# DEVELOPMENT AND APPLICATIONS OF HETEROCHIRAL DNA NANOTECHNOLOGIES

A Thesis

by

ADAM M. KABZA

Submitted to the Office of Graduate and Professional Studies of
Texas A&M University
in partial fulfillment of the requirements for the degree of

DOCTOR OF PHILOSOPHY

| | |
|---|---|
| Chair of Committee, | Jonathan T. Sczepanski |
| Committee Members, | Frank Raushel |
| | Wenshe Liu |
| | Junjie Zhang |
| Head of Department, | Simon North |

August 2020

Major Subject: Chemistry

# ABSTRACT

Nucleic acids serve as the molecular blueprint for all life on earth. Oligonucleotides hybridize to form the classic double helix architecture by aligning complementary bases to hydrogen bond with one another following a trivial set of rules termed Watson-Crick (WC) base pairing. WC base pairing rules state that adenine (A) residues always pair with thymine (T) residues and likewise guanine (G) residues always pair with cytidine (C) residues in the double helix conformation. This straightforward design principle is what endows nucleic acids with immense information storage capacity in order to encode life. Furthermore, this principle makes DNA a choice candidate for abiological nano-engineering. Through rational design of WC base pairing, it is possible to design limitless synthetic nucleic acid molecular architectures, both static and dynamic, with unparalleled precision. This unique feature of DNA has brought about the development of DNA nanotechnology. This area of research centers around using DNA to design dynamic as well as static nucleic acid architectures and systems with unprecedented functionality. With advances in synthesis, DNA nanotechnology has expanded to encompass all variety of modified and unmodified oligonucleotide systems capable of performing complex decision making tasks and even interacting with living systems as potential diagnostic and therapeutic tools. Despite the innovation that has come about in the past 40 years, numerous challenges remain in the application of DNA nanotechnology in vivo.

Until recently, DNA nanotechnology has remained in a predominantly homochiral paradigm. Even modified nucleobases have the naturally occurring D-stereochemistry in the ribose sugar ring. As a result, all of these polymers are subject to off target hybridization, protein interaction, and degradation. This body of work will cover structure based heterochiral interactions as well as the creation of sequence specific interactions between oligonucleotide enantiomers, a completely new phenomenon in the field of DNA nanotechnology. Heterochiral DNA nanotechnology is the study of fundamental interactions between oligonucleotides of opposing chirality, D- and L-. The utilization of L-oligonucleotides in biological systems provides several unique advantages over

the natural D-stereoisomer. L-DNA/RNA cannot be degraded by native enzymes, is typically not recognized by DNA/RNA binding proteins and is incapable of forming contiguous Watson-Crick base pairs with the native D-polymer. The work herein describes the various facets in which these unique properties may be exploited to design DNA nanotechnologies using L-DNA and L-RNA. Critically, we generalize sequence specific information communication between oligonucleotides of opposite chirality, as a result, the design principles described may be applied to all existing DNA nanotechnologies. Furthermore, we expect that the application of L-nucleic acids will find broad applications in biological chemistry as a whole as we move into the future.

# DEDICATION

To my mother and father, Dr.'s Lucyna and Konrad Kabza, without whom none of my journey would have been possible. Their teachings and knowledge have and will forevermore serve as a guiding light in all of my lifes pursuits. To my sister, Alice Kabza, who has always grounded me with her unwavering free spirit. Finally, to my loving partner, Gayle Bornovski, who always make sure I am cared for and loved throughout my most challenging moments.

# ACKNOWLEDGMENTS

I would like to thank my advisor, Dr. Jonathan Sczepanski, for accepting me to his lab and allowing me to pursue the ideas I proposed and providing me with an environment to be learn and be creative. I want to personally thank my close colleague Dr. Brian Young. Dr. Young guided me in lab and importantly, provided me with a constant source of conversation about not only nucleic acids chemistry, but all of biological chemistry literature as a whole. Our discussions culminated in us working together to develop many of the ideas presented in this work. I would also like to thank Nandini Kundu for always being willing to help and support throughout our time in graduate school together. Nandini and Brian have become my lifelong friends and helped me to grow tremendously as both a person and a scientist during my tenure at Texas A&M. I would also like to thank Dr. Deb Banerjee, Dr. Sougata Dey, Dr. Yu, and Chuck Deckard, for tolerating my silly rants and bad jokes. Without this incredible group of individuals, none of my success would have been possible.

CONTRIBUTORS AND FUNDING SOURCES

## Contributors

This work was supported by a thesis (or) dissertation committee consisting of Professors Jonathan Sczepanski (chair), Wenshe Liu, and Frank Raushel of the Department of Chemistry and Professor Junjie Zhang of the Department of Biochemistry and Biophysics.

DMA-001 and DMA-169 molecules were provided graciously by Dr. Amanda Hargrove's group as part of a collaboration. Certain data exhibited in Chapter 4 were collected in collaboration with Dr. Brian Young of the Department of Chemistry. Gayle Bornovski helped to edit this document carefully.

All other work conducted for this dissertation was completed by the student independently.

## Funding Sources

Graduate study was supported by the Cancer Prevention and Research Institute of Texas (CPRIT) under Grand Number RR150038, as well as the National Institutes of Health (NIH) under Grant Numbers R35GM124974 and R21EB027855. The contents of this dissertation are solely the responsibility of the author and do not necessarily represent the official views of CPRIT or the NIH.

TABLE OF CONTENTS

Page

LIST OF FIGURES

FIGURE Page

# 1. INTRODUCTION AND LITERATURE REVIEW

The twentieth century saw incredible scientific discoveries that greatly impacted all of society. Arguably the two most important discoveries of this era were quantum mechanics and the structure and function of nucleic acids. Together these two discoveries catapulted humanity into the digital age, saving countless lives and reshaping our understanding of the fundamental physics and biochemistry of life on earth. This was the beginning of the nanotechnology revolution. Countless advancements in optics, synthesis, particle physics, and molecular and cellular biology were made during this time [1] [2] [3] [4] [5] [6] [7]. We began to understand the fundamental building blocks, atoms and molecules, of matter, and how these building blocks were organized and interacted in both animate and inanimate systems. A critical advancement during this era is DNA nanotechnology, a broad field encompassing all technologies which utilize nucleic acids as synthetic building blocks and tools to create totally man-made devices, tools, biochemical circuits, and therapeutics which operate in ways not observed in nature. By understanding and exploiting the fundamental properties of this ubiquitous biopolymer, thousands of new biological technologies have been discovered, many of which have been effectively tested in living organisms [8] [9] [10].

DNA nanotechnology may be roughly categorized into two sub-fields or research; 1) Static, structural nanotechnologies, and 2) Dynamic nanotechnologies. Despite this split, there is significant overlap between these two categories of research because all DNA nanotechnologies rely on the same principles of WC hybridization. The critical distinction to be made is that static, structural technologies, focus on how higher order (tertiary and quarternary) structures of nucleic acids interact with one another, and dynamic technologies focus on how nucleic acids with complementary sequences recognize and interact with one another (secondary structure interaction) in real time [11] [12] [13] [14]. In this chapter I will provide a review of the field and introduce the relevant background and innovations as they relate to this work. Chapters 2 and 3 will cover structural nanotechnologies and chapter 4 will cover dynamic nanotechnologies. The following body of work encompasses the development of multiple new DNA nanotechnologies, termed heterochiral DNA

nanotechnologies which fully integrate L-DNA, the unnatural enantiomer of native D-DNA, into contemporary DNA nanotechnology.

### 1.0.1 Overview of nucleic acids

Nucleic acids constitute the fundamental building blocks of all life on earth. They each consist of four basic monomeric units, termed (deoxy)ribonucleotides, adenine, cytosine, guanine, and thymine (uridine for RNA) (Figure 1.1). Each sugar base has attached to it a nitrogenous, aromatic group, which confers the identity of the unit (A, C, G, or T/U). The primary distinction between DNA and RNA is that DNA lacks a $2'$ hydroxyl within its ribose sugar chemical structure. Although seemingly subtle, the presence or absence of this hydroxyl group drastically affects the stability of the respective polymers and as a result, dictates the different roles that DNA and RNA perform in the context of living systems. DNA participates as a molecular information storage entity, permanently and reliably storing all of the information necessary to create a living organism. This is only possible because the lack of a $2'$ hydroxyl endows DNA polymers with a half life of $\approx$ 4.6 billion years in terrestrial conditions. Conversely, RNA only has a half life of $\approx$15 minutes under the same conditions. However, despite lacking intrinsic stability, RNA is capable of assuming myriad high order tertiary and quarternary structures that DNA cannot and can be much more easily broken down into its basic substituents, two properties which make it an excellent dynamic molecular messenger and (in certain instances) machine. Together, DNA and RNA constitute two out of three of the polymers described in the central dogma of molecular biology, with the third being polypeptides (Figure 1.2) [3].

Briefly, DNA stores information in the classic double helix configuration which can then be transcribed into RNA, the messenger, which goes on to be translated into polypeptides which constitute proteins and enzymes, the working polymers of the cell [15]. Although initially the central dogma was thought to be absolute truth, our understanding of nucleic acids has evolved tremendously, forcing a re-organization of this central tenet. Specifically, two overarching discoveries have occurred. The first being that not all DNA within a cell codes for proteins, and in fact, the majority of DNA in the cell does not code for proteins, only roughly 2% does [16] [17] [18].

Second, that not all RNA is simply translated into proteins. In fact, RNA can act as a messenger (mRNA), control genetic expression (short interfering RNA or siRNA, long noncoding RNA or lncRNA and riboswitches), and even function as an oligonucleotide enzyme, or ribozyme, by catalyzing important chemical reactions within the cell such as splicing mRNAs and acting as a vital component of ribosomes, the molecular machinery that translates RNA into proteins [19] [20] [21]. Together, these discoveries have reshaped our understanding of the role nucleic acids play in biological systems and has resulted in countless innovations in fundamental biological chemistry as well as modern medicine. In the following sections I will review the current literature concerning oligonucleotide structure, DNA nanotechnology and its applications, as well as L-oligonucleotides and how they pertain to DNA nanotechnology and this body of work as whole.

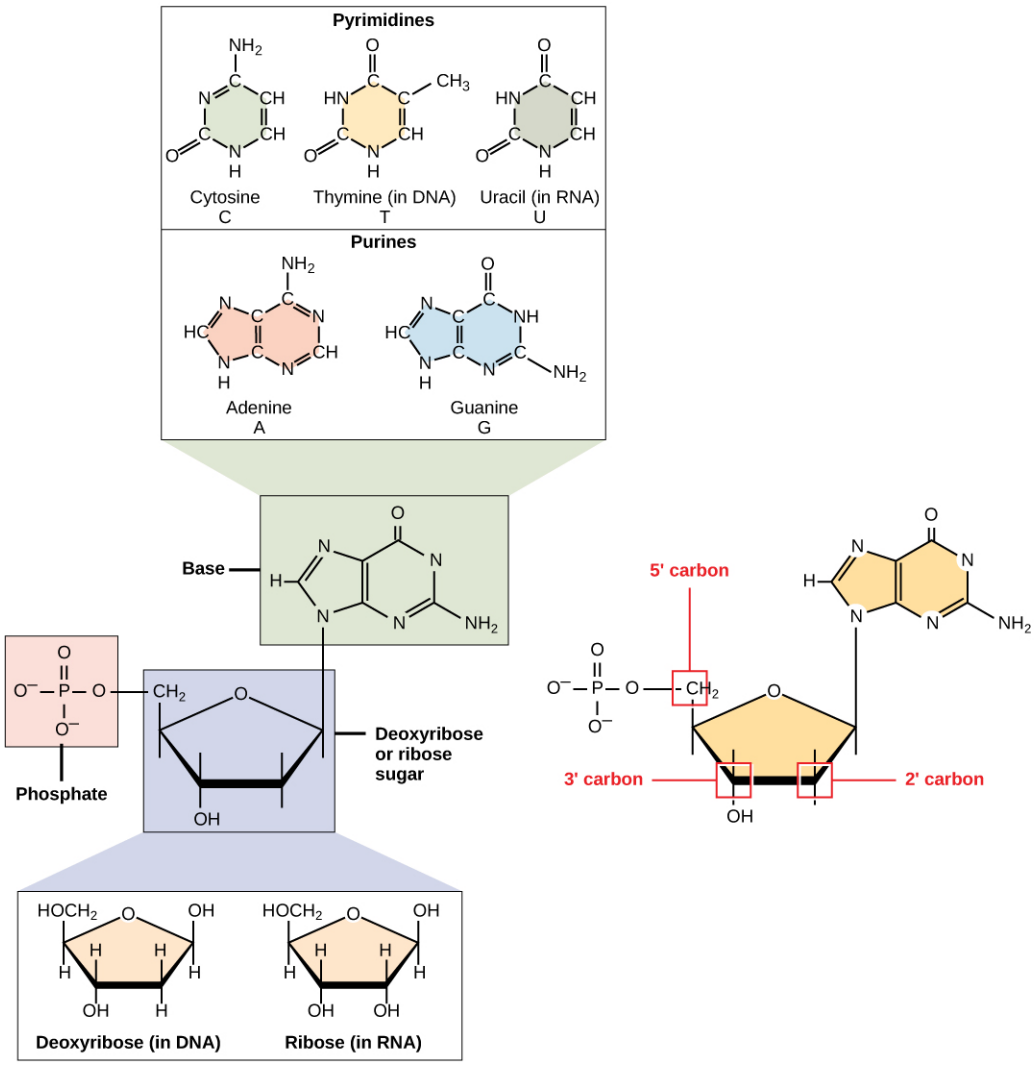


Figure 1.1: Chemical structures of DNA and RNA monomers. DNA is composed of deoxyribose sugar, with nitrogenous bases Cytosine, Thymine, Adenine, and Guanine. RNA is composed of ribose sugar with the same nitrogenous bases as DNA except Thymine is replaced by Uracil. The presence or absence of a hydroxyl moiety at the 2′ carbon distinguishes RNA from DNA respectively. Both polymers have nitrogenous bases protruding from the 1′ carbon and phosphate groups protruding from the 5′ carbon. The hydroxyl group at the 3′ position takes part in phosphodiester bond creation to build a polymer from monomeric units. Adapted under CC AK 4.0, access for free at https://openstax.org/books/biology-2e/pages/1-introduction.

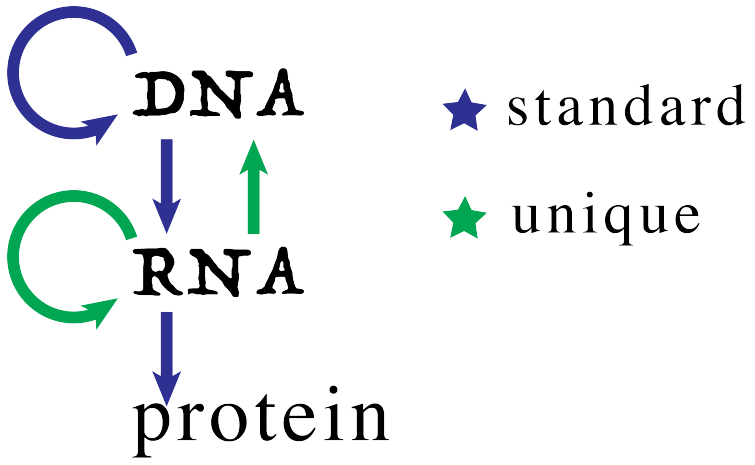


Figure 1.2: Cartoon representation of the contemporary central dogma of molecular biology. The arrows represent transfer of sequential information, categorized as standard (occurring in most cells) and unique (occurring under very specific conditions). The standard transfers of information are DNA $\rightarrow$ DNA (replication), DNA $\rightarrow$ RNA (transcription), and RNA $\rightarrow$ protein (translation). The unique cases represent RNA $\rightarrow$ RNA (RNA replication) and RNA $\rightarrow$ DNA (reverse transcription).

### 1.0.2 Oligonucleotide Structure

At the most basic level DNA and RNA are built of monomeric units linked together through a phosphodiester backbone (Figure 1.3). DNA consists of a core deoxyribose (RNA has a core ribose) sugar unit bound to an aromatic nitrogenous base at the C1′ carbon position. There are two types of nitrogenous bases-purines, adenine and guanine, and pyrimidines cytosine, thymine (DNA) and uridine (RNA) (Figure 1.1). The nitrogenous bases are capable of forming hydrogen bonds with one another following WC base pairing rules stating that A pairs with T/U (DNA/RNA respectively) through two hydrogen bonds and G pairs with C through three hydrogen bonds (Figure 1.3). Base pairing is the fundamental interaction that structures nucleic acids, including our entire genome, and regulates virtually all interactions between biologically relevant nucleic acids [22] [23] [24]. The 3′ and 5′ carbons linked on either end to a phosphate group which, in the context of the polymer, is a phosphodiester linkage. The 5′ position of each nucleotide is tethered to the 3′ position of the adjacent nucleotide through this phosphodiester linkage (Figure 1.3) [1].

The canonical DNA double helix typically consists of two DNA polymers twisted around one another and oriented in anti-parallel fashion with the 5′ end of one polymer adjacent to the 3′ end of the complement. (Figure 1.3). The phosphodiester backbone faces outward, away from the central axis of the double helix, thus orienting this negatively charged group towards solvent (water) and effectively solvating large nucleic acid polymers. The bases face inward toward pointing toward the longitudinal axis, allowing hydrogen bonding to take place between complementary bases and for $\pi$-$\pi$ stacking to occur between the $\pi$-orbitals of the aromatic bases which are oriented parallel to the longitudinal axis. This stacking interaction effectively occurs through the entire length of the double helix. Taken together, these two non-covalent interactions are what endow DNA with unparalleled stability and making it the optimal molecule for long term high fidelity data storage. Consequently, given the polyanionic nature of the phosphodiester backbone of oligonucleotides, the strength of the double helix duplex, as well as other high order structures can be mediated by the presence of mono- and divalent cations e.g. Na and $Mg^{2+}$ [25]. Furthermore, the concentrations of these cations can be used to modulate the kinetics of dynamic DNA systems in which the

organization of WC base pairs changes over time. The importance of nucleic acids in biological systems has compelled the characterization the kinetic and thermodynamic parameters commanding DNA/RNA structures [26] [27] [28] [29] [30] [31]. In fact, it is now possible to accurately predict oligonucleotide secondary structure under a variety of salt and oligonucleotide concentrations rapidly using open source programs such as mFold and NUPACK [32] [28].

DNA is capable of assuming various double helix conformations as well as other tertiary structures. Most commonly, a DNA duplex assumes a B-form helix (Figure 1.4A) [33]. The B-form helix has a right hand twist about its axis and is compacted quite tightly along its longitudinal axis with the shortest full turn length out of the three helical conformations. Conversely, the Z-form double helix has a left hand twist and a longer full helix turn length than B-form DNA. This atypical helical conformation is only formed under specific salt concentrations (Figure 1.4B). The A-form double helix, like B-form, has a right hand twist about its longitudinal axis and has the longest full helix turn length of the three types. The A-form helix is the preferred conformation of RNA duplexes (Figure 1.4C)

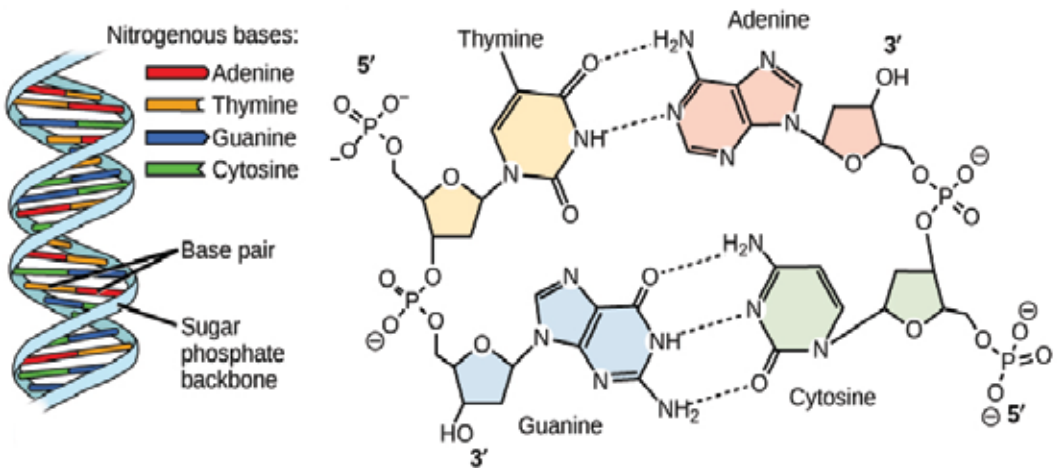


Figure 1.3: Cartoon representation of the structure of a DNA double helix at various scales. (a) the full double helix depicting base pairing, the major groove and the minor groove. The double helix is asymmetric about its longitudinal axis which gives rise to the two groove dimensions. (b) A closer look at the base pairing between A and T and C and G. The antiparallel arrangement of strands is also shown. (c) Chemical structure and molecular orientation of the polymer. Hydrogen bonding is denoted by dotted lines between bond donors and acceptors within the nitrogenous bases. The orientation of the sugar rings and phosphodiester backbone is also shown. Adapted under CC AK 4.0, access for free at https://openstax.org/books/biology-2e/pages/14-2-dna-structure-and-sequencing

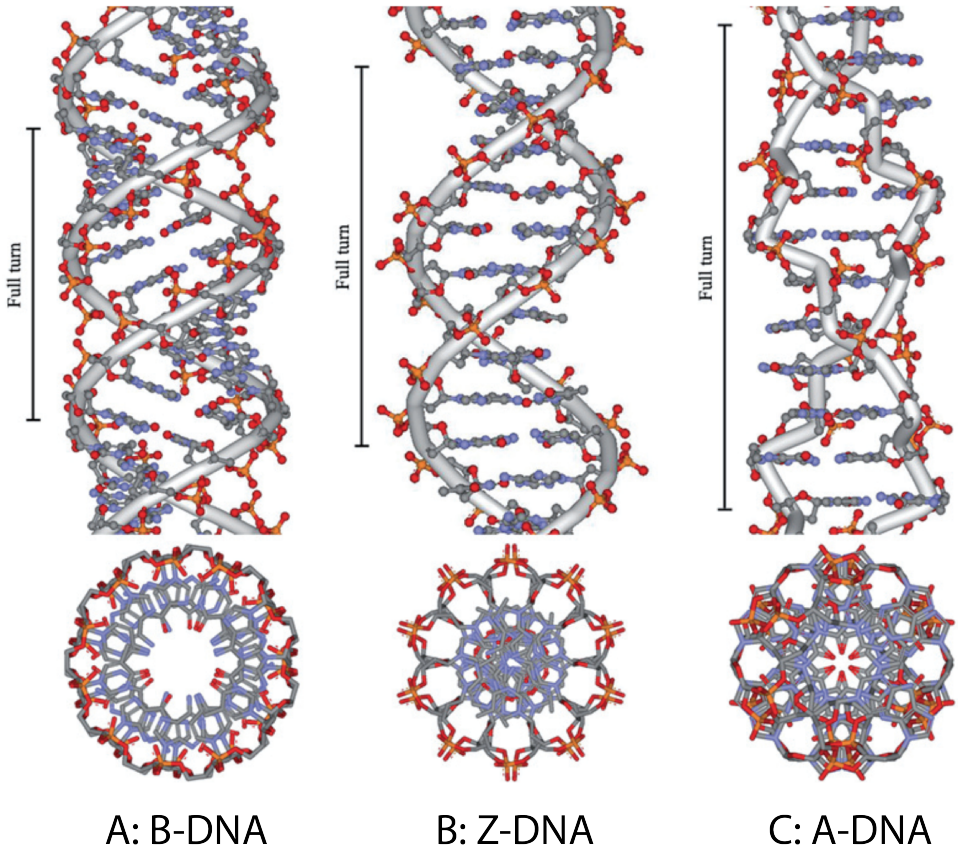


Figure 1.4: DNA double helix conformations. (A) The B-form DNA double helix is the most commonly occurring conformation of DNA. B-DNA has a right handed twist about the longitudinal axis with an average vertical base separation distance of 3.4 nm and approximately X bases per full turn. (B) The Z-form DNA double helix has a left handed twist and is only formed under specific salt concentrations. (C) The A-form DNA helix is another right handed twist helix with a different geometry from B-form. A-form helix is the preferred conformation of RNA double helixes. Adapted from Ref. 33 under CC AK-NC-3.0

## 1.1 DNA nanotechnology and its applications

In 1982 Nadrian Seeman published a seminal article titled 'Nucleic acid junctions and lattices' in the Journal of theoretical biology [34]. This work laid the foundations for what would eventually become DNA nanotechnology. Briefly, this article discusses the parameters that are necessary for an oligonucleotide sequence to fold into unnatural configurations by selectively designing the oligonucleotide sequence in such a way as to maximize Watson-Crick base pairing at precisely chosen subsequences of the full polymer. These rationally designed oligonucleotide sequences typically lack any sequence homogeneity with their natural counterparts. This revolutionary work reshaped the landscape of synthetic applications of DNA in biological chemistry. Importantly, this demonstrated that oligonucleotides are a premier candidate for bottom-up engineering of nanomaterials and nanodevices. However, at the time there were limitations to the length, quantity, and quality of synthetically prepared oligonucleotides, making it difficult to implement these ideas in an in vitro setting. As a result, it would be nearly twenty more years before DNA nanotechnology unraveled into the field it has become today.

The straightforward design principles of Watson-Crick base pairing make DNA a versatile and effective material for engineering nano- (<100 nm) to mesoscale (>100 $\mu$m) systems. With complete control over sequence identity through solid-phase DNA synthesis, it is possible to achieve control of such nanomaterials/devices down to a resolution of 3.4 nm (the spacing of adjacent base pairs in a typical B-form DNA helix). This has facilitated the rapid and diverse creation of scores of DNA machineries and architectures through the programmed hybridization of complementary oligonucleotides. Initially, DNA nanotechnology centered around the construction of unique, but static, nucleic acid structures [35] [36] [37] [38]. In these static systems, only the final, most thermodynamically stable structure is of interest, with the intermediate folding steps being a means to and end. However, recently, there has been great interest in the development of dynamic DNA systems which rely on spatio-temporaly resolved oligonucleotide interaction and hybridization. At their core, dynamic DNA systems rely upon the strand-displacement reaction. I will discuss this reaction in explicit detail in section 1.1.1. Briefly, a strand-displacement reaction allows for

one strand of DNA to displace another DNA strand from a preformed partial double helix, releasing the incumbent strand into solution. The released strand may go on to interact with other oligonucleotides as desired. Myriad dynamic DNA systems have been developed using the strand-displacement reaction including molecular tweezers, boolean circuits, catalytic signal amplifiers, autonomous walkers and rotors, and rearrangeable nanostructures [39] [40] [41] [42] [43] [44].

Essentially, DNA nanotechnology may be viewed as the simplest method for engineering nanomaterials and nanostructures with complete control of the three-dimensional configuration of matter to a resolution of approximately 3.4 nm. Currently no other technology or material exists that matches the precision of this bottom-up nanoscale design approach. Moreover, the simplicity of generating oligonucleotides with a variety of modifications even further expands the versatility of nucleic acids as a material for engineering nanoscale diagnostics and therapeutics as I will discuss in more detail in the following sections. Furthermore, because DNA/ RNA are present within all living organisms, one can envision the implementation of any DNA device within living cells and organisms, interacting with the natively expressed oligonucleotides in order to diagnose, treat, and attenuate systemic abnormalities. In the following sections I will more closely analyze the various existing static and dynamic DNA nanotechnologies which I have outlined here and provide impetus for the overarching goals of my research in this area.

### 1.1.1 Strand-displacement reactions

DNA strand displacement occurs when two strands of partial, or full, complementarity hybridize with one another, releasing one or multiple pre-hybridized strands in the process. In the first step of strand-displacement reactions, an initial oligonucleotide (Input A) interacts with an exposed complementary region 3* (known as a toehold) from a second oligonucleotide (blue strand in Complex X, BX, Figure 1.5B) which is in a partial duplex with a third, shorter oligonucleotide (red strand in Complex X, RX, Figure 1.5B) [11]. As shown in Figure 1.5A, sequence identity is denoted by either numbered or lettered domains which represent subsequences of the oligonucleotide. Complementary domains are denoted by a * where A* is complementary to A.

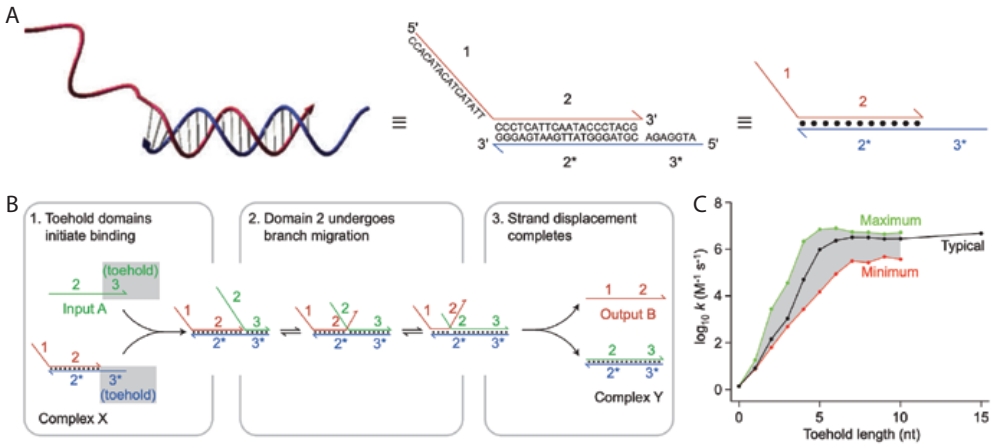


Figure 1.5: DNA strand-displacement reaction mechanism and notation. (A) Definition of sequence domain representation and hybridization illustrations. The individual strands are represented as lines with the half arrow indicating the 3′ end of the strand. Domains represent subsequences of the full length oligonucleotide and are denoted by numbers with complementary domains denoted by a * symbol. Hybridization is indicated by black circles between complementary domains. (B) The three steps of a full strand-displacement reaction. (C) Kinetic plot of strand-displacement reactions each with different toehold domain lengths, demonstrating the toehold length dependence of the kinetics of strand-displacement reactions. This data also indicates a plateau to the reaction speed beyond a toehold length of approximately 8. Adapted from Ref. 11 with permission from Nature.

The length and base composition of the toehold region directly influences the kinetics of nucleation (initial binding to the toehold domain) and by extent, the overall strand displacement reaction (Figure 1.5C). Longer and more G/C rich toeholds generate a more stable nucleation duplex since GC basepairs intrinsically have 50% more hydrogen bonds per base pair, increasing the probability of moving onto the second step of strand-displacement rather than the dissolution of the nucleated complex. The next step of strand-displacement is known as branch migration. Branch migration begins when the toehold nucleated strand (Input A) begins to compete with the incumbent strand (RX) for hybridization to strand BX. It is well known that at the terminal ends of DNA double helixes, the base pairing behaves dynamically, a process referred to as fraying or breathing [27] [45]. As a result, as the terminal nucleotides of the Complex X duplex which are adjacent to the toehold domain breath, the nucleated strand Input A competes for hybridization with strand RX in a stepwise manner. In this fashion, one base pair at a time, Input A may displace strand RX by migrating all the way through the RX/BX duplex. This process occurs in a random walk fashion, driven forward by enthalpy since the final duplex generated (Complex Y) is more thermodynamically stable than Complex X. This is because the final duplex has overall more base pairs and is more stable than the initial duplex. Importantly, this process may be designed to occur not by enthalpy, but rather entropy, where a strand displacement utilizing one input releases two output strands [46]. With the release of strand Output B, an output signal has been generated from an input signal (Input A) through this strand displacement event. The released strand may now go on to interact with other partial duplexes in downstream strand displacement events, or act as a signaling molecule to generate a detectable readout such as a fluorescent signal. In the following sections I will discuss a variety of possible reaction schemes which rely on strand displacement reactions.

The first example of a dynamic DNA device employing strand-displacement reactions to operate was a so called molecular tweezer reported by Neumann's lab (Figure 1.6) [43]. The initial complex consists of three strands of DNA. The first strand A is labeled at its $5'$ end with a tetrachlorofluorescein (TET) fluorescent dye (wavelength) and at its $3'$ end with carboxy-tetramethyl-

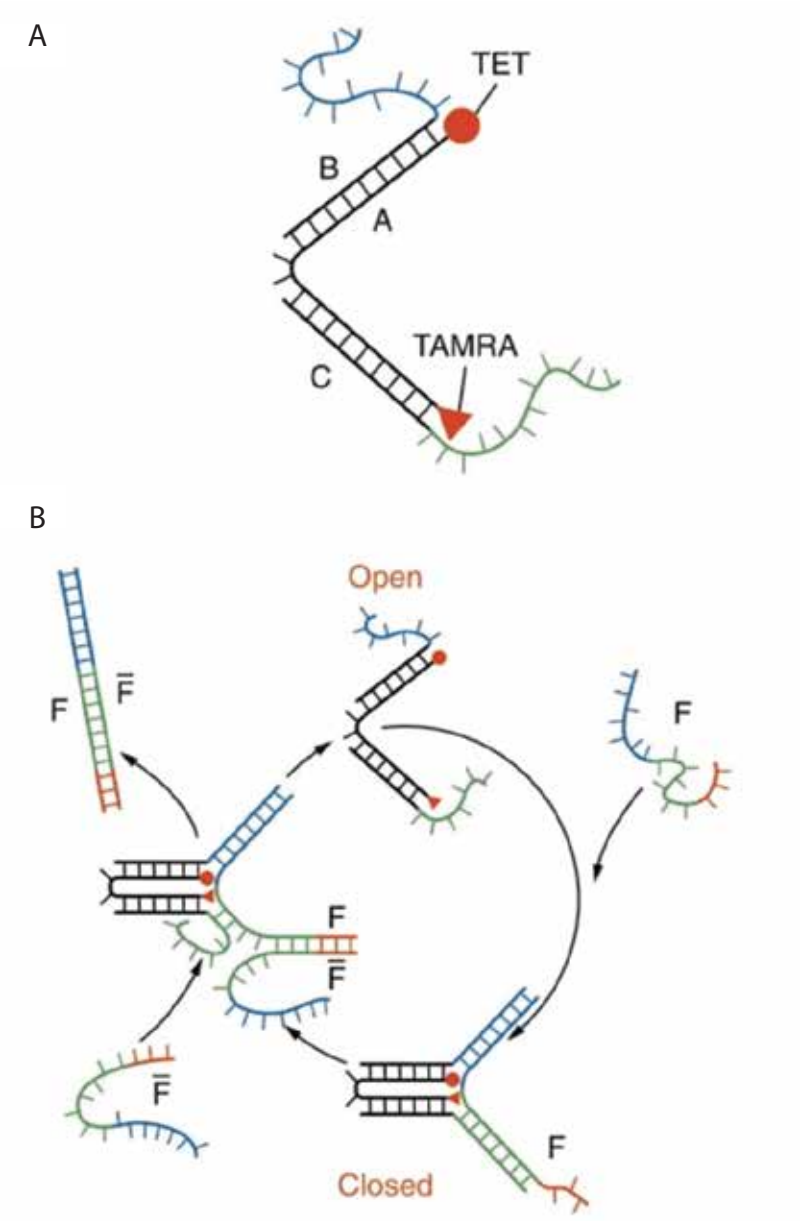


Figure 1.6: A DNA fueled dynamic DNA device. (A) Description of the TET and TAMRA fluorescent labeling of the 'tweezers'. (B) A cartoon schematic demonstrating the opening and closing of the molecular tweezers for one cycle of fuel addition. Initially, the tweezers are in an open conformation. When the fuel strand 'F' is introduced, it hybridizes to exposed toehold domains on strands B and C (blue and green subsequences respectively), forcing the TET and TAMRA dyes into close proximity, enabling FRET. This is the closed conformation of the tweezers. Next, the Fbar strand, which is complementary to the fuel strand F, is introduced. Fbar nucleates to the exposed toehold domain of F (orange), and through branch migration frees the tweezers as waste duplex F/Fbar is generated, leaving the tweezers in their initial open state. These steps together constitute one cycle of closing and opening. Adapted from Ref. 43 with permission from Nature.

rhodamine (TAMRA) fluorescent dye (wavelength). Strand A is hybridized to strands B and C through complementary sequence domains with a single stranded flexible region separating the two partial duplexes. Strands B and C have single stranded overhang regions at the 5′ or 3′ overhangs respectively. In the inactive state, the fluorophores remain on average separated and the tweezers are considered in the open conformation. Upon addition of a fuel strand F, which contains domains complimentary to the single stranded overhangs of strands B and C, and a toehold domain for downstream fuel sequestration, the tweezers become closed through hybridization of F to B and C. When this occurs, the single stranded flexible region of strand A bends, forcing the TET and TAMRA dyes into proximity, enabling Forster Resonance Energy Transfer (FRET) to occur, indicating that the tweezers are in a rigid closed state. Strand F was designed with its own single stranded overhang which acts as a toehold for a fully complementary strand F* to nucleate to, branch migrate through B/F and C/F duplexes, thus re-opening the tweezers and releasing an F/F* waste duplex. By consecutive additions of strands F and F*, this dynamic DNA device could be cycled through the opened and closed states at least 7 times. This work demonstrated the potential to utilize DNA strand-displacement reactions to operate nucleic acid based nanodevices with complete control over functionality and reaction kinetics.

A critical innovation in dynamic DNA nanotechnology was the likening of strand-displacement reactions to digital (boolean) logic gates, with high and low electric current being replaced by high and low oligonucleotide concentration. The first example of this analogy was reported by Winfree and coworkers in 2006 [41]. This analogy allows abstraction of boolean logic into a DNA context and confers the ability for DNA to not only store information as it does in living systems, but also to perform complex computations and decision making tasks following a boolean paradigm. An input strand may be treated like an input electrical current in a digital circuit. Similarly, strands released from a displacement event behave like an output electrical current in digital circuitry. Overall, it is possible to treat cascaded DNA strand-displacement reactions as boolean (digital) circuits. In their initial report, the authors designed an AND, NOT and OR gate as well as a thresholding gate for leak signal suppression (Figure 1.7). The rational design of such cascaded systems is possible due

to the immense effort that has gone into the kinetic and thermodynamic characterization of DNA duplexes over the past seventy years [26] [27] [28] [29] [30] [31] [25] [47]. By understanding these parameters of DNA double helixes, it is possible to rationally design complex, multi-component DNA circuits. Theoretically, there is no limit to the complexity of DNA based circuits. However, in reality there are numerous roadblocks to the design and implementation of strand-displacement circuits both in vitro and in vivo. The two most prominent challenges are 'leak', or the generation of output signal with no input present, and in vivo specificity and stability [48]. Winfree and coworkers have developed many important advances towards the minimization of aberrant leak signal by designing leak suppressing duplexes which depress low background signal, but do not affect overall signal when input is present [49] [50] [51]. Seelig et. al. has also contributed powerful solutions to these issues. Prominently, the spatially resolved DNA circuit in which each gate is anchored to a large DNA nanostructure, preventing spurious interactions between circuit components [52]. Furthermore, the use of modified oligonucleotides in the sequence design of DNA circuit gates has also been extensively studied and utilized [11] [12]. To date there have been incredible advances in the application of D-DNA nanotechnologies in a cellular context [12] [53] [54]. For example, DNA point accumulation for imaging in nanoscale topography (DNA-PAINT), utilizes transient DNA hybridization of fluorophore-quencher labeled docking strands onto a target. The binding and unbinding event causes a switch in the fluorescent state of the docking strand, allowing imaging with sub-10-nm resolution using total internal reflection microscopy [55] [56]. Furthermore, DNA nanostructures have been used as for cargo delivery into cells, DNA strand displacement reactions and molecular beacons have been used to detect endogenous nucleic acids in living cells [57] [58] [59]. Despite these advances however, the issue of applying strand-displacement reaction cascades in vivo remains a massive challenge. Specifically, chemically modified oligonucleotides which confer stability against nuclease enzymes, are still capable of hybridizing with off-target endogenous nucleic acids, and have altered kinetic and thermodynamic properties from the native polymer, making rational design difficult and unpredictable. I will discuss such modifications in more detail in section 1.3. Altogether, these issues leave much

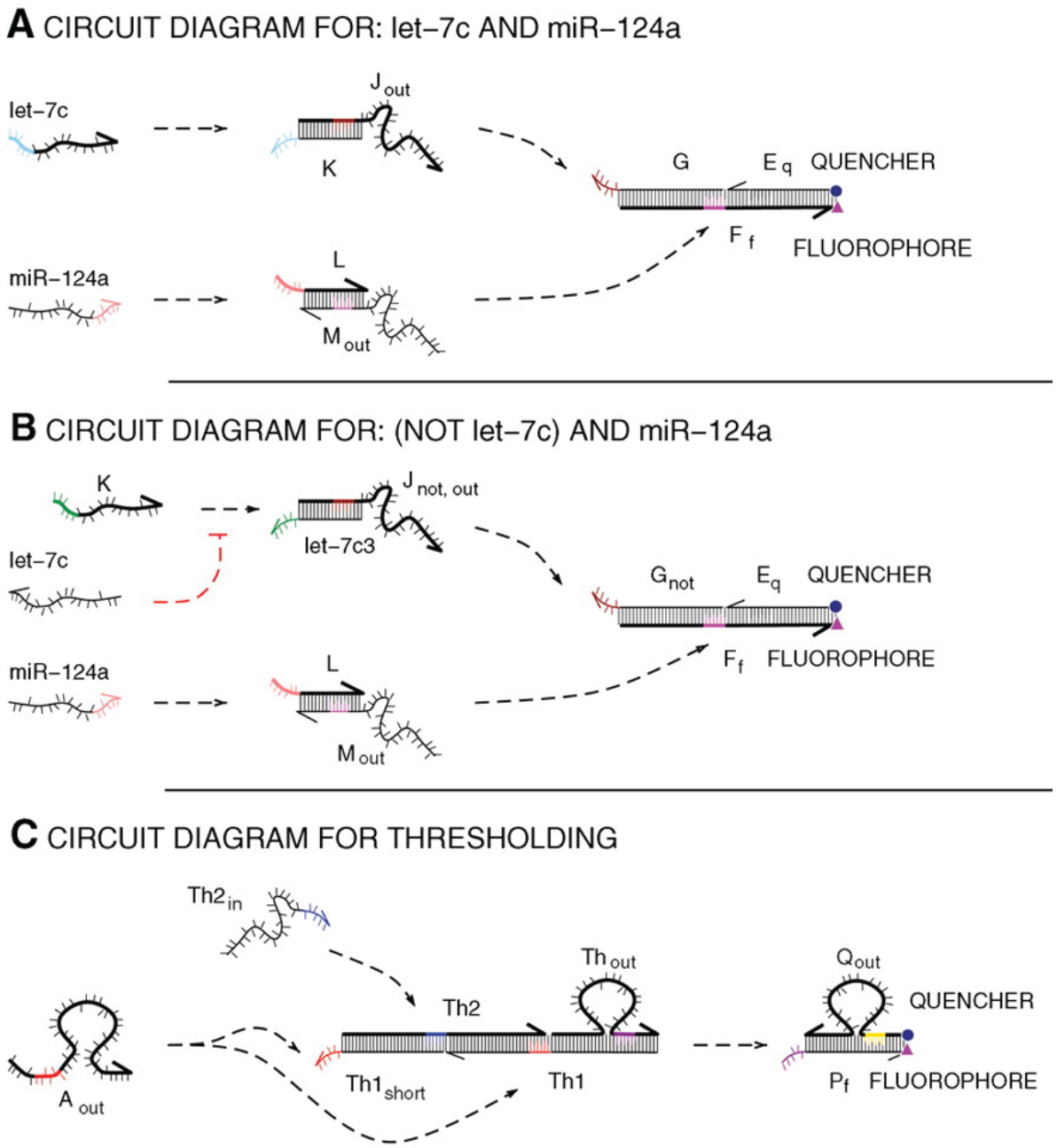


Figure 1.7: Demonstration of cascaded DNA strand-displacement reactions acting as boolean logic gates. (A) A DNA based AND gate requiring both let-7c and miR-124a RNA inputs in order to activate a fluorescent signal. (B) A DNA based NOT-AND gate which requires the absence (NOT) let-7c miRNA AND the presence of miR-124a in order to activate the final fluorescent signal. (C) A thresholding gate which is a three input AND gate requiring only two unique inputs $A_{OUT}$ and $Th2_{in}$, where $A_{OUT}$ is required to be the first and third input. $Th2_{in}$ is present before the experiment begins. At substoichiometric concentrations of $A_{OUT}$, very little output signal is generated. When the concentration of $A_{OUT}$ is in twofold excess to the gate complex will generate positive signal. Adapted from Ref. 41 with permission from Science.

to be desired for the application of strand-displacement reactions in biologically relevant systems. In section 1.4 Goals, I will introduce the technologies I have developed to bridge this gap with the remaining chapters explicitly detailing all aspects of these systems.

#### *1.1.1.1 DNA computation*

As mentioned above, strand-displacement reactions may be abstracted into boolean logic gates analogous to digital circuit gates [41]. This unique property makes DNA an excellent candidate for molecular computing. Boolean logic traditionally utilizes three base operations, AND, OR, and NOT, in order to perform complex computations through a systematic concatenation of these three operators. When a signal (in our case an input DNA molecule(s)) is presented at a gate, the operator makes a decision of YES or NO (release or no release of an output strand respectively) whether to pass signal on beyond its position. Because there are only two possible outcomes for each operator, boolean logic circuits behave as a binary algebra. Consequently, when these three operators are applied in a cascading, feedback, and feedforward fashion, they can be used to perform complex computations. These operators may be visualized as truth tables, logic gates, or Venn diagrams (Figure 1.8) [60]. Digital computers perform sophisticated task processing and decision making using digital boolean logic gate operations. By emulating these operations on a DNA platform, it is theoretically possible to achieve computational complexity rivaling that of silicone based technologies. Although currently no DNA based circuit even remotely reaches the complexity of contemporary digital technology, this is a rare example of a biological molecule capable of being engineered to perform synthetic computations. An interesting distinction between nucleic acid computation and its digital counterpart is that there is no real distinction between hardware and

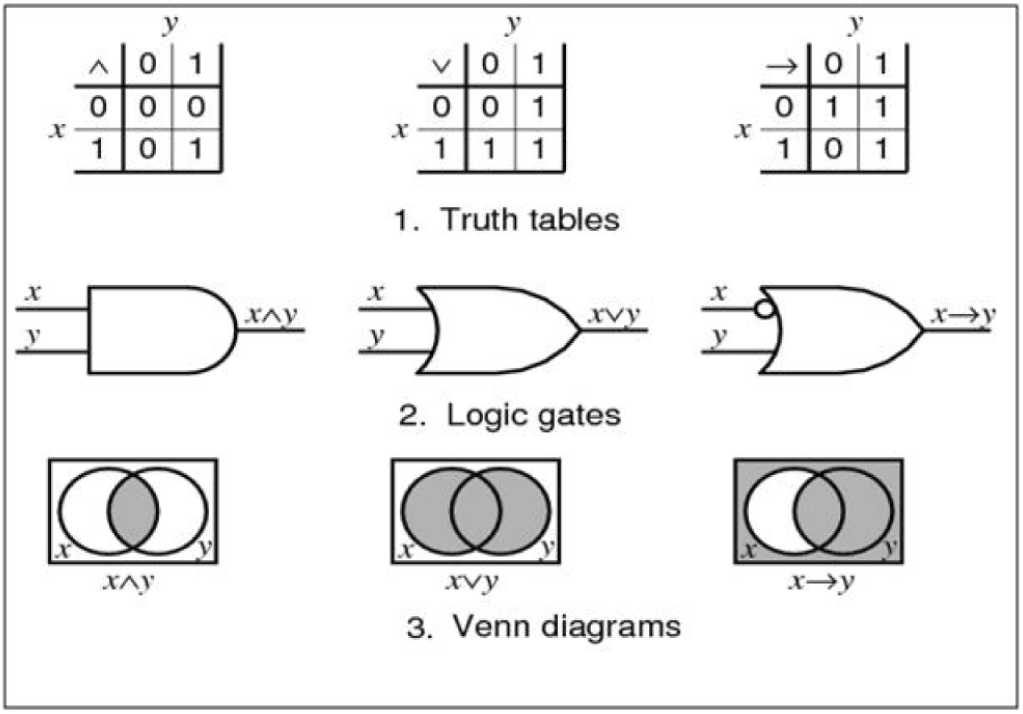


Figure 1.8: Diagram of various representations of Boolean logic operations. (a) Truth tables where '1' represents ON and '0' represents OFF. (b) Logic gates with formal notation defined as: AND and two variations of OR. (c) Venn diagrams with the shaded region designating the final signal generated by the corresponding operation. These operations may be performed using DNA strand displacement reactions. This facilitates the use of DNA for biomolecular computation. Adapted from Ref. 60 from IEEE Computer Society open access journal.

software in DNA computation. DNA not only behaves as the structural component (hardware), but also as the signal transducer (software), greatly simplifying the engineering of nucleic acid based computational systems. Furthermore, unlike its silicone counterpart, because cellular processes are dictated by nucleic acid transcription, translation, and replication, DNA computations systems can be directly integrated into live genetic circuitry to make real time decisions regarding the immediate state of the cell. It is important to note that although enzymatic reactions may be utilized to perform trivial computations, it is impossible to generalize rules for employing enzymes for sophisticated multicomponent circuits.

The first example of DNA computing came from Adleman in 1994 where he used a cycle of DNA hybridization events and polymerase chain reactions (to amplify signal) to solve the Hamiltonian path problem [61]. In graph theory, a Hamiltonian path is defined as a path in a graph that visits each vertex exactly once. Although in this case enzymes were necessary (PCR) to amplify signal, DNA hybridization events alone performed the computations required to solve the problem. Since then, countless examples of DNA based computation have been demonstrated. As our understanding of dynamic DNA systems evolves, so does the complexity and scale of the computation. Contemporary DNA computation has been used to create DNA neural networks, compress information (DNA fountain), encrypt information, and perform complicated decision making tasks with hundreds of input and output strands [62] [63] [64] [65] [50] [66]. Furthermore, general chemical reaction kinetics have been abstracted to DNA computational platforms [67]. All of these technologies rely solely on DNA strand-displacement reactions, demonstrating the immense versatility of this unique reaction. Together, these advancements are leading towards the integration of complex computational systems in living and artificial biological systems [68] [65]. By modeling gene regulatory pathways with DNA computation, one can envision effectively 'hijacking' cellular gene paths and potentially correcting malignancies and other aberrant genetic expression patterns to treat diseases (Figure 1.9) [69]. Furthermore, the same concepts may also be applied in synthetic biology, bringing us closer to the creation of totally synthetic organisms.

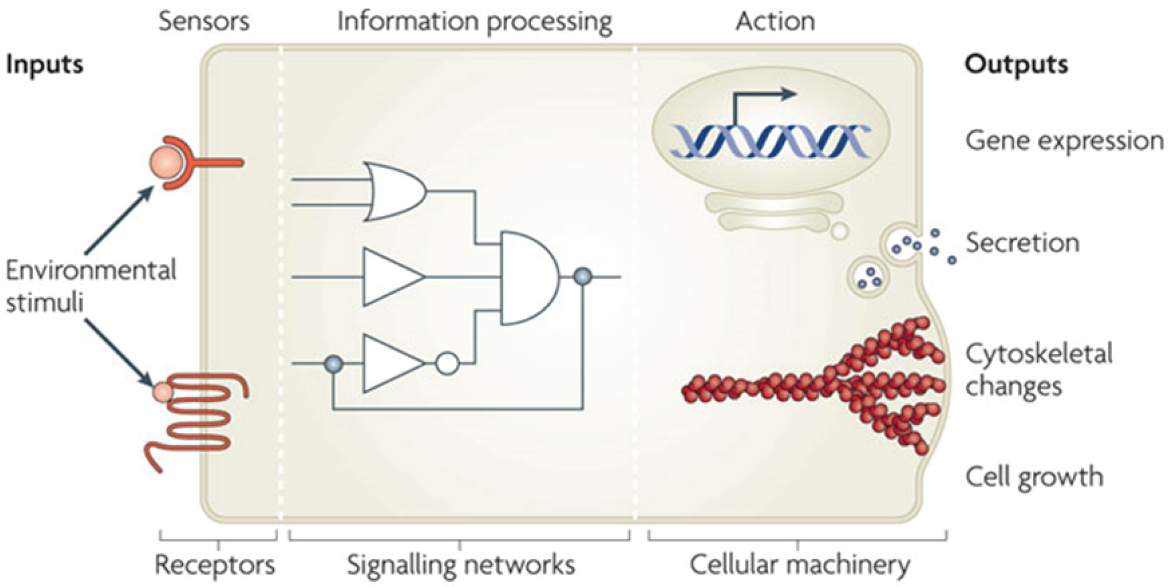


Figure 1.9: Cartoon representation of how cellular information processing may be visualized as a boolean logic circuit where environmental stimuli behave as input signals, and gene expression and physiological changes are output signals. Dynamic DNA nanotechnologies naturally fit into this system, allowing for the rational design of nucleic acid circuits which precisely attenuate diverse facets of cellular activity. Adapted from Ref. 69 with permission from Nature.

#### *1.1.1.2 DNA cryptography and data storage*

DNA has proven itself a reliable material for the storage of data; it is the blue print for all life on earth. With modern synthetic capabilities, it is now possible to 'write' anything using the four letter (A, C, G, and T) alphabet of DNA. This translation is analogous to translating information into binary for computers to interpret. Although this is DNAs most famous form of information storage, utilizing the properties of DNA for the storage of historical, social, scientific, and environmental information has gained traction in the past two decades. Specifically, DNA lends itself to very long term data storage on the order of thousands to millions of years. There are several key factors that distinguish nucleic acids as superior long term storage material over their digital counterpart. The first being that DNA will likely never be outmoded. Briefly, this means that the enzymes which process and read DNA and which are utilized to retrieve information from nucleic acid sequences will always be available to perform this task. The second factor is DNAs incredibly information rich sequence space which is quarternary (A, C, G, T bases) as opposed to digital binary sequence space. In fact, for a given string of N nucleotides, there are $2^N$ times as many DNA sequences as there are strings N binary digits long [70]. Depending on the method of information storage, the information density of nucleic acids can reach 215 petabytes per gram of DNA. For context, one petabyte is equivalent to 1024 terabytes, so one gram of DNA has equivalent data storage capacity as >220,000 1terabyte hard drives [63]. Furthermore, even if a storage oligonucleotide becomes damaged in some fashion (i.e. radiation damage or hydrolysis), as long as reasonably long subsequences remain intact, much information may still be retrieved by sequencing the fragments. A major disadvantage for the utilization of DNA for data storage is the difficulty of information retrieval from the stored DNA sequence(s). Modern state of the art DNA sequencing methods are still orders of magnitude slower than digital computing for data processing. However, this is unimportant when the goal is to safely store information for future generations to have a reliable encyclopedia of contemporary life.

Like dynamic DNA computation, DNA data storage is analogous to digital data storage and retrieval. Importantly, the information stored in DNA sequences requires encryption in order to

avoid reading by an unwelcome party. This challenge has spawned the area of DNA cryptography. Cryptography is defined as the practice of creating and breaking codes. The process of storing information cryptographically is known as encryption. Encryption techniques have existed almost as long as written language. In the digital age, almost all information being processed by computers is encrypted to some degree. However, with every encryption technique discovered, a new code cracking technique arises. As a result, DNA based cryptography might be the next advancement in unbreakable encryption algorithms. The sheer quantity of manipulation and analytical methods available for nucleic acids means there is limitless potential for developing unbreakable codes on DNA platforms. To date multiple groups have encrypted various information using DNA [71]. Recently in 2017, Erlich and Zielinski utilized a method known as DNA Fountain to store an entire computer operating system, a film, and other files which totaled $2.14 \times 10^6$ bytes of data [63]. With sequence coverage equivalent to that of a single Illumina sequencing tile, the authors retrieved all of this information with zero error. These examples demonstrate the power and versatility of using DNA for abiological data storage and encryption. As technologies advance and make the synthesis of even larger scale DNA architectures, as well as advances in nucleic acid modifications and sequencing technology, DNA cryptography and information storage will likely become a more mainstream DNA nanotechnology in the years to come.

### 1.1.2 Aptamers

With the discovery of catalytically active RNA molecules in 1980 it became apparent that oligonucleotides are capable of more functions than strictly information storage and messaging [72]. Aptamers comprise a class of functional, single stranded oligonucleotides, which bind a ligand with high affinity and specificity. In fact, the word aptamer comes from the latin term *aptus*- to fit [73]. Aptamers are obtained by applying a desired evolutionary pressure to a random pool of oligonucleotides in successive cycles to 'select' for functional oligonucleotides, this process is termed in vitro selection. There are two key properties of nucleic acids that make them excellent candidates for rational library screening: they are structurally diverse molecules and they are easily

replicated and amplified by standard enzymatic methods in vitro. Furthermore, nucleic acids sequence identity dictates the structure of the oligonucleotide, meaning the phenotype (structure) of a polymer is directly related to the genotype (sequence) of the polymer. This makes identification of functional oligonucleotides trivial using standard sequencing technologies. Aptamers and in vitro selection were originally discovered simultaneously by three independent research groups in 1990 [73] [74] [75]. Ellington et al. designed an in vitro selection scheme (Figure 1.10) to discover organic dye binding RNA molecules and coined the term aptamer. Gold and Tuerk selected an RNA molecule which binds to the bacteriophage T4 DNA polymerase enzyme and coined the term SELEX or, Systematic Evolution of Ligands by EXponential enrichment. Joyce and Robertson carried out the first in vitro selection for a catalytically active RNA molecule, termed a ribozyme, which specifically cleaved single stranded DNA. These discoveries demonstrate the versatility of nucleic acids as functional polymers and layed the groundwork for generating aptamers and nucleic acid enzymes.

It is virtually impossible to rationally design an aptamer or nucleic acid enzyme. A nucleic acid polymer of length $N$ may be represented by $4^N$ possible sequences since there are four nucleotides possible at each position in the oligonucleotide, A, C, G, and T/U. Thus, a DNA sequence of length 50, has $\approx 10^{30}$ possible sequence variants. Current computational limits preclude the ability to predict all possible structures and functional applications of sequence libraries so vast. It is for this reason that in vitro selection is such a powerful technique. By subjecting a library of single stranded oligonucleotides to a predetermined selection pressure such as the binding of a ligand, it is possible to sieve out and dispose of non-functional sequences, thereby enriching the minute subset of oligonucleotides which are capable of performing the desired function.

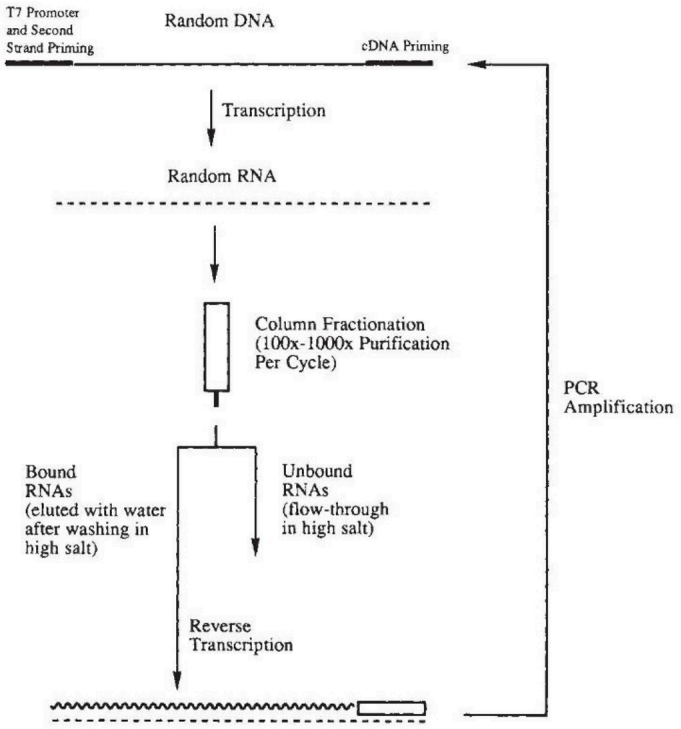


Figure 1.10: Schematic representation of the steps of an in vitro selection experiment. First, a DNA library with an internal random region flanked by primer binding domains, a T7 promoter region, and restriction sites for cloning, is synthesized using solid-phase DNA synthesis. This material is then transcribed using T7 RNA polymerase and standard reaction protocols. In the following step, which is the *selection* step of this procedure, the transcribed random RNA pool, typically consisting of $\approx 10^{15}$ unique molecules is exposed to the desired target ligand which is itself immobilized to a surface. During the selection step, multiple washing steps are performed to remove non-binding polymers. Finally, the binding molecules are eluted with low salt buffer, reverse transcribed into cDNA which is PCR amplified to generate a new and enriched random pool of oligonucleotide sequences, ready to repeat the cycle. Adapted from Ref. 73 with permission from Nature.

Through repetition and systematically increasing the selection pressure, or stringency, it is possible to obtain oligonucleotides with unprecedented functionality [76] [77] [78]. To date, thousands of aptamers with myriad ligand types ranging from single ions to whole cells have been successfully selected by employing some iteration of in vitro selection [79] [80]. Moreover, as mentioned above, catalytic chemical functionality has been selected in the selection of ribozymes and DNAzymes. Modern selections have employed chemically modified nucleobases in place of the native monomers, scaled selections to select for thousands of aptamers simultaneously in high throughput methods, employed high throughput sequencing technologies and have even been successfully performed for totally synthetic oligonucleotide analogues in particular L-nucleic acids [81] [82] [83] [84].

#### *1.1.2.1 L-Aptamers*

Aptamers comprised of L-nucleic acids were first discovered by Furste and coworkers in 1996 and termed spiegelmers [85] [86] [81]. Spiegel is German for mirror. L-nucleic acids are the enantiomers or mirror image of natural D-nucleic acids and their properties will be discussed in more detail in section 1.3.0.1 below. In order to select for an aptamer consisting entirely of L-RNA, a mirror-image in vitro selection was performed [87] [88]. The binding modality of L-aptamers utilizes the rule of reciprocal chiral substrate specificity [89]. For example, if an L-peptide binds to a natural D-oligonucleotide, then the enantiomeric D-peptide will bind the enantiomeric L-oligonucleotide. Conversely, this means that if a D-oligonucleotide binds an unnatural D-peptide, the same sequence L-oligonucleotide will bind the natural L-peptide identically. By exploiting this reciprocity, it is possible to perform in vitro selections using a native D-oligonucleotide library, which may be enzymatically amplified, against D-peptides to obtain a final L-oligonucleotide which binds the biologically relevant L-peptide target. Since their discovery, L-aptamers have been generated against a variety of targets including structured RNA elements [83]. L-nucleic acids are choice candidates for generating biostable aptamers since the stereospecificity of biological environments renders them immune to enzymatic degradation and off target binding interactions.

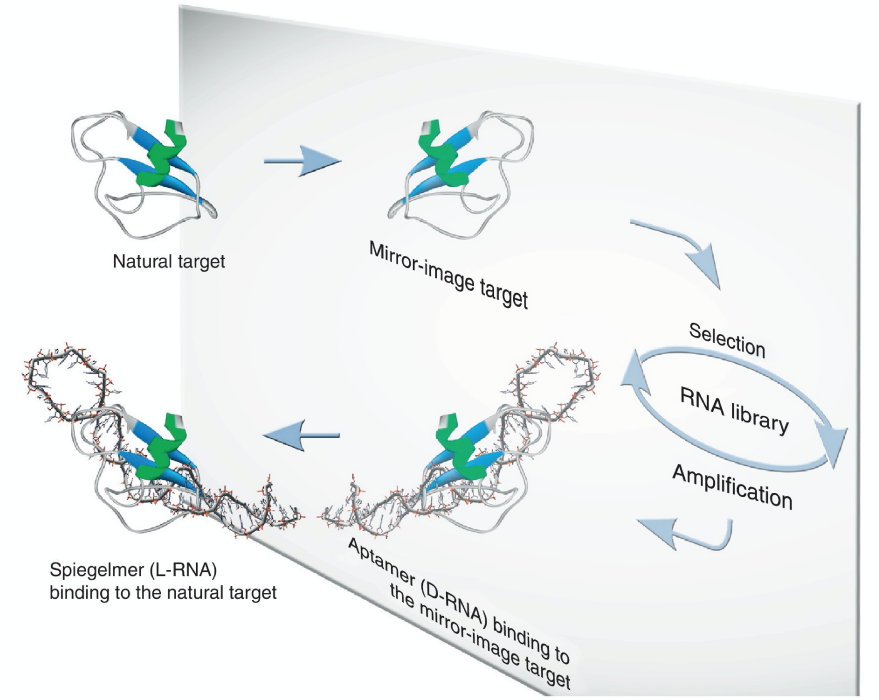


Figure 1.11: Cartoon representation of a mirror image selection scheme. The mirror-image target is used as the selection target in order to use natural D-oligonucleotide library which may be manipulated enzymatically for selection procedures Adapted from Ref. 87 with permission from Elsevier.

Significant effort has been put towards understanding and modeling nucleic acid tertiary structure [90] [91]. Despite this, a large void remains in predicting oligonucleotide structures [92]. However, there are examples of all variety of nucleic acid crystal structures including aptamers and nucleic acid enzymes. The earliest example of a high resolution crystal structure of an aptamer was reported by the Stockley lab in 1998 [93]. In this work, an RNA aptamer bound to its protein target, bacteriophage MS2 coat protein, was crystallized and diffracted with 2.8 angstrom resolution. (Something about what they were able to observe in that paper). Since then, aptamers and NAzymes bound to various target classes have been crystallized and countless new tertiary RNA/DNA structural motifs have been reported [94] [95]. Understanding the structure of aptamers is important in the rational design of selection libraries. If a particular sequence-structural element confers increased binding affinity for some class of targets, then a library may be designed with randomized regions flanking that element. In this way it is possible to use a shorter randomized region, shrinking the overall size of the initial pool, and increasing the chances of finding high affinity aptamers.

#### *1.1.2.2 Structure-switching Aptamers*

As mentioned before, because aptamers, ribozymes, and DNAzymes, are all composed of nucleic acids, they all must follow standard WC base pairing rules. As a result, all of these unique classes of oligonucleotide molecules may be directly integrated with all other DNA nanotechnologies. Structure-switching aptamers (Figure 1.11) are a class of aptamers which are initially restrained from folding into their active conformation by hybridization with a partially complementary strand [96] [97]. The strength of hybridization is calculated to be slightly less than the binding energy of the aptamer:ligand complex so that only in the presence of the ligand will the aptamer fold appropriately and releasing the locking strand, hence the name structure-switching. By employing a fluorescent aptamer or a fluorophore quencher pair in the restraining oligonucleotides, in a strategy like this, a biosensor is created. Furthermore, this strategy is amenable to general strand-displacement reactions whereby the unfolded aptamer acts as the incumbent strand

in a strand-displacement reaction, thus acting as a downstream sensor for strand-displacement circuits. There are numerous examples of structure-switching aptamers being integrated into logic circuits and detection schemes [98]. For example, Zhu et. al. designed a logic circuit in which the first toehold domain is blocked by a hybridized DNA aptamer, which upon binding a target small molecule unhybridizes, opening the toehold for circuit activation, thus converting a small molecule into a DNA logic output [99]. Furthermore, Wang and colleagues used a structure switching approach to trigger a fluorescent signal upon binding of a cell surface receptor and direct accumulation of a prodrug at the target tissue [100]. Fluorogenic aptamers have also been used for cellular localization studies as well as structure-switching strand displacement reactions for in vivo detection of microRNAs [101] [102]. Ribyzomes and DNAzymes likewise have been utilized in similar structure-switching strategies to develop biosensors for various targets of biological relevance [103] [104]. These examples further showcase the unique and vast versatility of oligonucleotides in biological chemistry. Chapter 4 will also discuss the applications of L-aptamers in heterochiral DNA nanotechnologies, in particular strand-displacement circuits.

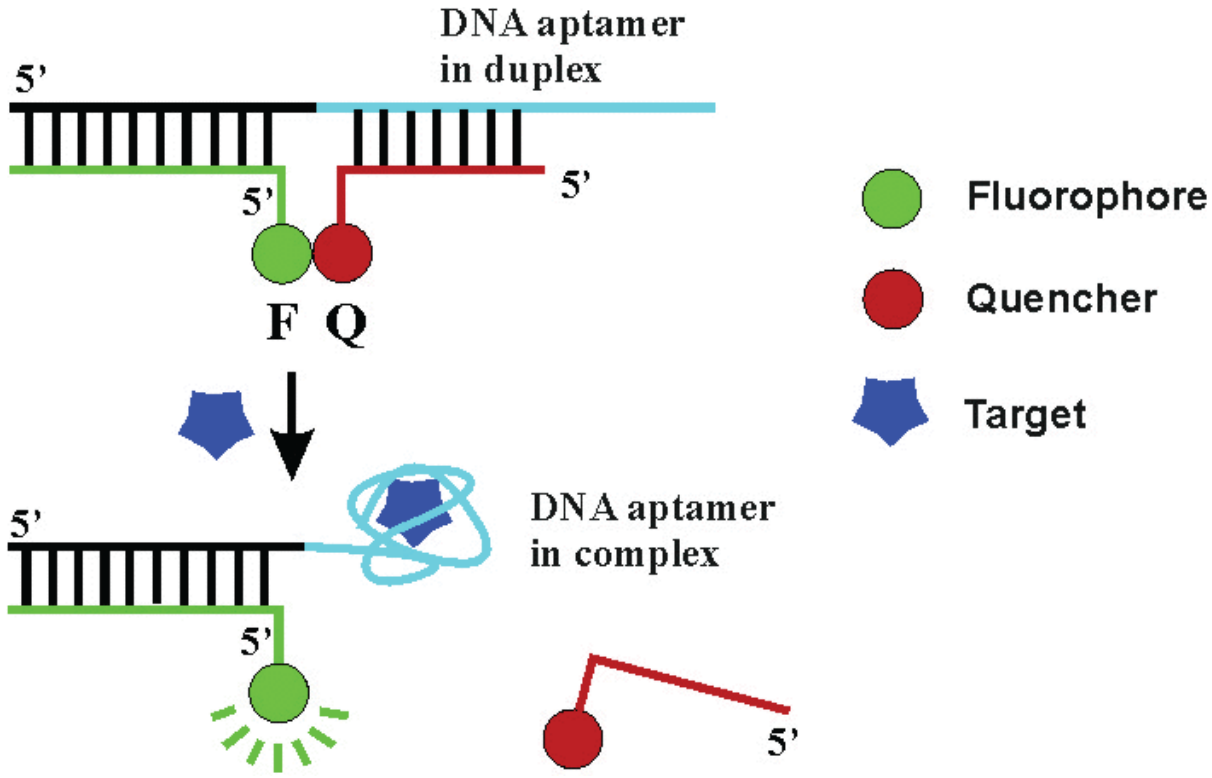


Figure 1.12: Cartoon representation of a structure switching biosensor. The DNA aptamer (cyan) binding domain is synthesized with additional 5′ sequence in order to construct a nicked duplex. The green and red strands are labeled with a 5′ fluorescent dye and 3′ quencher modification respectively. When hybridized to the aptamer sequence, the fluorophore and quencher are in close proximity of one another, effectively quenching the fluorescent signal of the dye. When the aptamer target molecule is introduced, the exposed aptamer binding domain begins to fold and bind the target. The base pairing between the aptamer and quencher strand is less energetically favorable than the aptamer:target complex, resulting in release of the quencher strand and concomitant activation of the fluorescent dye. Adapted from Ref. 96 with permission from ACS.

## 1.2 Nucleic acid synthesis

The commercialization of automated solid-phase oligonucleotide synthesis in the 1990's reshaped the landscape of nucleic acid chemistry and cell and molecular and synthetic biologies. This technology made available high quality, high fidelity, and large (>100 nt) oligonucleotides for standard research labs at an affordable price. Leading up to this, numerous synthetic strategies were attempted [105] [106]. In the early 1980's, the Caruthers lab developed phosphoramidite nucleoside monomers which became the standard oligonucleotide synthetic reagents [107]. Phosphoramidite monomers are relatively stable solids which, under proper conditions, may be stored for years prior to use (Figure 1.13). They have fast reaction kinetics and routinely generate consistent coupling yields of >98%. Synthesis occurs in the solid phase which is most commonly a chemically functionalized controlled pore glass (CPG) or polystyrene (PS).

The iterative nature of phosphoramidite chemistry allows to the inclusion of myriad oligonucleotide modifications at any position of the polymer, so long as the modification is amenable to the phosphoramidite method. A selection of such modificaitons will be discussed in the following section.

## 1.3 Nucleic acid modifications and analogues

Typically the goal of modifying nucleic acids is to increase the polymers stability against enzyme mediated degradation. The predominant types of modifications are backbone modifications, such as phosphorothioate, phosphoramidate morpholino, and phosphoroamidate linkages, as well as modifications at the $2'$ position of the deoxyribose sugar. Common types of $2'$ modifications include locked nucleic acids (LNAs), $2'$-O-Methyl, and $2'$ fluorine (Figure 1.13) [59] [108]. Although all of these modifications increase the stability against enzymatic degradation, most confer in increased cytotoxicity and immunogenicity in vivo relative to the native polymer. Furthermore, these modifications tend to effect the kinetics and thermodynamics of hybridization, requiring extensive post-modification testing to ensure the modified oligonucleotide functions as desired. These are substantial challenges which have greatly impeded the use of oligonucleotides as drugs. L-nucleic

| Name | Modification Type | Structure |
|---|---|---|
| dA-CE DNA Phosphoramidite | N/A | 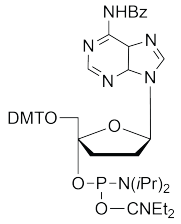 |
| LNA, 2′-O-Methyl | 2'-Hydroxyl | 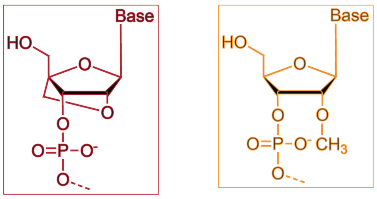 |
| Phosphoroamidate, Phophorothioate, Phosphoroamidate morpholino | Phosphate Backbone | 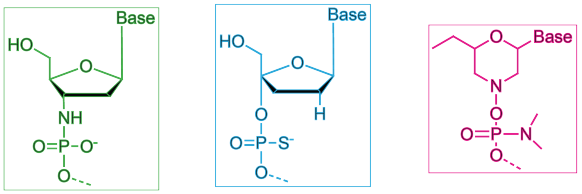 |

Figure 1.13: Structures of unmodified and various modified oligonucleotide monomers. The standard DNA (row 1) phosphoramidite used in solid-phase synthesis. This particular phosphoramidite is an adenine base. Examples of 2′-Hydroxyl modified oligonucleotides (row 2); locked nucleic acids (LNAs) are sterically constrained due to the methylene linker between carbon C4′ and the 2′ hydroxyl resulting in nuclease resistance and tighter WC basepairing. In row 3 are shown various phosphate backbone modifications which confer nuclease stability.

acids, the enantiomer of the natural D-nucleic acids, are an often overlooked oligonucleotide modification that we believe is a prime candidate for application in nucleic acid technologies. Subsection 1.3.0.1 details this modification.

Many non-base modifications of oligonucleotides are routinely employed in DNA synthesis. Fluorophore and quencher modifications have been used to develop molecular beacons as well as DNA circuit output signals (Figure 1.14). Linker modifications such as sulfur, azide, and biotin, discussed in the Aptamer section, have found ubiquitous application in various nucleic acid technologies. The ability to incorporate any phosphoramidite reagent into an oligonucleotide sequence routinely allows for infinite possible unique sequences to be easily synthesized, and together with the programmability of WC base pairing allows us to engineer any imaginable dynamic or static nucleic acid systems from these unique polymers.

#### *1.3.0.1 L-ONs as an optimal nucleic acid modificaiton*

In the following chapters, L-DNA will be the most commonly used oligonucleotide modification. The interplay of D- and L-DNA is the foundation of all heterochiral DNA nanotechnologies. The first example of L-DNA, the enantiomer of natural D-DNA, was reported by Gary Ashley in 1984 [109]. This is a unique modification in which the three chiral carbon centers of the (deoxy)ribose sugar have inverted L-stereochemistry, in contrast to the natural D-stereochemistry (Figure 1.15). Interestingly, no examples of L-DNA/RNA have been observed in nature to date and the reasons for this remain a hot topic of debate [110] [111] [112]. The enantiomeric monomers are prepared as phosphoramidites in exactly the same fashion as their D-counterparts. As a result, design and synthesis of oligonucleotides containing the L-enantiomer modification is straightforward. Enantiomers by definition exhibit identical physical properties. As a result, L-oligonucleotides retain identical solubility properties, hybridization kinetics, and duplex thermal stability to the D-enantiomer. As a result, any existing design principles established for D-DNA systems may be directly adapted to L-DNA based nanotechnologies. This greatly simplifies the optimization required when moving from an unmodified to a modified system as compared to the modifications

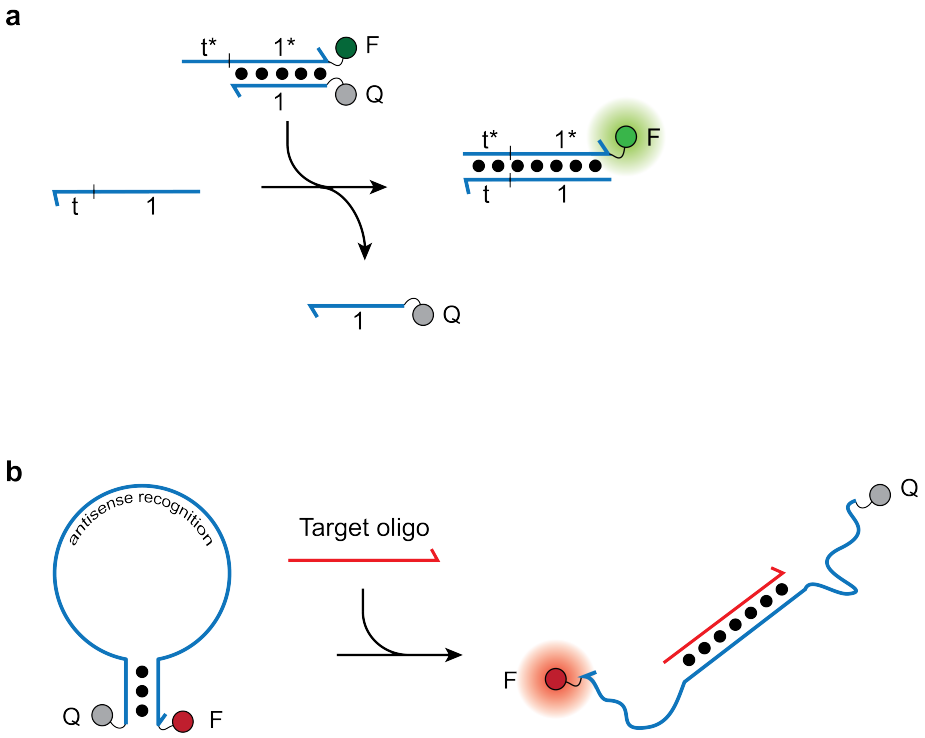


Figure 1.14: Examples of fluorophore-quencher pairs for the detection of nucleic acids. a) A strand displacement reaction wherein a pre-formed quenched duplex is activated by an input strand. The quencher strand is released through branch migration, allowing the fluorophore to fluoresce. b) Classic molecular beacon probe design. A short duplex region separated by a large unstructured antisense recognition region. When the target oligonucleotide hybridizes to the antisense region, the fluorophore and quencher are separated by the rigid recognition duplex, allowing the fluorphore to generate signal.

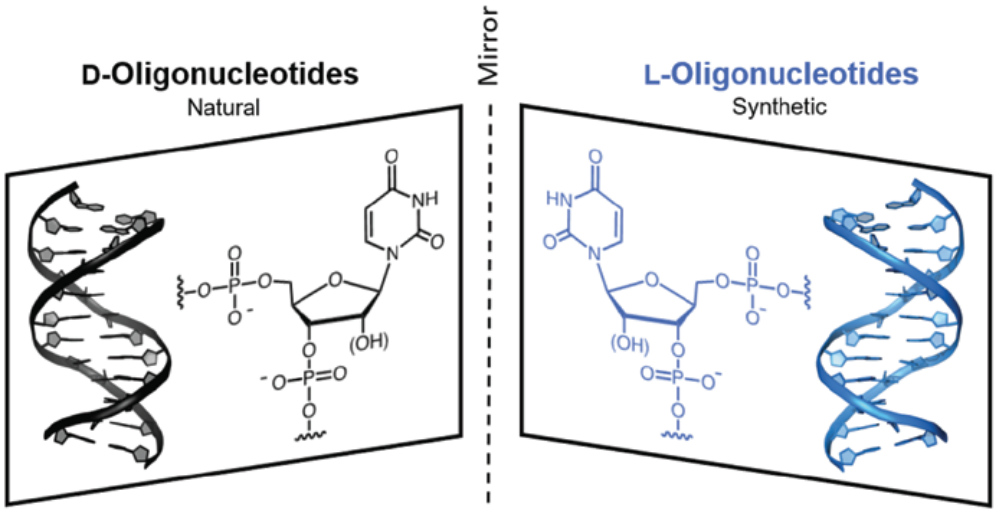


Figure 1.15: Comparison of D-DNA and L-DNA. D-DNA and D-RNA are the naturally occurring enantiomers shown in black on the left. L-DNA and L-RNA are the synthetic enantiomers of the natural counterparts, shown in blue to the right.

discussed above. This body of work centers around the integration of L-nucleic acids into contemporary DNA nanotechnolgy systems and to expand on these systems given the unique properties of these modified oligonucleotides.

#### *1.3.0.2 Peptide Nucleic Acid*

Peptide nucleic acids (PNAs) represent a unique class of backbone modified oligonucleotides. In place of the standard sugar-phosphodiester backbone of natural nucleic acids, PNA consists of an N2-aminoethyl-glycine peptide backbone, with the nitrogenous DNA base protruding from each repeating nitrogen atom in the backbone (Figure 1.16) [113] [114]. In addition to having no charge, the backbone of PNA is achiral. The steric dimensions of PNA almost exactly mimic those of DNA and RNA, allowing it to hybridize to other PNAs, DNAs, and RNAs following standard WC base pairing rules [115] [116]. The N-terminus and C-terminus of PNA are analogous to nucleic acids $5'$ and $3'$ ends respectively. PNA is capable of hybridizing to its complement as a homo-duplex in an antiparallel fashion similar to natural DNA as well as a parallel orientation. However, the lack of chirality in the backbone causes on average half of the duplexes to have a right hand twist and the other half to have a left hand twist.

Nielsen and colleagues initially synthesized this analogue in 1991 to generate an enzyme resistant polymer capable of hybridizing to native nucleic acids. The non-ionic and flexible nature of the backbone markedly increases the $T_m$ of PNA for complimentary nucleic acids (both DNA and RNA) when compared to all combinations of native nucleic acid duplexes. Furthermore, the neutral backbone makes the duplex stability of PNA homo- and hetero-duplexes independent of salt concentration. In 1998 Giesen et. al. reported a formula for predicting the thermal stability ($T_m$) of PNA/DNA heteroduplexes [117] [118]. Their model is a modified version of the previously reported nearest neighbor model which describes the duplex stability based on experimentally accessible thermodynamic terms [27] [29]. The thermodynamic terms considered in this model are the standard enthalpy and entropy of adjacent bases in a particular sequence. Giesen et al extends this model by using thermodynamically accessible terms for the bases in a PNA polymer changing the equation from:

$$T_m(\text{calc}) = \frac{\Sigma\Delta H^0}{R \times ln(\frac{C_t}{n}) + \Sigma\Delta S^0}$$

to:

$$T_m pred = c_0 + c_1 \times T_m nnDNA + c_2 \times f_{pyr} + c_3 \times \text{length}$$

This work has made designing PNA/DNA and PNA/RNA duplexes with precise hybridizaiton enthalpy values possible. Furthermore, PNA is synthesized using standard FMOC peptide synthesis methods [119]. Consequently, it is straightforward to synthesize countless desired PNAs with any modifications available for FMOC chemistry. Together these qualities make PNA an obvious candidate for integration with DNA strand-displacement reactions.

Despite these promising qualities, PNAs have two critical drawbacks; 1) solubility, especially as polymer length and number of purines increases; and 2) synthetic limits in tandem with solubility issues restrict polymer length to <40 bases. As a result, PNA is only capable of being integrated with DNA nanotechnologies that utilize shorter sequences. Most prominently, PNAs have been used in oligonucleotide delivery, antisense applications, and strand- displacement reactions [120] [121] [122].

As mentioned above, PNA is an oligonucleotide analogue with no inherent chirality. As a result of this, PNAs are capable of WC hybridization with oligonucleotides of either D- or L-stereochemistry [123]. In Chapter 4 I will detail how this unique property is exploited in order to design heterochiral strand displacement reactions. This observation bridges the gap in heterochiral sequence information transfer that had stood since L-oligonucleotides were first reported.

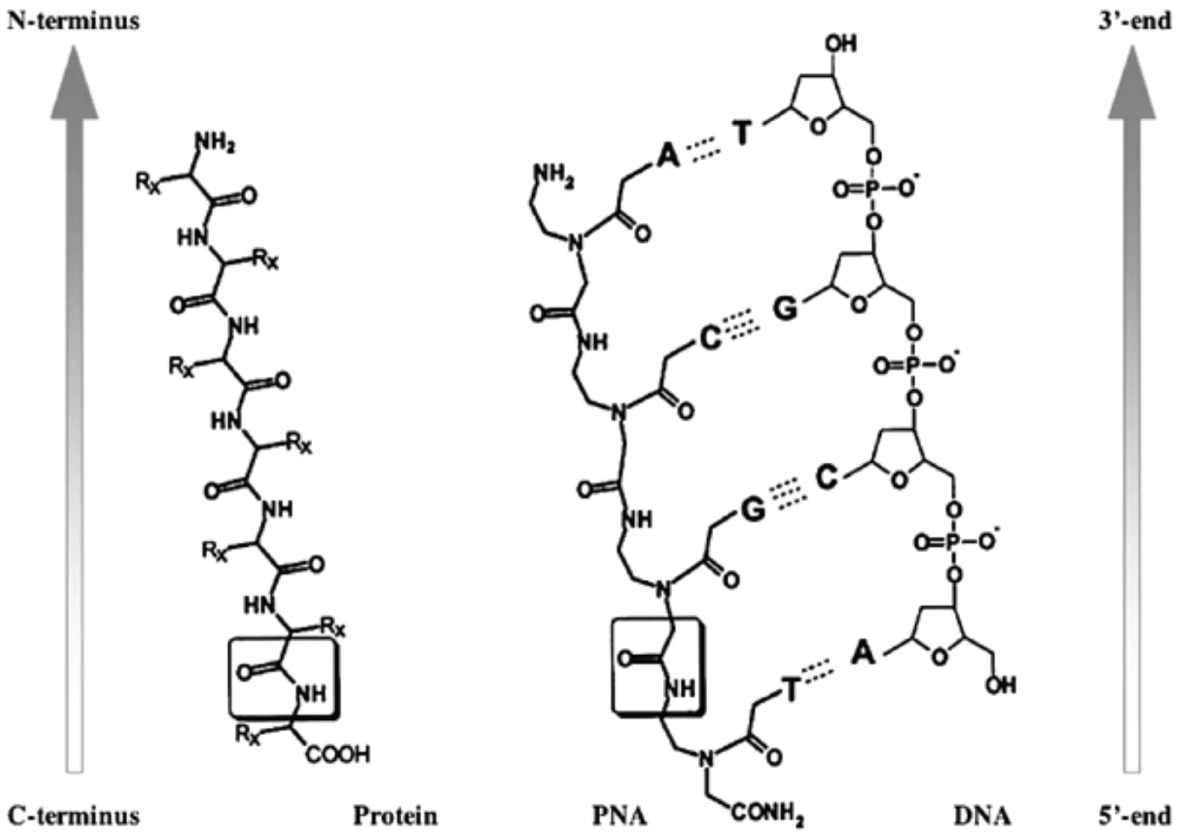


Figure 1.16: Comparison of DNA and PNA atomic structures. The PNA backbone is composed of 2-aminoethly glycine linkages in place of the natural phosphodiester backbone with the nucleotide base protruding from the amino nitrogen via a methylene carbonyl tether. The amide bond characteristic of both PNA and peptides is boxed in. PNAs are described using peptide conventions. The N-terminus is analogous to a DNA 5′ end and the C-terminus is analogous to a DNA 3′ end. PNA is capable of hybridizing to DNA in both a parallel and antiparallel fashion, however the preferred anti-parallel orientation is shown here. Adapted from Ref. 113 with permission from Springer.

## 1.4 Goal of this research

DNA nanotechnologies have proven to be versatile and applicable tools in biological chemistry as well as molecular, cell and synthetic biology both in vitro and in vivo. However, despite the great efforts put forth towards developing stable and low background systems through the use of modified nucleic acids, the issues of off target hybridization, protein binding and enzyme mediated degradation remain at the forefront of challenges facing the integration of such technologies in living systems. It is the goal of this body of work to attempt to reshape the landscape of DNA nanotechnology by looking through the chemical mirror at a novel class of nucleic acid modifications, L-oligonucleotides. L-ONs biostability, minimal off target interaction with native biomolecules and identical physical properties to the native enantiomer, make them a prime candidate for in vivo applications of DNA nanotechnology.

To this end, in Chapter 2 we discuss a new class of RNA binding L-aptamers by selecting the first chemically modified L-RNA aptamer which binds precursor-miR-19a, inhibiting its Dicer mediated biogenesis to miR-19a [124]. In Chapter 3, we present a novel high-throughput screening methodology which exploits the specific binding characteristics of L-aptamers for structured D-RNA targets in order to screen for small molecules with specific RNA binding properties. Together these two chapters represent a contribution to the fundamental understanding of tertiary structural interactions between nucleic acids of opposing chirality. In the first half of Chapter 4 we present a new biochemical reaction termed heterochiral strand-displacement [125]. This work generalizes the expansion of all existing DNA nanotechnologies onto an L-nucleic acid platform. Building from this work, the second half of Chapter 4 introduces a direct application of the heterochiral strand-displacement reaction in the design of an L-DNA based nucleic acid circuit [126].

As a whole, the work presented herein represents a new perspective to approaching mainstream DNA nanotechnology and establishes L-nucleic acids as premier alternatives to the classic oligonucleotide modifications employed in the last fifty years.

# 2. A CHEMICALLY MODIFIED L-RNA APTAMER*

The functions of RNAs often depend on their specific secondary and tertiary structures, which can serve as important recognition elements mediating RNA-RNA and RNA-protein interactions. RNA structures also play critical roles in a variety of diseases, including viral infections, neurological disorders, and cancer [127] [128] [129]. As a result, there is significant interest in the development of reagents that selectively target RNAs. Such reagents could advance the development of new tools to study RNA function and therapeutics to treat RNA-mediated diseases. However, the discovery of molecules that are capable of binding RNA structures with high affinity and specificity has proven challenging when using current approaches. Targeting RNA by using small molecules, for example, is often hampered by poor selectivity as a result of the negatively charged backbone and structural redundancy of RNA [130] [131]. In addition, RNAs with extensive secondary structures are often inaccessible to traditional hybridization-based reagents, which also suffer from significant off-target effects [132] [133]. Therefore, novel strategies for targeting structured RNAs are needed.

Aptamers are adept at binding targets with high specificity and affinity, however, they are typically unsuited for binding other oligonucleotides for numerous reasons. D-aptamers selected against ON targets typically utilize base-pairing to recognize and bind their intended target. This is due to the fact that base-pairing is a very stable form of ON interaction. However, this precludes the ability to select for D-aptamers which bind through tertiary interactions with their target because complimentary ONs will always win a selection. Additionally, aptamers consisting of D-nucleic acids are prone to nuclease degradation, off-target hybridization, and other nonspecific interactions with various cellular entities. The poor biostability and specificity of D-aptamers in cells essentially precludes the possibility of employing aptamers as drugs for cellular targets. The current state of the art method for applying D-aptamers in cellular contexts is to either utilize a

*Reprinted with permission from "An L-RNA aptamer with expanded chemical functionality that inhibits microRNA biogenesis" by Adam M. Kabza and Jonathan T. Sczepanski, 2017. *ChemBioChem.*, 18, pp. 1824-1827, 2017.

chemically modified library containing a modification which imparts nuclease stability, or to systematically chemically modify a selected aptamer in such a way as to retain target affinity and specificity while increasing stability. Despite the availability of such technologies, all D-aptamers, regardless of what chemical modifications are present on them, are capable of Watson-Crick base-pairing with ONs of the same stereochemistry. In order to select an aptamer capable of specifically binding a natively expressed ON target with minimal off-target effects and high biostability, a different sort of chemical modification must be utilized. One modification that stands out for overcoming these problems is L-DNA, the stereoisomer of natural D-DNA. As described in the introduction, L-nucleic acids solve nearly all of the issues plaguing current state of the art aptamer technologies. In 2013 Sczepanski et. al. published the first L-aptamer which binds a D-RNA target, the trans-activation response element of HIV or TAR element [83]. This was accomplished by designing and utilizing a peculiar selection scheme, mirror-image SELEX. Figure 2.1 depicts a cartoon representation of a mirror image selection.

To facilitate isolation of L-aptamers with novel RNA-binding properties, we employed a cationic nucleotide, 5-aminoallyl-uridine, during the mirror image in vitro selection process. Through this effort, we identified a modified L-RNA aptamer (MLRA) capable of binding oncogenic precursor microRNA-19a (pre-miR-19a) with exceptional affinity, and we showed that cationic modification is absolutely critical for binding. Furthermore, formation of the MLRA-pre-miR-19a complex inhibited Dicer-mediated cleavage of the pre-miR, thus blocking formation of the mature functional microRNA. The MLRA reported here not only represents the first L-aptamer to be evolved by using modified nucleotides but also the first modified aptamer (of any type) to be selected against a structured RNA target. Our results demonstrate that functionalized L-aptamers, which are intrinsically nuclease-resistant, provide an attractive approach for developing robust RNA-binding reagents. In this chapter we advance mirror image selection technology into the next generation by employing a chemical modification in one RNA base, uridine. Specifically, we utilize a 5 aminoallyl uridine nucleotide as a chemically modified nucleobase in order to select a chemically modified L-aptamer with novel binding properties against a naturally occurring D-RNA hairpin,

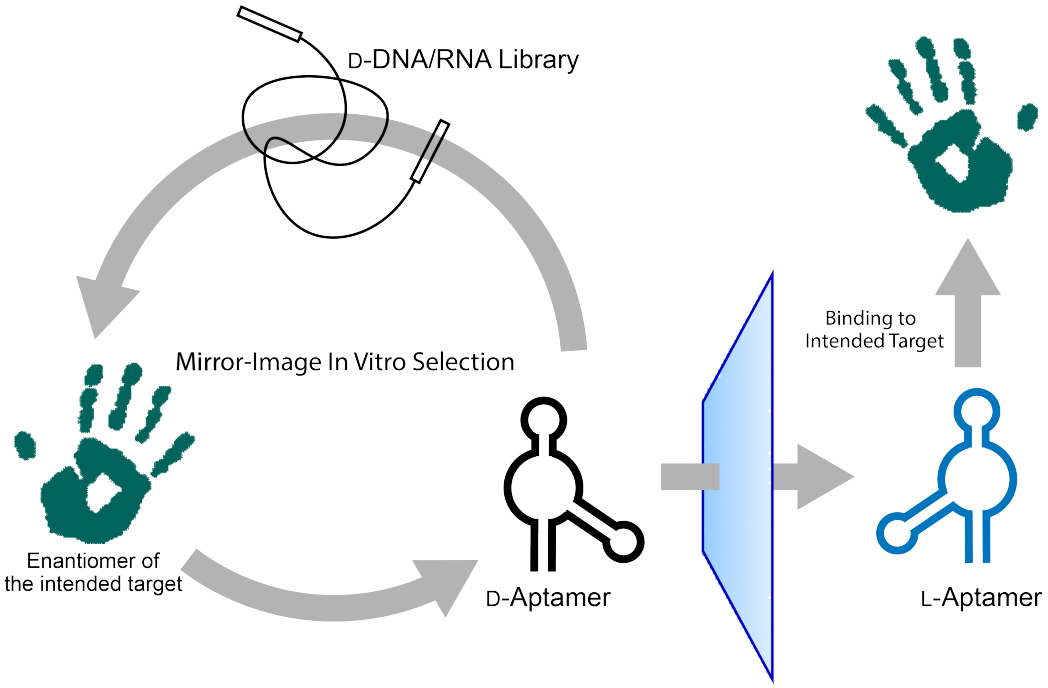


Figure 2.1: Cartoon illustration of a mirror-image selection scheme. First a D-Aptamer is selected against the L-RNA version of the naturally occuring D-RNA. Upon completion of the selection procedure, an L-stereochemistry version of the selected aptamer is chemically synthesized which binds the natural D-RNA target as intended. Adapted from Ref. 124 with permission from Wiley.

precursor microRNA-19a.

## 2.1 Results

Previous studies have shown that L-aptamers are capable of selectively binding pre-miR hairpins, thereby inhibiting production of the mature miR [134]. Motivated by these findings, we chose pre-miR-19a as the initial target for developing an MLRA (Figure 2.2a). MiR-19a is a member of the oncogenic miR-17/92 cluster, and its upregulation has been shown to promote proliferation of both bladder and prostate cancer cells [135] [136] [137]. Thus, identification of reagents that inhibit miR-19a biogenesis could provide a viable approach to treat these diseases.

In order to obtain an MLRA capable of binding pre-miR-19a, we carried out a mirror image in vitro selection experiment employing an L-RNA version of the pre-miR-19a hairpin that was biotinylated at its 3′-end (Figure 2.3, Figure A.1) [85]. The starting pool of modified D-RNA (Figure A.3) was prepared by T7 RNA polymerase transcription, employing 5-aminoallyl-UTP in place of UTP. This modification was previously shown to be compatible with standard in vitro selection methods and facilitates interactions between aptamers and negatively charged ligands [137] [138]. The selection experiment was initiated by mixing the modified RNA pool ( $10^{14}$ unique molecules) together with L-pre-miR-19a in a reaction mixture containing 5 mM $MgCl_2$, 20 mM NaCl, 50 mM KCl, 0.1% Tween 20, and 25 mM Tris (pH 7.6). D-RNAs that bound that bound L-pre-miR-19a were captured on streptavidin coated magnetic beads, which were subsequently washed with the binding solution. D-RNAs that remained bound throughout the washing procedure were eluted with NaOH, reverse-transcribed, and amplified by PCR. The resulting DNA was used to transcribe a new pool of modified D-RNA to begin the next round of in vitro selection. The selection pressure was gradually increased over successive rounds by reducing the concentration of both the modified D-RNA library and L-pre-miR target, and the duration of the washing periods was also gradually increased (Figure 2.4, Figure A.2). Following round 5, the binding and washing steps were carried out under simulated physiological conditions (1 mM $MgCl_2$, 20 mM NaCl, 50 mM KCl, 25 mM Tris pH 7.6, 37 °C) to encourage isolation of aptamers that could function within a biological context. After 11 rounds of selection, the enriched RNA pool was cloned and sequenced

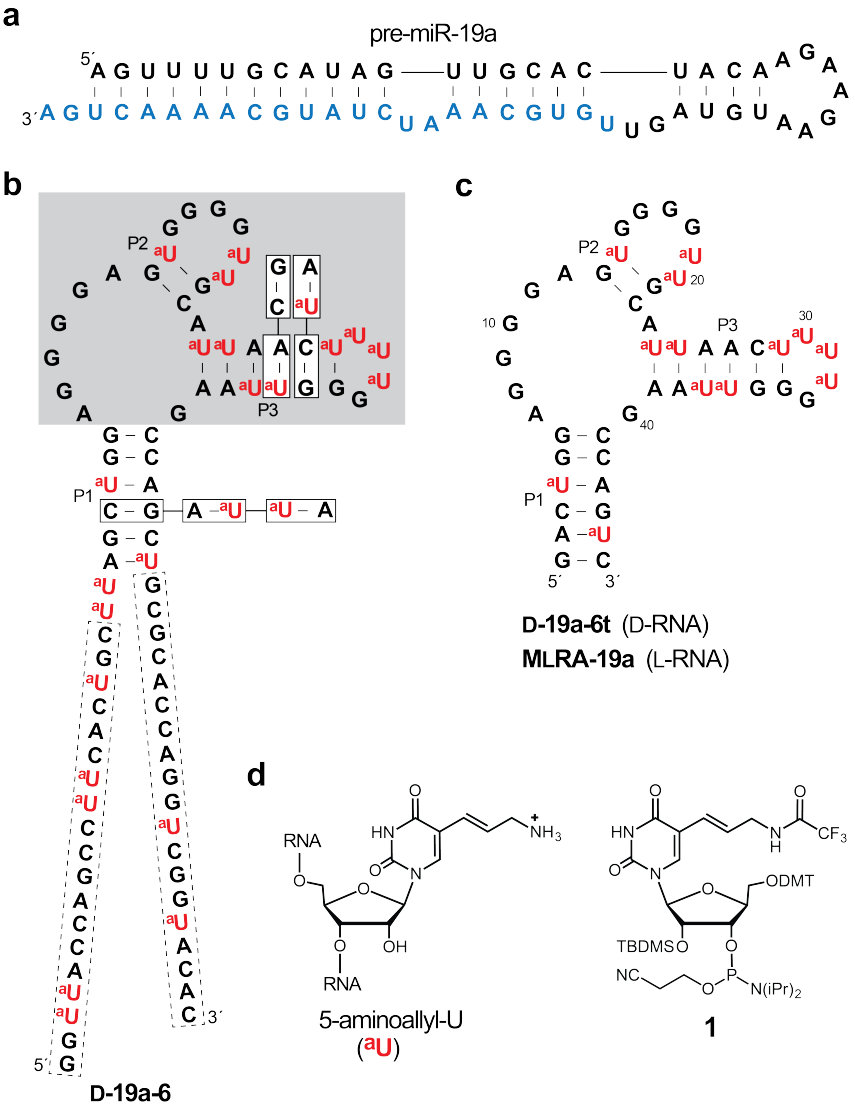


Figure 2.2: Sequence and secondary structure of pre-miR-19a and corresponding aptamers. A) Full-length pre-miR19a (blue sequence indicates mature miR-19a-3p). B) Clone D-19a-6, with the primer-binding sequences in boxes (...). The shaded area indicates the region of high sequence conservation following the reselection experiment, and compensatory base pair covariations are indicated. C) Truncated aptamers D-19a-6t (D-RNA) and MLRA-19a (L-RNA). D) The 5-aminoallyl-uridine ($^{a}$U) modification and the corresponding L-nucleoside phosphoramidite (1) employed in this work. Adapted from Ref. 124 with permission from Wiley.

(Figure 2.5).

Several unique clones were analyzed for binding L-pre-miR-19a by using an electrophoretic mobility shift assay (EMSA). Of the five clones tested, D-19a-6 (Figure 2.2b) had the lowest apparent $K_d$ value (<1 nM). Thus, all further studies were based on this clone. A succession of 3′ and 5′ truncations of D-19a-6 revealed that as many as 20 nt could be removed from both ends, indicating the primer-binding sites were unnecessary for binding.

To further determine the nucleotides of D-19a-6 that were critical for binding L-pre-miR-19a, the original random sequence domain of D-19a-6 was mutated to yield a population wherein all possible sequences carrying seven mutations or less were represented. This library was subjected to three additional rounds of in vitro selection against L-pre-miR-19a, and the final enriched pool of RNA was cloned and sequenced (Figure A.3b). Alignment of the sequence variants revealed a highly conserved region within the central portion of the mutated domain, which strongly suggests these residues are critical for ligand binding (Figure 2.2b). In contrast, the flanking segments were highly variable, indicating that base pairs within the proposed P1 stem were interchangeable. Together, these observations were used to design a minimal aptamer, D-19a-6t, that contained 46 nt (Figure 2.2c). D-19a-6t binds L-pre-miR-19a with a $K_d$ value of 0.72 nM under physiological conditions and in the presence of excess tRNA (Figure 2.3). Importantly, a version of D-19a-6t containing uridine (U) rather than $^{a}$U was unable to bind L-pre-miR-19a, demonstrating the aptamer's dependence on this cationic modification (Figure 2.4a/b M0, Figure A.6).

To investigate which $^{a}$U residues are essential for binding of L-pre-miR-19a, we systematically replaced various $^{a}$U residues with cytidine (C), being sure to retain base pairing where appropriate (Figure 2.4a). Although not an ideal substitution, this strategy enabled D-19a-6t variants to be easily synthesized by in vitro transcription. Substitutions with U or a more closely related analogue would have required an extensive synthetic effort. Replacement of $^{a}$U14, $^{a}$U19, $^{a}$U20, and $^{a}$U29-$^{a}$U32 with C (M2-M7) significantly reduced the affinity of D-19a-6t for L-pre-miR-19a (Figure 2.5b), thus suggesting that these residues are critical for binding. In contrast, replacing $^{a}$U24/A39, $^{a}$U25/A38, $^{a}$U36/A27, and $^{a}$U37/A26 base pairs within the P33 stem (M8 and M9)

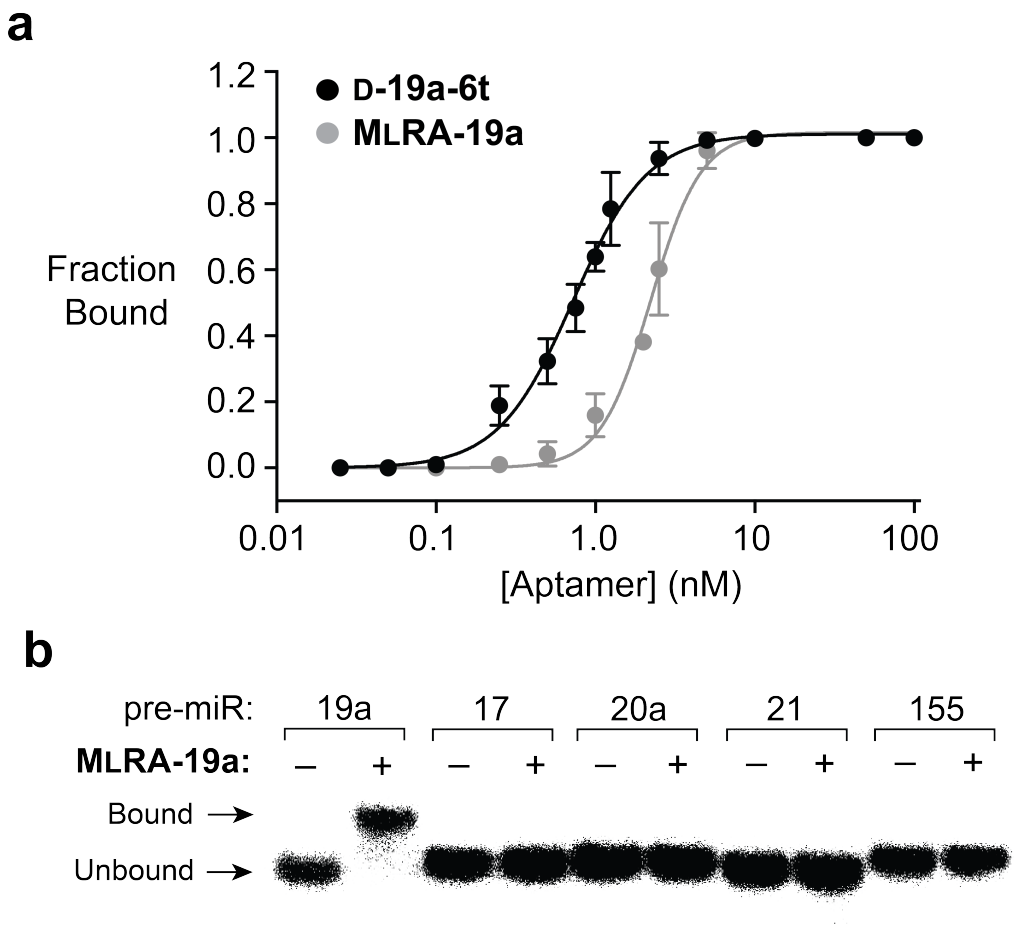


Figure 2.3: Binding affinity and specificity of aptamer-pre-miR-19a complexes. A) Saturation plot for binding of either D-19a-6t or MLRA-19a to L- or D-pre-miR-19a, respectively. B) EMSA demonstrating the specificity of MLRA-19a for pre-miR-19a. All mixtures contained 0.05 nM [5′-$^{32}$P]-labeled pre-miR, 10 nM MLRA-19a, 1 mM $MgCl_2$, 150 mM KCl, 20 mM NaCl, at pH 7.6 and 37°C. Adapted from Ref. 124 with permission from Wiley.

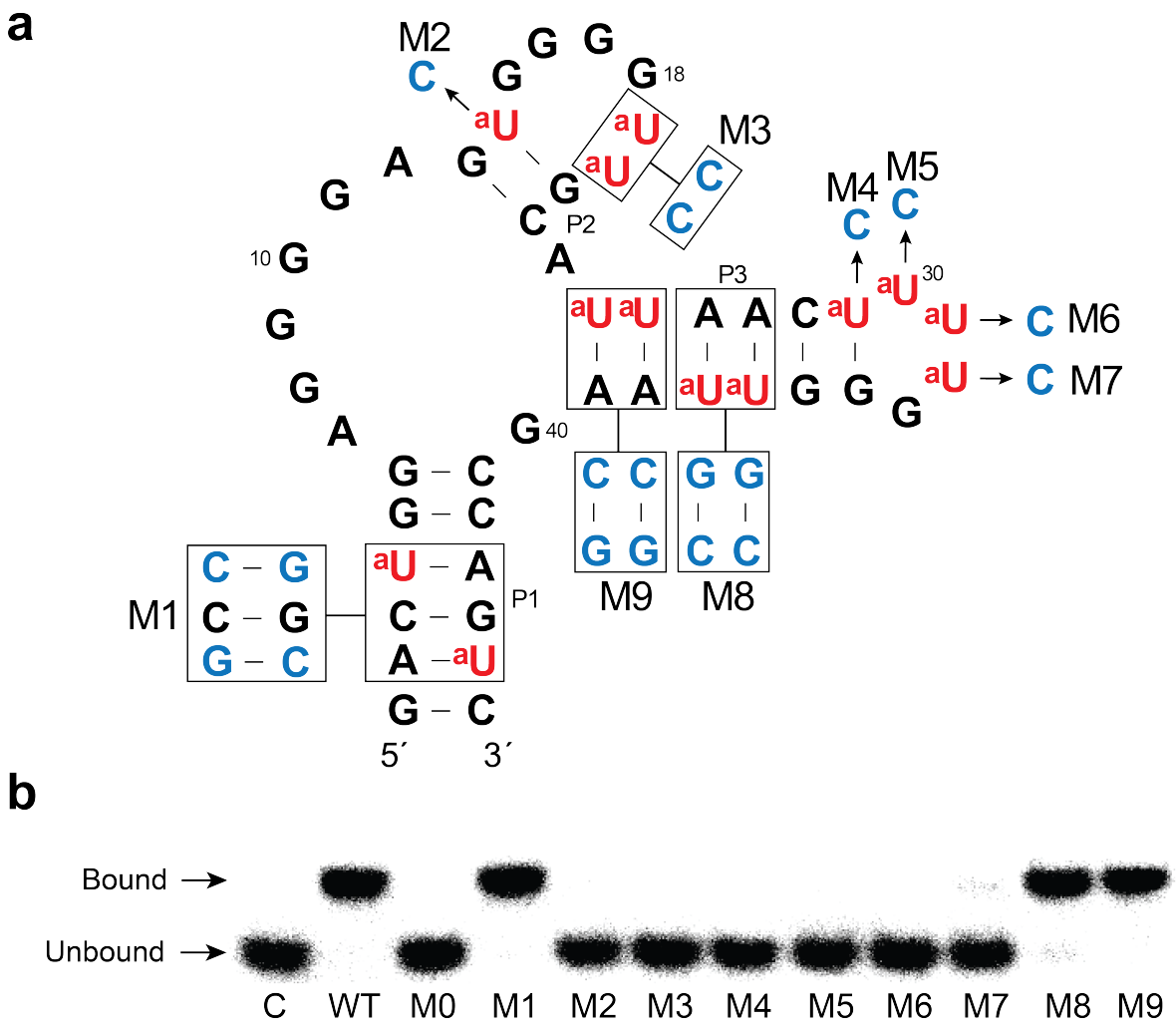


Figure 2.4: Mutational analysis of D-19a-6t. A) Mutations introduced into D-19a-6t (M0-M9). M0 is D-19a-6t containing uridines rather than $^{a}$U. B) EMSA used to reveal the effects of the mutations described in A. All mixtures contained 0.05 nM[5′-$^{32}$P]-labeled L-pre-miR-19a, 10 nM of the indicated mutant aptamer, 1 mM MgCl2, 150 mM NaCl, at pH 7.6 and 37 °C. Adapted from Ref. 124 with permission from Wiley.

and $^{a}$U4/A43, and $^{a}$U45/A2 base pairs within the P1 stem (M1) with cytidine or guanosine had no influence on binding. This suggests that the primary role of both stems is structural, and the cationic functional groups are dispensable. These observations were consistent with compensatory base pair covariations identified at several positions within the P1 and P3 stems following the reselection experiments (Figure A.4a).

We next prepared an L-RNA version of 19a-6t by solid-phase RNA synthesis (Figure A.7). The $^{a}$U modification was incorporated by using phosphoramidite 1 (Figure 2.2d), which was obtained from a commercial source. The resulting modified L-RNA aptamer, MLRA-19a, bound the native D-pre-miR-19a hairpin with a $K_d$ value of 2.2 nM under physiologically relevant conditions (1 mM $MgCl_2$, 20 mM NaCl, 150 mM KCl, 25 mM Tris pH 7.6, 37 °C, Figure 2.3a). This interaction is slightly weaker than what was determined for the D-19a-6t:L-pre-miR-19a complex ($K_d$ = 0.72 nM), which reflected the somewhat lower quality of synthetic L-RNA compared to D-RNA that is prepared enzymatically [134]. Nevertheless, binding of pre-miR-19a by MLRA-19a represented one of the tightest interactions between an aptamer and a structured D-RNA target reported to date, irrespective of stereochemistry. Given that the majority of previously reported RNA-binding aptamers utilize WC pairing, the exceptional affinity of MLRA-19a for pre-miR-19a demonstrates that merging heterochiral recoginition with cationic modifications facilitates discovery of nucleic acid interactions that are potentially superior to what can be achieved through hybridization alone [139]. No binding was observed between MLRA-19a and several non-cognate pre-miRs (Figure 2.3b), including two other members of the miR-17/92 cluster (pre-miR-17 and pre-miR-20a).

To gain insight into the region of binding of MLRA-19a to pre-miR-19a, we performed an in-line probing analysis of the pre-miR in the presence and absence of MLRA-19a (Figure 2.5) [140]. Several nucleotides within the loop domain of pre-miR-19a underwent a significant conformational change in the presence of excess MLRA-19a, as evidenced by either an increase or decrease in hydrolytic cleavage compared to pre-miR-19a alone. These data strongly suggest that MLRA-19a binds the pre-miR primarily through nucleotides in the loop domain.

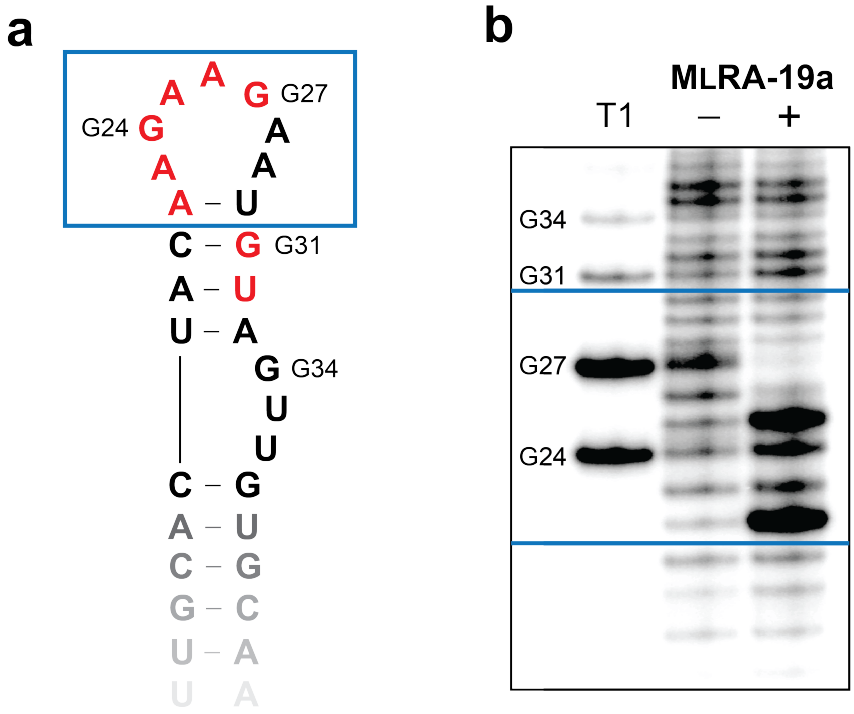


Figure 2.5: In-line probing analysis of pre-miR-19a in the presence and absence of MLRA-19a. A) Distal loop domain of pre-miR-19a, with loop nucleotides in boxes (blue line). Residues that underwent a significant conformational change in the presence of excess MLRA-19a during the in-line probing assay are colored red. B) PAGE analysis and autoradiography of [5′-$^{32}$P]-labeled pre-miR-19a after the in-line probing assay. Area between the blue lines indicates the loop domain boxed in A. Partial digest by ribonuclease T1 (cleaved after G residue) is shown to the left (T1). Adapted from Ref. 124 with permission from Wiley.

Consistent with these findings, MLRA-19a also bound sever other short D-RNA hairpins, as long as they retained the distal loop associated with pre-miR-19a (Figure A.8). In contrast, MLRA-19a poorly bound a version of pre-miR-19a in which the distal loop was replaced by a generic tetraloop (5′-GAAA-3′, Figure A.8).

On the basis of its binding to the loop domain of pre-miR-19a, we anticipated that MLRA-19a would inhibit Dicer-mediated cleavage of the pre-miR into mature miR-19a. To test this, pre-miR-19a was incubated in the presence of human Dicer, together with various concentrations of MLRA-19a under physiologically relevant reaction conditions. MLRA-19a was found to inhibit pre-miR-19a processing in a concentration-dependent manner and nearly completely blocked Dicer-mediated cleavage at concentrations greater than 25 nM (Figure 2.6). The $IC_{50}$ value for this inhibition was 4 nM (Figure 2.6), which was at least 20-fold lower than all previously reported pre-miR-bound (unmodified) L-aptamers measured under similar conditions [83]. As expected, MLRA-19a had no significant effect on Dicer-mediated cleavage of pre-miR-21, demonstrating the specificity of this reagent (Figure 2.6c).

In summary, we have identified and characterized a modified L-RNA aptamer (MLRA-19a) capable of binding oncogenic pre-miR-19a with high affinity and specificity, and we showed that the cationic modification, 5-aminoallyl-uridine, is absolutely critical for binding. MLRA-19a is not only the first L-aptamer to be evolved by using odified nucleotides during the in vitro selection process but also the first modified aptamer (of any type) to be selected against a structured RNA target. This approach opens a route to precise targeting of a wide range of structured RNAs, thus addressing a long-standing challenge in RNA biochemistry and drug discovery [141].

Furthermore, our results suggested that L-aptamers, like their native counterparts, benefit from an expanded chemical repertoire. In the future, it will be important to screen additional modified nucleotides during the in vitro selection process in order to identify those functional groups most apt for RNA binding. Importantly, we showed that MLRA-19a inhibited Dicer-mediated processing of pre-miR-19a, which demonstrates the ability of MLRAs to modulate RNA function and provides impetus for future development of RNA-targeted MLRA therapeutics.

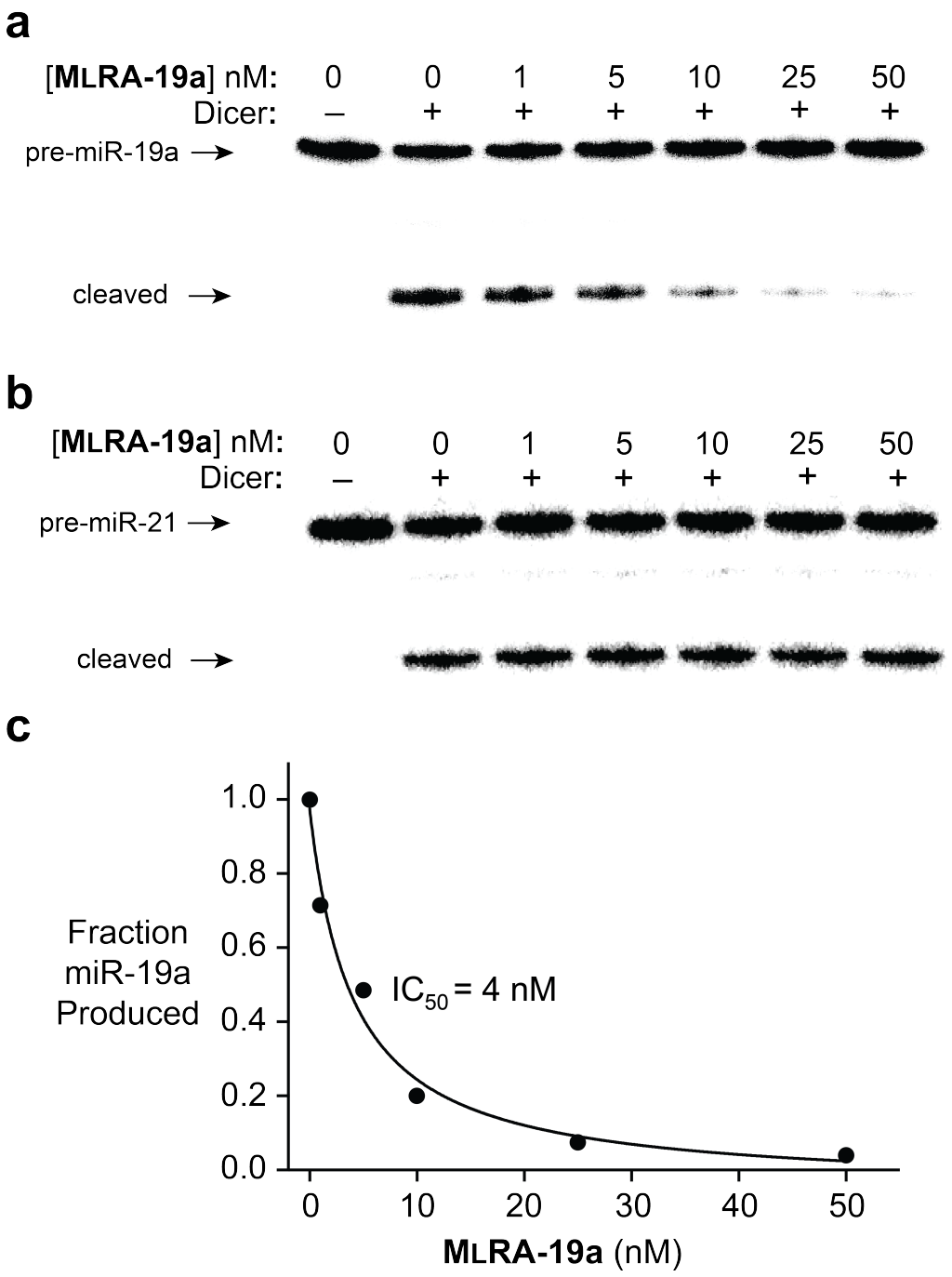


Figure 2.6: Inhibition of Dicer-mediated processing of pre-miR-19a by MLRA-19a. Autoradiograms of either A) [5′-$^{32}$P]-labeled pre-miR-19a or B)[5′-$^{32}$P]-labeled pre-miR-21 processing by human Dicer in the presence of MLRA-19a. Radioactvie pre-miR was incubated for 15 min with Dicer (5 nM) in the presence of varios concentrations of MLRA-19a. C) $IC_{50}$ value of MLRA-19a for inhibition of pre-miR-19a cleavage in A. Adapted from Ref. 124 with permission from Wiley.

## 2.2 Materials and Methods

### 2.2.1 Materials.

Oligonucleotides were either purchased from Integrated DNA Technologies (Coral-ville, IA) or prepared by solid-phase synthesis on an Expedite 8909 DNA/RNA synthesizer. Synthesizer reagents and D-nucleoside phosphoramidites were purchased from Glen Research (Sterling, Va). D-5-aminoallyl-UTP used in in vitro transcription reactions was purchased from ThermoFisher Scientific (Waltham, MA). L-nucleoside phosphoramidites, including the specialty phosphoramidite L-5-aminoallyl-UTP, were purchased from ChemGenes (Wilmington, MA). For coupling of degenerate nucleotides (N), the four nucleoside phosphoramidites were mixed at a concentration ratio of 3.0:2.0:2.3:2.5 for A:T:G:C respectively, to achieve equivalent coupling efficiencies. All oligonucleotides were purified by polyacrylamide gel electrophoresis (PAGE) and desalted by ethanol precipitation. Histidinetagged T7 RNA polymerase was purified from E. coli strain BL21 containing plasmid pBH161 (provided by Gerald Joyce, The Salk Institute for Biological Studies). Thermus aquaticus (Taq) DNA polymerase was prepared as described previously [142]. Superscript II reverse transcriptase and streptavidin coated magnetic beads (MyOne Streptavidin C1 Dynabeads) were purchased from Life Technologies (Carlsbad, CA). [$\gamma^{32}$P]ATP was purchased from Perkin Elmer (Waltham, MA) and dNTPs were purchased from Sigma Aldrich (St. Louis, MO). Mass spectrometry analysis was performed by Novatia LLC (Newtown, PA).

### 2.2.2 RNA library preparation

. A dsDNA library was generated from a templated extension of 1.5 nmol reverse primer (R1) on 1 nmol of template (Lib1). The reaction was performed in a 1 mL volume for 45 minutes at 42°C containing 8 U/$\mu$L Superscript II reverse transcriptase, 3 mM $MgCl_2$, 75 mM KCl, 10 mM DTT, 50 mM Tris (pH 8.3), and 0.5 mM each of the four dNTPs. The products of the extension reaction were ethanol precipitated and resuspended in 45 $\mu$Lultrapure water. This DNA was added directly into a 100 $\mu$L transcription reaction containing 10 U/$\mu$L T7 RNA polymerase, 0.001 U/$\mu$L

Inorganic pyrophosphatase (IPP), 25 mM $MgCl_2$, 2 mM spermidine, 10 mM DTT, 40 mM Tris (pH 7.9), and 5 mM of each of the four NTPs, where UTP was replaced with 5-aminoallyl-UTP. The reaction mixture was incubated at 37 °C for 2 hours, concentrated by ethanol precipitation, and purified by denaturing polyacrylamide gel electrophoresis (PAGE). The product (RNA Lib1, Figure A.3a) was eluted overnight at room temperature in buffer containing 200 mM NaCl, 10 mM EDTA, and 10 mM Tris (pH 7.5).

### 2.2.3 In vitro selection.

A 250 $\mu$L reaction mixture containing 2 nmol of the above RNA (RNA Lib1), 50 mM KCl, 20 mM NaCl, and 25 mM Tris (pH 7.6) was annealed at 70 °C for 1 minute and allowed to cool slowly to room temperature. To this mixture was added a second solution (250 $\mu$L) containing 10 mM $MgCl_2$, 50 mM KCl, 20 mM NaCl, and 25 mM Tris (pH 7.6) to obtain a final 500 $\mu$L reaction mixture having a $MgCl_2$ concentration of 5 mM. The reaction mixture was added onto 1.67 mg of Streptavidin Dynabeads, which were previously blocked with yeast tRNA (1 mg/mL), and incubated at room temperature for 1 hour. This constitutes the negative selection step (N.S., Figure A3). The supernatant was removed and the beads discarded to remove any bead-binding oligonucleotides. To the retained supernatant was added 100 pmol of pre-miR-19a (S1) and the solution was incubated at room temperature for 30 minutes. This constitutes the positive selection step (P.S., Figure A.3). At this point, 3.3 mg of Dynabeads (blocked with 1 mg/mL yeast tRNA) were added. After incubating for 15 minutes at room temperature, the beads were washed five times with 1 mL of the selection buffer (SB: 5 mM $MgCl_2$, 50 mM KCl, 20 mM NaCl, and 25 mM Tris pH 7.6) in order to remove weakly bound molecules. The retained RNA was eluted using two 150 $\mu$L portions of a stripping solution containing 25 mM NaOH and 1 mM EDTA. Both aliquots were quickly combined into a solution containing 30 $\mu$L of 3 M NaOAc, 30 $\mu$Lof 1 M Tris (pH 7.6), and 4 $\mu$L glycogen (1 mg/mL, Roche Diagnostics, Indianapolis, IN). The RNA was then ethanol precipitated and used directly in a 50 $\mu$L reverse transcription reaction containing 10 U/$\mu$L RT, 3 mM $MgCl_2$, 75 mM KCl, 10 mM DTT, 50 mM Tris (pH 8.3), and 0.5 mM each of the four dNTPs, which was incubated at

42 °C for 45 minutes. The resulting cDNA was added as a template into a 1 mL scale PCR and amplified for approximately 15 cycles (PCR conditions: 95 °C for 2 minutes, 95 °C for 30 seconds, 50 °C for 30 seconds, 72 °C for 1 minute, repeat for N cycles). The amplified DNA was ethanol precipitated and approximately half of the material was used to generate a new RNA library for the next round of in vitro selection. Figure A.2 summarizes selection conditions for each round. The first two rounds of in vitro selection were carried out at 22 °C due to previous observations that selection experiments initiated at 37 °C often failed to enrich functional aptamers. Following round 11, the enriched dsDNA pool was cloned into E. coli using the TOPO TA cloning kit (Life Technologies, Carlsbad, CA). Bacteria were grown for 16 hours at 37 °C on LB agar plates containing 50$\mu$g/mL kanamycin. Individual colonies were amplified by PCR and sequenced by Eton Biosciences Inc. (San Diego, CA).

### 2.2.4 Reselection of clone D-19a-6.

In order to clearly define the nucleotides within D-19a-6 that were critical for binding L-pre-miR-19a, we carried out a reselection experiment using a S12 mutagenized library based on D-19a-6 (Lib2, Figure A.3c), which was prepared by solid-phase oligonucleotide synthesis. The mutagenized region was synthesized with a degeneracy of 0.12 at each position, which yields molecules that have an average of 7 mutations relative to D-19a6. The mutagenized DNA library (Lib2) was purified by denaturing PAGE (8%, 19:1 acrylamide:bis-acrylamide) and transcribed as described above. The new mutated RNA library (RNA Lib2, Figure A.3c) was subjected to three rounds of in vitro selection as above (see Figure A.2b), and the final pool was cloned and sequenced as described for the original selection experiment.

### 2.2.5 In vitro transcription of D-RNA aptamers.

DNA templates used to prepare D-19a-6t and related mutants (see Figure 2.4 in the main text) were generated by cross-extension of two overlapping synthetic oligonucleotides (Figure A.6).

The oligonucleotides (200 pmol each) where annealed in a 25 $\mu$L mixture containing 6 mM $MgCl_2$, 150 mM KCl, 20 mM DTT, and 100 mM Tris (pH 8.3), which was heated at 90 °C for 1 minute and then cooled slowly to 22 °C. The volume was then adjusted to 50 $\mu$L using a solution containing 1.0 mM of each of the four dNTPs and 16 U/$\mu$L Reverse Transcriptase and incubated at 42 °C for 45 minutes. Following ethanol precipitation, the resulting dsDNA was added to a transcription reaction mixture containing 10 U/$\mu$L T7 RNA polymerase, 0.001 U/$\mu$L Inorganic pyrophosphatase (IPP), 25 mM $MgCl_2$, 2 mM spermidine, 10 mM DTT, 40 mM Tris (pH 7.9), and 5 mM of each of the four NTPs, where UTP was replaced with 5-aminoallyl-UTP. After incubating for 2.5 h at 37 °C, reaction mixture was ethanol precipitated and the RNA purified by denaturing PAGE (10%, 19:1 acrylamide:bis-acrylamide).

### 2.2.6 Preparation of D-pre-miR19a (S3).

Full length D-pre-miR-19a was prepared by ligation of two synthetic RNA oligonucleotides (sequences below). A 500 $\mu$L reaction containing 5 nmol of RNA1, 10 nmol of RNA2, 1 mM ATP, 50 $\mu$L DMSO (1.4 M), 10 mM $MgCl_2$, 1 mM DTT, and 50 mM Tris (pH 7.5) was annealed at 70 °C for 1 minute and slowly cooled to room temperature. T4 RNA ligase was added to a final concentration of 0.4 U/$\mu$L and the reation mixture was incubated at room temperature over night ($\tilde{1}$6 h). The RNA was concentrated by ethanol precipitation, and the ligated material was purified by denaturing PAGE (10%, 19:1 acrylamide:bis-acrylamide). RNA1. 5′-AGUUUUGCAUAGUUGCACUACAAGA-3′ RNA2. 5′-pAGAAUGUAGUUGUGCAAAUCUA-UGCAAAACUGA-3′

### 2.2.7 Electrophoretic mobility shift assay.

Dissociation constants for aptamer-pre-miR complexes were determined as described previously [134]. Briefly, a trace amount (0.05 nM) of either [5′-$^{32}$P]- labeled S2 or S3 was incubated with various concentrations of either D-19a-6t or MLRA-19a, respectively, in a 20 $\mu$L reaction mixture containing 1 mM $MgCl_2$, 150 mM KCl, 20 mM NaCl, 0.01 mg/mL tRNA, and 25 mM Tris (pH

7.6). After a 30 min incubation at 37 °C, the samples were loaded onto a non-denaturing polyacrylamide gel (8%, 19:1 acrylamide:bis-acrylamide), which contained 1 mM $MgCl_2$, 150 mM KOAc, 20 mM NaOAc and 25 mM Tris (pH 7.6). The samples were electrophoresed at 70 mA ( 37 °C) for 2 hours. The gel was imaged by autoradiography for 2.5 hours, and bound and unbound materials were quantitated using a Typhoon FLA-9500 Molecular Imager purchased from General Electric Co. (Boston, MA).

### 2.2.8 In-line probing analysis of pre-miR-19a.

A 10 $\mu$L reaction mixture containing 3 $\mu$M of [5′-$^{32}$P]- labeled D-premiR-19a (Figure A.5), either none or 18 $\mu$M MLRA-19a, 5 mM $MgCl_2$, 150 mM KCl, 20 mM NaCl, and 25 mM Tris (pH 7.6), was incubated at 37 °C for 48 hours. The cleavage products were resolved by denaturing PAGE (15%, 19:1 acrylamide:bis-acrylamide) and analyzed using a Typhoon FLA-9500 Molecular Imager (GE, Boston, MA).

### 2.2.9 Dicer inhibition assay.

Dicer cleavage was carried out in a 20 $\mu$L reaction mixture containing 1 nM [5′-$^{32}$P]-labeled D-pre-miR-19a (Appendix Figures), 5 nM human Dicer protein, various S14 concentrations of MLRA, 20 mM NaCl, 150 mM KCl, 0.05 mg/mL tRNA, 10 mM DTT, and 25 mM Tris (pH 7.6), which was incubated for 15 minutes at room temperature. Following the reaction, an aliquot was removed and quenched with a two-fold volume of 95% formamide solution containing 10 mM EDTA and the cleavage products were resolved by denaturing PAGE (10%, 19:1 acrylamide:bis-acrylamide). The gel was imaged by autoradiography and the fraction cleaved was quantitated using a Typhoon FLA-9500 Molecular Imager (GE, Boston, MA).

# 3. A MIRROR IMAGE FRET ASSAY FOR THE IDENTIFICATION OF SMALL MOLECULE RNA INHIBITORS.

High throughput screening approaches have dominated the drug discovery field since the advent of automated experimental robots. These processes allow for millions of small molecules to be tested in millions of various conditions for specific types of activity ranging from binding biologically relevant molecules to selectively inducing cancerous cell death [143]. The vast majority of high throughput approaches rely upon fluorescence based detection methods given the rapid data collection and processing which is possible using advanced instrumentation [144]. One commonly utilized approach for high-throughput screening in particular is the displacement assay. Briefly, in a displacement assay, a test molecule is mixed with its intended target which has been preemptively bound by a known competitor. The pre-bound complex is typically engineered to have a quenched fluorescent signal which activates only when the test molecule successfully displaces, or outcompetes, the control competitor. The high signal gain, versatility (amenable to variety of solution conditions), and speed of data collection make fluorescent displacement assays popular in drug discovery [131].

Aptamers are a unique class of affinity reagents well suited to applications in high throughput screening technologies [145]. Their key advantages lie in their vast target recognition capabilities, spanning from single ions to whole cells, their ease of production and modification through solid phase synthesis, and their high specificity and affinity for the target. Furthermore, it is straightforward to include fluorescent and quenching modifications onto aptamers. Together these properties make aptamers ideal candidates for fluorescent based displacement techniques.

The predominant classes of fluorescence detection are fluorophore-quencher pairs, fluorescence polarization, and Forster Resonance Energy Transfer (FRET) interactions [146] [147]. In this work we focus on developing an aptamer displacement assay which utilizes FRET for signal output. FRET interactions occur when two fluorophores have overlapping emission and excitation spectral bands. As a result, when a pair of such fluorophores move into close proximity of one an-

other, when the fluorophore with a higher energy excitation wavelength (donor) becomes excited, the excitation energy is transferred through Forster resonance energy transfer (FRET), a nonradiative energy transfer process, to the other fluorophore (acceptor), thus exciting the acceptor. The emission spectrum of the acceptor is collected to obtain FRET data. Figure 3.1 depicts the spectral overlap of a pair of FRET active fluorophores, cyanine 3 and cyanine 5 (Cy3 and Cy5 respectively) [148]. In this work we hypothesize that by labeling an L-aptamer and its D-RNA target with a pair of FRET active fluorophores, we could design a scalable and high-throughput FRET knockdown assay for the discovery of small molecule RNA inhibitors which tightly and specifically bind structured RNA targets.

Despite the surge in high-throughput screening methodologies in the past quarter century, it remains a stark challenge to develop high performance and cost effective assays for the discovery of small molecule RNA inhibitors [131] [149] [150]. Given the lack of diversity of RNA secondary structure, virtually all small molecules which bind an RNA target will also bind countless other RNAs. This poses an extremely difficult barrier to the engineering of a screening method which can effectively provide high quality results with minimal false positives and down-stream off target effects. Moreover, RNA tertiary structure is highly dynamic and as such requires the screening assay to work properly under conditions which mimic the physiological environment of the RNA target in question [151]. It is for these reasons that we believe an L-aptamer based approach can be superior to the current state of the art methods since L-aptamers exhibit high affinity and specificity for their intended targets, bind through explicitly tertiary interactions, can be quickly generated also in a high-throughput manner, and bind under physiologically relevant conditions. Thus, we have devised a fluorescence based FRET method to quickly screen potentially thousands of small molecules for target binding activity (Figure 3.2). This approach rely's on the inhibition or knock-down of FRET signal between an L-aptamer and its D-RNA target by a small molecule, with the knock-down of FRET signal constituting a positive hit. The issue of weeding out false positives is implicitly resolved based on the design of the experimental method and is discussed in detail below. In the following sections we report the design and application of L-aptamer based

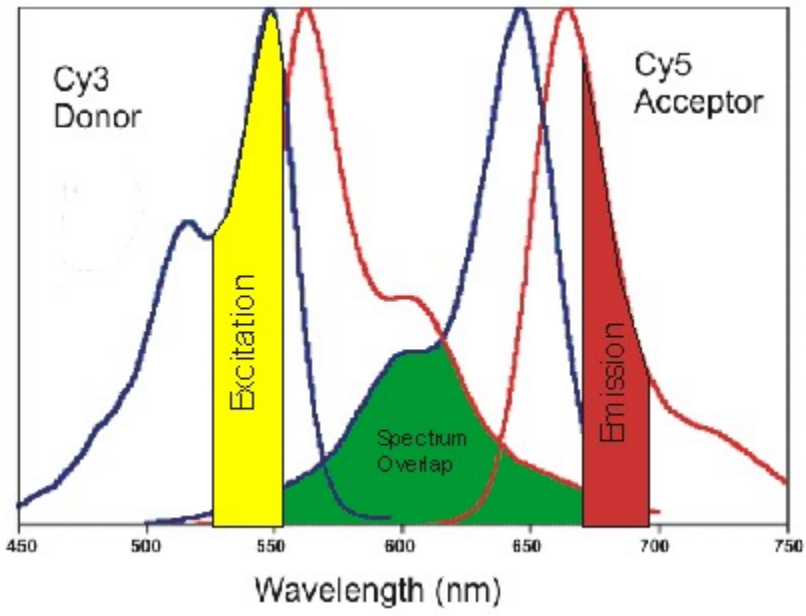


Figure 3.1: Fluorescence spectrum of Cyanine 3 and Cyanine 5 dyes showing the spectral overlap of excitation and emission wavelengths. The emission wavelength of Cyanine 3 overlaps with the excitation wavelength of Cyanine 5 so that when the two fluorophores are in close physical proximity to one another, upon excitation of Cy3, the excited Cy3 may nonradiatively transfer its energy to the ground state Cy5 thus generating an excited Cy5 which emits at its standard wavelength (690 max). Adapted from Ref. 150 under copyright AK CC 4.0

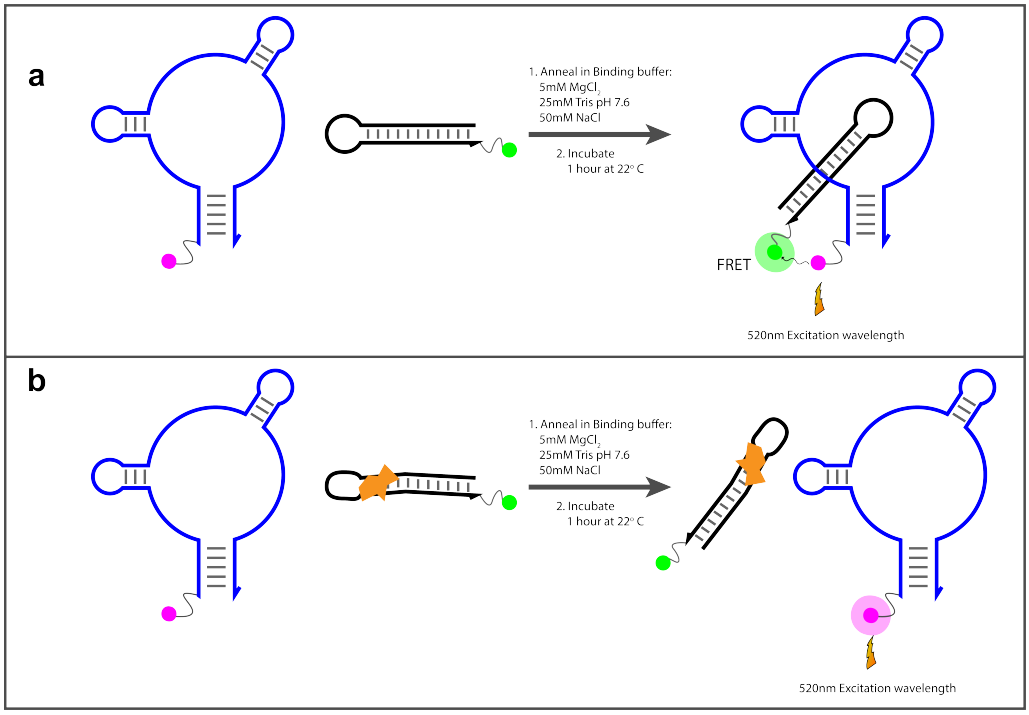


Figure 3.2: Cartoon representation of FRET signal generation and inhibition. (a) L-aptamer binding to D-RNA target in order to produce a positive FRET signal by bringing Cy3 and Cy5 fluorescent dyes into close proximity of one another. (b) Small molecule binding to D-RNA target thus perturbing the native structure, consequently preventing proper L-aptamer binding, thus inhibiting the generation of FRET signal between Cy3 and Cy5.

displacement FRET assay. We demonstrate the simplicity, versatility, and scalability of the design and describe how this may be implemented in a more industrial setting with no need for specialized equipment.

### 3.1 Results

Initially we set about determining if an L-aptamer and its D-RNA are capable of generating a FRET signal when labeled with an appropriate pair of fluorophores (Cy3 and Cy5). FRET interactions are highly distance dependent [152]. Due to the distance dependence of FRET, it is critical to ensure that in the absence of any small molecules, the L-aptamer and its D-RNA target are capable of generating a FRET signal upon binding. Without clear crystallographic data, it is difficult to determine the optimal positions for labeling of the aptamer and target. However, through a rational design approach it is straightforward to test a combination of labeling positions until a measurable FRET signal is produced by the aptamer:target complex. Most commonly, direct fluorophore phosphoramidite coupling, azide/alkyne click linkers, and NHS ester succinimide linkers are installed at the 3′ and/or 5′ end of either oligonucleotide to achieve the desired fluorescent labeling. The flexibility in labeling of oligonucleotides is beneficial for designing complex FRET interaction systems especially if the binding modality of the aptamer is not well understood. We chose to synthesize the L-6-4t TAR aptamer with a 5′ Cy3 phosphoramidite directly coupled to the terminal 5′ G. This labeling position was chosen for the simplicity of its incorporation. Next, a truncated version of the HIV-TAR RNA hairpin was synthesized in its natural D-sterochemistry configuration with a 3′ Cy5 fluorophore which was incorporated into the oligonucleotide by using a Cy5 labeled controlled pore glass (CPG) resin for oligonucleotide synthesis. As a result of our incorporation techniques, both dyes are present at the terminal ends of stable duplexes and are expected to have low flexibility, reducing the chance for binding to occur without a concomitant increase in FRET signal. Figure 3.3a/b depicts the L-6-4t and D-TAR RNA [83] constructs we have synthesized which generate a positive FRET signal upon binding. Once a FRET signal has been achieved, it is important to determine conditions under which FRET knockdown sensitivity is maximized. Two critical steps are required to achieve this; 1) determining the binding

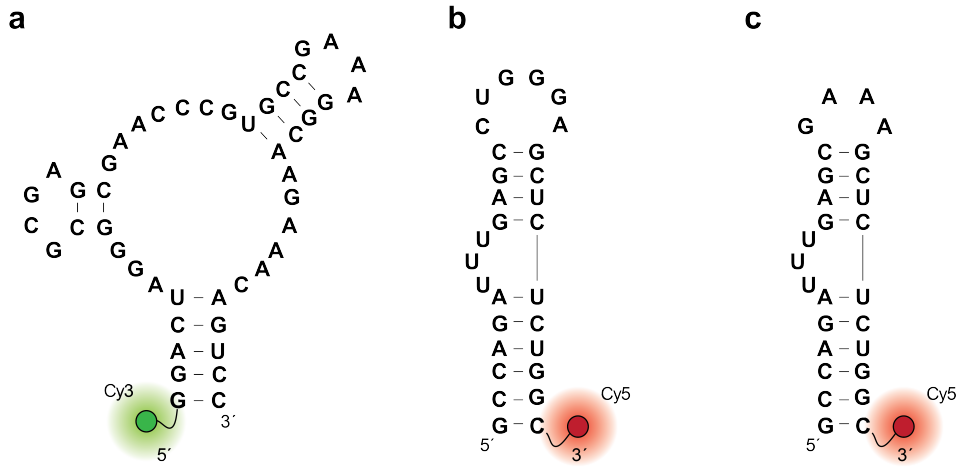


Figure 3.3: Sequences and predicted secondary structures of (a) TAR aptamer containing 5′ Cyanine 3 (Cy3) dye label, (b) Native TAR hairpin containing 3′ Cyanine 5 (Cy5) dye label, and (c) Mutant TAR hairpin with GNRA loop containing a 3′ Cy5 label.

affinity of the Cy3 labelled L-6-4t for the D-TAR target in the expected screening conditions, and 2) generating a FRET efficiency titration curve to determine the the aptamer and target concentrations where FRET disruption is most sensitive [153]. It is important to note that the conditions under which the aptamer was selected restrict the conditions under which the screening will be performed. As a result, the expected small molecule libraries must be soluble and stable under the conditions which the aptamer is functional. However, this is also advantageous since aptamers can easily be selected to bind under physiologically relevant conditions, greatly increasing the chances that upon screening a small molecule library, any positive hits will faithfully bind the target in vivo.

In order to determine the binding affinity of the Cy3 labeled L-aptamer for the Cy5 labeled TAR hairpin a series of electrophoretic mobility shift assays (EMSAs) were performed. A variety of conditions mimicking various potential screening conditions (Figure 3.4) were used when performing these EMSAs in order to demonstrate the versatility of L-aptamers in a high throughput screening method. In fact, varying DMSO concentration from 0% to as high as 10% showed little impact on L-6-4ts ability to bind the TAR hairpin. After determining the binding affinity under screening conditions, we selected a concentration at which $\approx$65% of target was bound to the aptamer (200 nM, Figure 3.5) and proceeded to perform a FRET titration experiment where the aptamer (donor) concentration was held constant at 200 nM and the TAR target (acceptor) concentration was varied between 25 nM and 2 $\mu$M (Figure 3.5) to generate a FRET activity curve which is somewhat analogous to the EMSA binding curve. This is to ensure that the concentrations of donor and acceptor molecule lie within the maximal slope region of the FRET activity curve and thus the FRET signal highly sensitive to disruptions in binding. In parallel, a FRET activity curve was also generated for a mutated version of the truncated TAR hairpin (Figure 3.3c). The L-6-4t TAR aptamer is incapable of binding the mutated loop sequence and so this mutant target acts as a non-specific FRET control molecule as indicated by the absence of a curve in the titration experiment.

With these parameters determined we moved on to screening known TAR binding small molecules

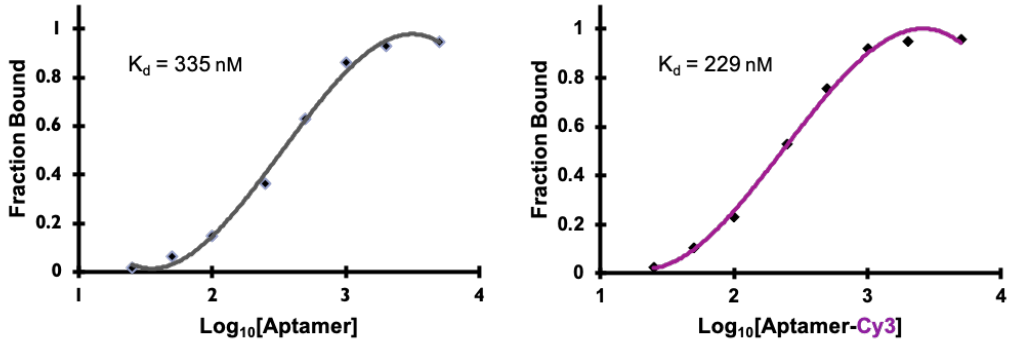


Figure 3.4: Comparison of dissociation constants of unlabeled (left) and Cy3 labeled (right) TAR aptamers. Fraction bound was determined by native EMSA. Dissociation constant values were approximated from the model equation at $y = 0.5$. The fluorescently labeled aptamer binds with a slightly higher affinity than the unlabeled variant.

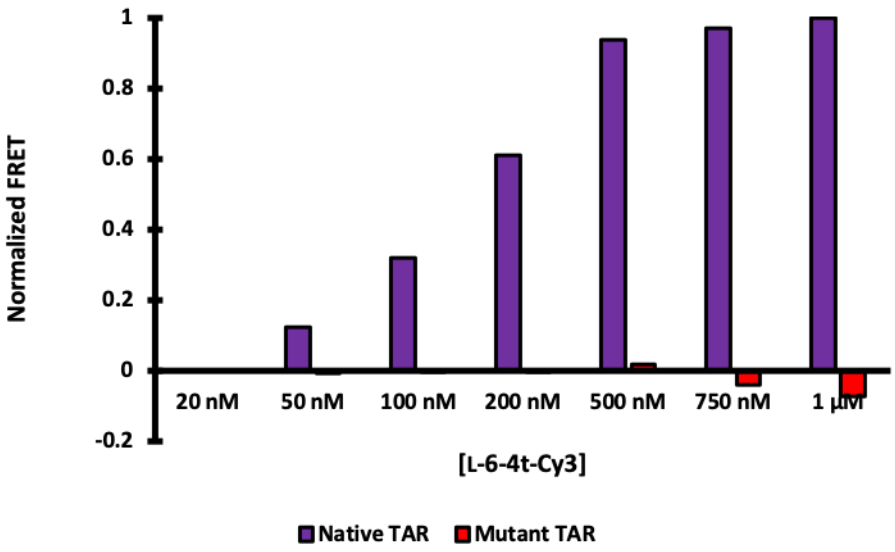


Figure 3.5: Titration of L-6-4t-Cy3 aptamer against native TAR (Figure 3.3b) in purple and mutant TAR (Figure 3.3c) in red. Target concentration is held constant at 200 nM. From this data we observe that at equimolar concentrations of target and aptamer the FRET signal is the most sensitive to disruptions. We expect that these concentrations will provide a most sensitive and reliable assay.

and peptides for FRET knock down activity. Three control molecules were chosen for this purpose: TAT peptide (GRKKRRQRRRPQ), Neomyocin, and native (unlabeled) L-6-4t TAR aptamer [154] [155] [83]. For each competitive inhibitor, $K_d$ values were estimated from previously reported values. To test FRET knockdown activity each molecule was titrated over a range of concentrations well below, equal to, and well above the estimated $K_d$ into reactions containing 200 nM TAR or 200 nM mutant TAR and incubated for 2 hours at 23 °C. The small molecules are pre-incubated with the target because the L-6-4t aptamer has been previously demonstrated to have a very slow off-rate, making the assay cumbersomely slow when attempting to directly disrupt a pre-formed aptamer:target complex. After incubating the small molecules with the target, the L-aptamer is added to the reaction to a final concentration of 200 nM. After the addition of aptamer, the reactions were incubated another 2 hours at 23 °C before FRET data was collected (Figure B.1). FRET data was corrected and normalized according to previously reported protocol [156].

After demonstrating that these well characterized TAR binding molecules are capable of inhibiting FRET signal through competitive binding, we proceeded to testing various dimethylamiloride (DMA) derivatives (Figure 3.6) developed in Dr. Amanda Hargroves laboratory at Duke University as part of a collaboration to scale up our screening method [157] [158] [159]. The same series of FRET inhibition experiments were performed, however, two derivatives (Figure 3.6) were used in place of the control molecules. Each molecule was subjected to an aptamer displacement FRET inhibition assay as described above. In each case, the molecule is tested for activity using a mutant TAR variant as a negative control. Figure 3.7 depicts the results a triplicate averaged aptamer displacement FRET inhibition experiment. In this experiment, DMA-169 competes with L-6-4t-Cy3 aptamer for binding to the native TAR hairpin (Figure 3.3b). Displacement of the aptamer is confirmed by a reduction in FRET signal as the Cy3 and Cy5 fluorophores appended to L-6-4t-Cy3 and the TAR hairpin are separated. We confirmed specificity by performing the same experiment using the mutant TAR target (Figure 3.3c) as well as the DMA-001 molecule which is incapable of binding the native TAR hairpin (Figure 3.8). The mutant target is a negative control

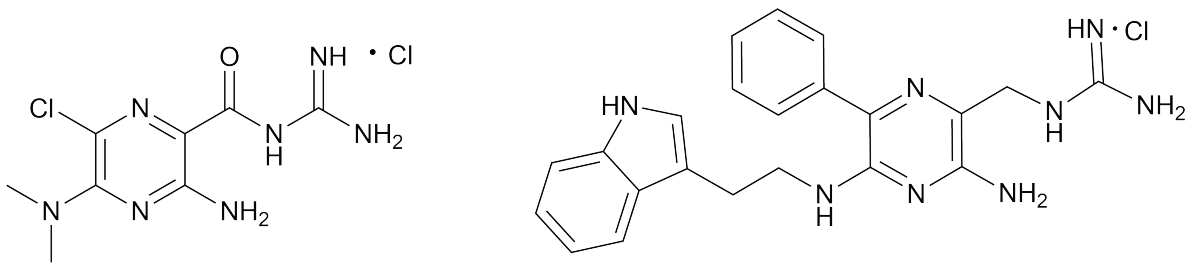


Figure 3.6: Chemical structures of dimethyl amiloride (DMA-001) and a synthetic derivative, DMA-169, which were used in developing the TAR aptamer displacement assay. Previous work in the Hargrove group (see main text for reference) has characterized these molecules interactions with TAR in great detail.

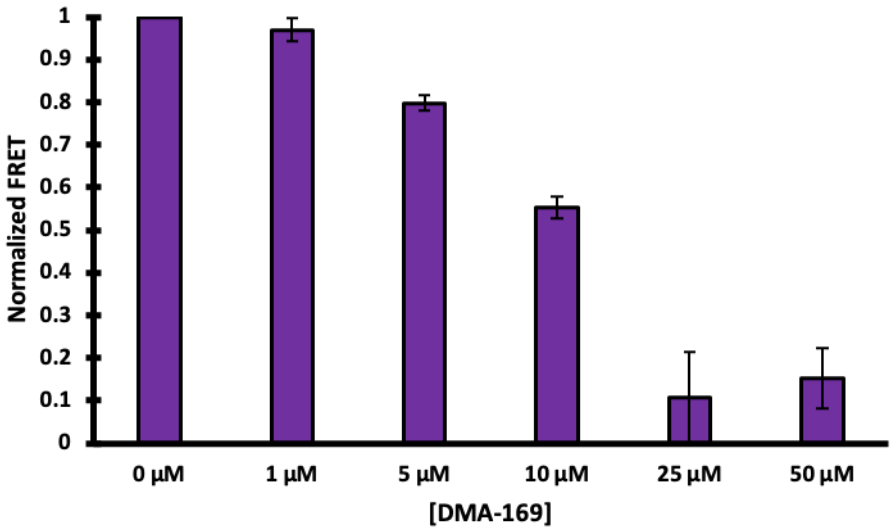


Figure 3.7: Triplicate averaged results of aptamer displacement FRET inhibition assay. The dimethylamiloride derivative DMA-169 clearly prevents aptamer binding, reducing FRET signal as its concentration increases. These results confirm that our method is reliable and motivate advancement into high throughput screening platforms.

for baseline FRET activity and aptamer specificity and DMA-001 is a negative control for aberrant attenuation of FRET signal by a small molecule similar to DMA-169 but lacking binding affinity for TAR. At high concentrations of DMA-169, the raw fluorescent signal, and concomitantly the corrected FRET signal, of the mutant TAR species is drastically affected by the high concentration of small molecule. Figure A.9 shows supporting data that DMA-169 non-specifically attenuates fluorescent signal of a variety of labeled oligonucleotides and free fluorophore. This effect is reproducible and does not impair the analysis of our results. For each individual reaction mixture there are two control reactions which are necessary for correct signal analysis. The first is a reaction mixture containing the small molecule at a particular concentration together with only aptamer present at the experimental concentration (200 nM). The second control is nearly identical, however the targets (native and mutant) are incubated with the small molecule at the experimental concentration (200 nM). Although it is typically only necessary to have one control reaction containing donor (aptamer) and another containing acceptor (target), in our experiments we observed that certain small molecules can attenuate the baseline fluorescent signal of the cyanine dyes (Figure B.2). As a result, it is critical to demonstrate that this attenuation is not caused by unwanted binding of the small molecule to the aptamer so we performed an in-line hydrolysis experiment where the Cy3 labeled L-aptamer was incubated under exact screening conditions (50 mM NaCl, 5 mM $MgCl_2$, 25 mM Tris pH 7.6, 2% DMSO, and 0.01 mg/mL tRNA) both in the presence and absence of DMA-169. After incubating for 24 hours at 23 °C, an aliquot of each reaction mixture was run down an analytical PAGE gel (15% 19:1 acrylamide:bisacrylamide) and scanned under Cy3 wavelengths in order to see if there was any difference in the hydrolysis pattern between the two mixtures (Figure 3.9). There was no detectable difference between any individual bands, implying that the molecule does not bind the aptamer. Although this effect requires the screening method to have significantly more control reactions, each control may be used as an individual in-line hydrolysis experiment, parallelizing both FRET inhibition detection and false positive screening.

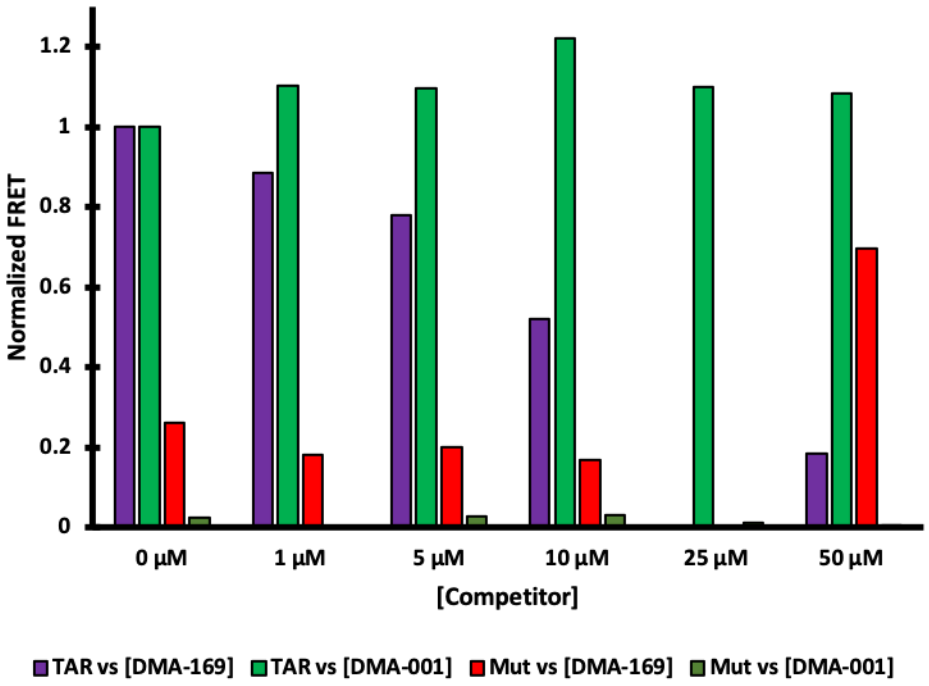


Figure 3.8: Control experiments demonstrating specificity of aptamer displacement FRET inhibition assay. The proper displacement FRET inhibition experiment using DMA-169 was performed as a positive control in this series of data (dark purple bars). As expected, molecule DMA-001 does not compete with the aptamer for target binding with no loss of FRET signal at any concentration (mint green bars). The mutant TAR species (Figure 3.3c) exhibits some background FRET signal with no evidence of FRET inhibition (red bars). In fact at higher concentrations of DMA-169 the raw fluorescent signal of the mutant TAR is non-specifically attenuated by the small molecule. When the mutant TAR is incubated with aptamer and DMA-001 little to no FRET signal is observed at all (dark green bars).

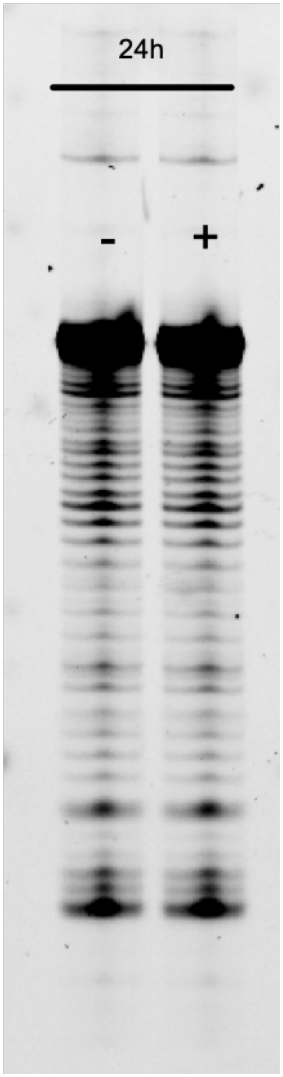


Figure 3.9: In-line hydrolysis of Cy3 labeled TAR aptamer construct in the absence (-) and presence (+) of inhibitor molecule DMA-169 demonstrating that DMA-169 does not bind the TAR aptamer non-specifically. This gel proves that the FRET knockdown effect is not a false positive due to binding of the L-aptamer rather than the intended D-RNA target.

During the optimization of these experiments, we observed that the concentration of tRNA present in the reaction seemed to diminish the ability of DMA-169 to compete with L-6-4t for target binding and FRET signal suppression. We decided to investigate this phenomenon further by performing a tRNA titration experiment (Figure 3.10a). We hypothesize that the DMA-169 molecule is promiscuously binding tRNA, a molecule rich in secondary and tertiary structure for small molecule binding, resulting in differences in assay sensitivity. In this experiment, the target and aptamer concentration are held constant at 200 nM and DMA-169 concentration is held constant at 10 $\mu$M across 3 aliquots. Into each reaction an increasing concentration of tRNA is added spanning ranging in two orders of magnitude. If the molecule is binding tRNA nonspecifically, then its ability to compete with the aptamer for target binding should be increasingly impeded as more tRNA is present in the reaction. The results in Figure 3.10a clearly demonstrate that increasing tRNA concentration reduces DMA-169s efficacy as a competitor with L-6-4t. Furthermore these findings motivated us to investigate how other nonspecific RNAs could affect the results of this assay. We chose to study the 363 bp TAR HIV-RNA transcript (Figure B.3) which was designed to be missing the TAR hairpin structure so the remaining RNA could behave as a nonspecific RNA blocker, analogous to tRNA in previous experiments. Figure 3.10b shows how with increasing HIV-RNA concentration, FRET signal is restored to match the control reaction. These experiments display an obvious weakness of small molecule RNA inhibitors, off target effects. The mirror image approach we employ in this work is expected to identify molecules with much higher specificity than what has been achieved to date. This is because L-aptamers bind their targets strictly through high affinity tertiary interactions, unique to the aptamer:target complex. As a result, it is expected that a molecule which disrupts such a tight and specific interaction will likewise exhibit a degree of specificity for the target. However, as mentioned above, the redundancy of RNA secondary and tertiary structure leaves identifying small molecules with decreased off target effects a difficult challenge.

In order to test if this experimental design is generalizable, we designed an analogous system using an L-DNA aptamer developed in our lab against precursor microRNA-155 [160]. The reason

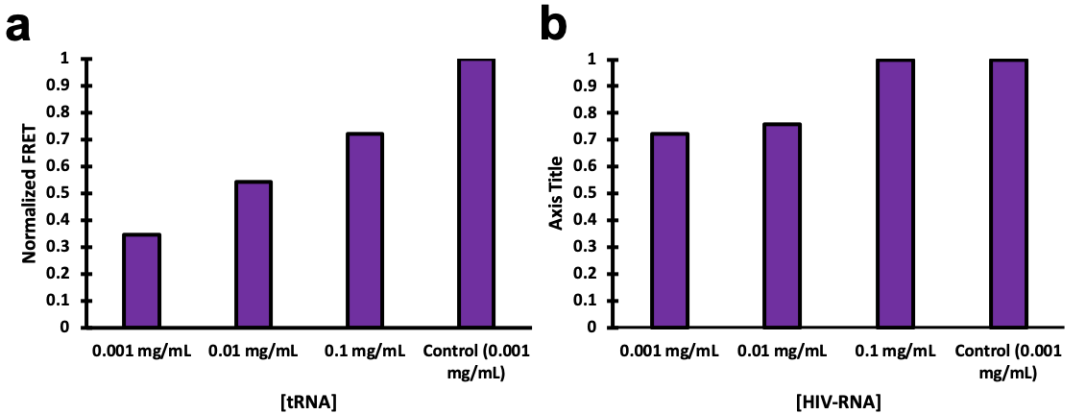


Figure 3.10: FRET reconstitution by nonspecific a) tRNA and b) HIV-RNA construct competitors. The increasing concentration of off target RNA sequesters the DMA-169, prohibiting competitive displacement of aptamer from TAR, causing FRET signal to remain high.

for our choice of using this aptamer and target pair is twofold; 1) we demonstrate that the choice of target is generalizable and 2) we demonstrate that aptamers consisting of either DNA or RNA may be used in this method. This latter point is especially significant as theoretically by using DNA aptamers, there is reduced chance of obtaining false positive results (i.e. small molecule disrupting FRET by binding the RNA aptamer rather than the RNA target) because DNA is lacking the $2'$ hydroxyl moiety and has a very different subset of secondary and tertiary structures when compared to RNA. Because the stereochemistry of the aptamer and target are opposite of one another, they bind only through tertiary structure motifs. This property greatly increases the sensitivity of the assay because if the target and aptamer were bound through duplex formation, many small molecules in a library would likely bind to the complex through base intercalation thus leading to countless false negative results. As before, we first obtained a FRET titration curve in order to determine at what concentrations of L-aptamer and target will FRET signal disruption have the highest sensitivity (Figure 3.11). We proceeded to testing FRET inhibition of the L-155 aptamer:pmiR-155 target by synthesizing an unlabeled (native) version of the L-155 DNA aptamer to act as a competitive binder (Figure 3.12). Additionally, we synthesized a mutant (murine) version of the pmiR-155 hairpin to act as a negative control to ensure the specificity of the assay. In Figure 3.11, it is clear that only the native pre-miR-155 hairpin generates a positive FRET signal in the presence of the aptamer at equimolar (500 nM) concentrations. Furthermore, the off target murine pmiR-155 variant exhibits only background FRET signal in the presence of aptamer.

Moving forward, we expect to test this experimental design in a high-throughput screening context as part of a collaboration with Dr. Amanda Hargrove at Duke University. Dr. Hargrove's group has recently published multiple articles focused on understanding the structure of TAR RNA for the discovery and development of novel RNA binding therapeutics [158] [159]. We aim to test the scalability of our approach using Dr. Hargrove's DMA derivative library as a benchmark test for scaling up into high throughput screenings. This library has already been screened for TAR binding, making it the perfect control library for the L-6-4t TAR aptamer in our system. Moreover, given the success of using this approach with the L-DNA aptamer, we would like to screen

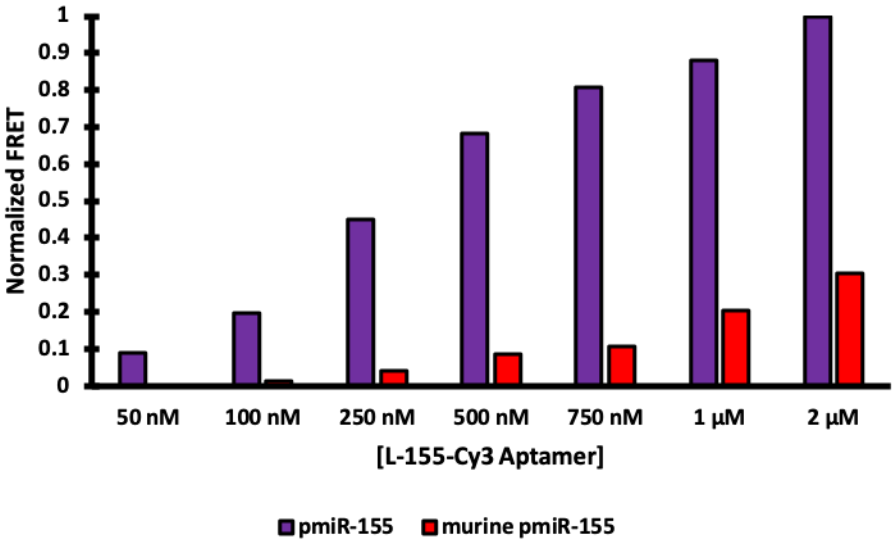


Figure 3.11: FRET titration curve for L-DNA pmiR-155 Aptamer. pmiR-155 concentration is held constant at 500 nM throughout each reaction mixture and L-aptamer concentration is varied between 50 nM and 2 $\mu$M

the same DMA library against pre-miR-155. This would provide insight into the promiscuity of these RNA binding small molecules, as well as potentially discover new small molecule drugs for pre-miR-155.

Previously groups have successfully applied aptamers to many diverse high throughput screening approaches [145] [161]. However, this work represents the first example of a high throughput approach using L-aptamers to screen for specific RNA binding characteristics. We expect that using L-aptamers, which bind their target through tertiary interactions, will increase the likelihood of discovering high affinity and high specificity small molecules against clinically relevant structured RNA targets. The unique features of L-aptamers will likely find diverse use in screening platforms moving into the future.

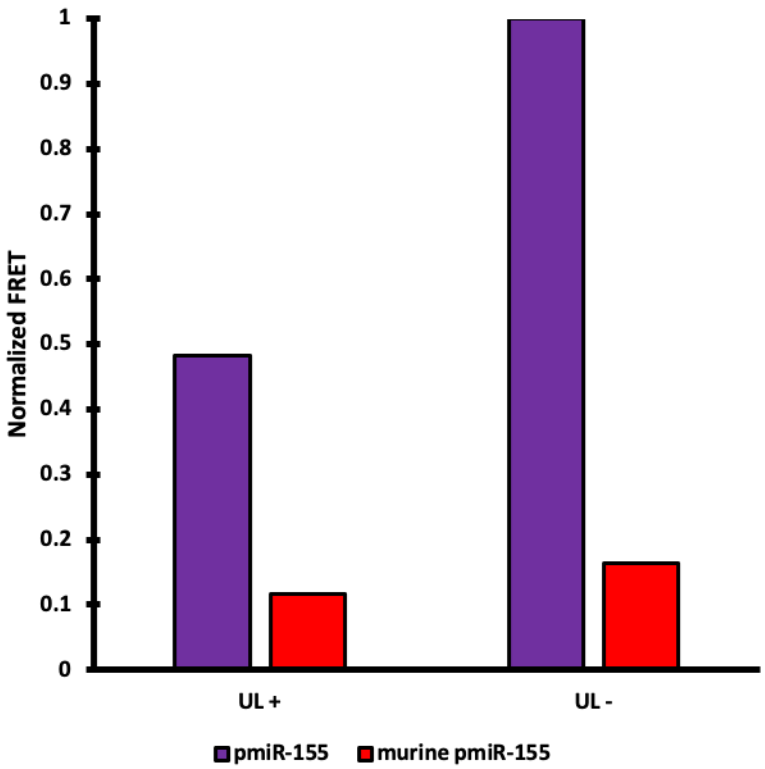


Figure 3.12: Demonstration of FRET inhibition by the addition of unlabeled L-DNA pmiR-155 aptamer. Purple bars show the FRET knockdown for the native pmiR-155 target. Red bars show both lack of FRET and FRET knockdown for the murine pmiR-155 variant showing the specificity of the L-aptamer for its proper target.

## 3.2 Materials and Methods

### 3.2.1 General

All oligonucleotides used in this work were prepared by standard solid-phase synthesis on an Expedite 8909 DNA/RNA synthesizer. DNA synthesizer reagents, D-nucleoside phsophoramidites, and fluorescent phosphoramidites/CPG supports were purchased from Glen Research (Sterling, Va). L-nucleoside phosphoramidites were purchased from ChemGenes (Wilmington, Ma). [Gamma-$^{32}$P]ATP was purchased from Perkin Elmer (Waltham, MA).

### 3.2.2 Oligonucleotide purification

Following synthesis, oligonucleotides were deprotected following manufacturer protocols. After cleavage and deprotection from the solid support, all oligonucleotides were purified by 15-20% polyacrylamide gel electrophoresis (PAGE 19:1 acrylamide:bisacrylamide). Purified material was excised from the gel, crushed up, and eluted overnight at 23 °C in an elution buffer consisting of of 200 mM NaCl, 10 mM EDTA, and 10 mM Tris (pH 7.6). The slurry was passed over a filter to remove gel chunks and the eluted material was first concentrated in an Amicon Ultra Centrfugal Filter (Millipore-Sigma) having a membrane pore size of 3kDa. Concentrated samples were desalted by standard ethanol precipitation.

### 3.2.3 FRET data collection and processing

All fluorescent signals were collected using a GloMax Discover multi-well plate reader from Promega Corp. (Madison, WI). Unless stated otherwise all TAR system reactions contained 200 nM of either aptamer and/or target, 50 mM NaCl, 5 mM MgCl2, 25 mM Tris pH 7.6, 2% DMSO, and 0.01 mg/mL tRNA, and were carried out at 23 °C for the indicated period of time. Prior to mixing, the aptamer and target are each annealed at 75 °C in buffer containing 50 mM NaCl, 5 mM $MgCl_2$, 25 mM Tris pH 7.6, 2% DMSO, and 0.01 mg/mL tRNA to ensure proper folding. Raw FRET data is collected by scanning first using at 660 nm/770 nm (bandpass filter; Cy5), followed by 520 nm/770 nm (bandpass filter; FRET), and finally 520 nm/580 nm (bandpass filter; Cy3). This order is chosen so as to minimize photobleaching of the fluorophores during data collection.

Each reaction mixture has two controls reactions associated with it. They are nearly identical to the reaction mixture however each control is missing either aptamer or target. All other conditions including inhibitor concentration are identical to the actual experiment. This control scheme is required in order to account for two important factors, 1) spectral overlap between Cy3 and Cy5 fluorophores and 2) attenuation of fluorophore signal by the small molecule. Consequently, only signal generated by FRET interaction is analyzed. The rationale behind this method is carefully detailed in an article from the Luger group [156].

### 3.2.4 Electrophoretic mobility shift assay

. Dissociation constants for aptamer-pre-miR complexes were determined following previously published protocols [134]. Briefly, a trace amount of 5′-$^{32}$P]-labeled Cy5-TAR was incubated with increasing concentrations of Cy3-L-6-4t aptamer in a 20 $\mu$L reaction mixture containing 50 mM NaCl, 5 mM MgCl2, 25 mM Tris pH 7.6, 2% DMSO, and 0.01 mg/mL tRNA. After a 30 minute incubation at 23 °C, the samples were loaded onto a non-denaturing PAGE gel (8% 19:1 acrylamide:bisacrylamide), which contained 5 mM $MgCl_2$, 50 mM NaOAc and 25 mM Tris pH 7.6. The samples were electrophoresed at 55 mA ( 23 °C) for 2.5 hours. The gel was then imaged by autoradiography for 1 hour. Bound and unbound materials were quantitated using a Typhoon FLA-9500 Molecular Imager purchased from General Electric Co. (Boston, MA).

### 3.2.5 In-line probing analysis of Cy3 L-6-4t and Cy5 TAR RNA

In-line hydrolysis reaction was performed by incubating either Cy3 L-6-4t or Cy5 TAR at 5 $\mu$M concentration were incubated in the presence or absence of a saturating amount (1 mM) of inhibitor molecule DMA-169, for 48 hours in a 20 $\mu$L reaction mixture containing 50 mM NaCl, 10 mM MgCl2, 25 mM Tris pH 7.6, 2% DMSO, and 0.01 mg/mL tRNA. The cleavage products were resolved by denaturing PAGE (15%, 19:1 acrylamide:bis-acrylamide) and analyzed using a Typhoon FLA-9500 Molecular Imager (GE, Boston, MA).

# 4. HETEROCHIRAL STRAND DISPLACEMENT CIRCUITS.*

The absence of a straightforward strategy to interface native D-DNA with its enantiomer L-DNA oligonucleotides of opposite chirality are incapable of forming contiguous Watson-Crick base pairs with each other has enforced a "homochiral" paradigm over the field of dynamic DNA nanotechnology [162] [163] [164] [165] [166]. As a result, chirality, a key intrinsic property of nucleic acids, is often overlooked as a design element for engineering of DNA-based devices [167], potentially limiting the types of behaviors that can be achieved using these systems. Here we introduce a toehold-mediated strand-displacement methodology for transferring information between orthogonal DNA enantiomers via an achiral intermediary, opening the door for "heterochiral" DNA nanotechnology having fully interfaced D-DNA and L-DNA components. Using this approach, we demonstrate several heterochiral DNA circuits having novel capabilities, including autonomous chiral inversion of DNA sequence information and chirality-based computing. In addition, we show that heterochiral circuits can directly interface endogenous RNAs (e.g., microRNAs) with bioorthogonal L-DNA, suggesting applications in bioengineering and nano-medicine [12]. Overall, this work establishes chirality as a design parameter for engineering of dynamic DNA nanotechnology, thereby expanding the types of architectures and behaviors that can be realized using DNA.

## 4.1 Results

PNA is an oligonucleotide analogue in which the sugar-phosphate backbone has been replaced with uncharged N-(2-aminoethyl)glycine units (Figure 4.1a). Like DNA and RNA, PNA obeys WC base-pairing rules, forming stable antiparallel duplexes with DNA [168]. In contrast to the native polymers, however, PNA has no inherent chirality [123] [169]. On the basis of this property, we concieved a novel toehold-mediated strand-displacement reaction (hereinafter called strand-

*Reprinted with permission from "Heterochiral dna strand-displacement circuits" by Adam M. Kabza, Brian E. Young, and Jonathan T. Sczepanski, 2017. *JACS*, 139, pp. 17715-17718, 2017.

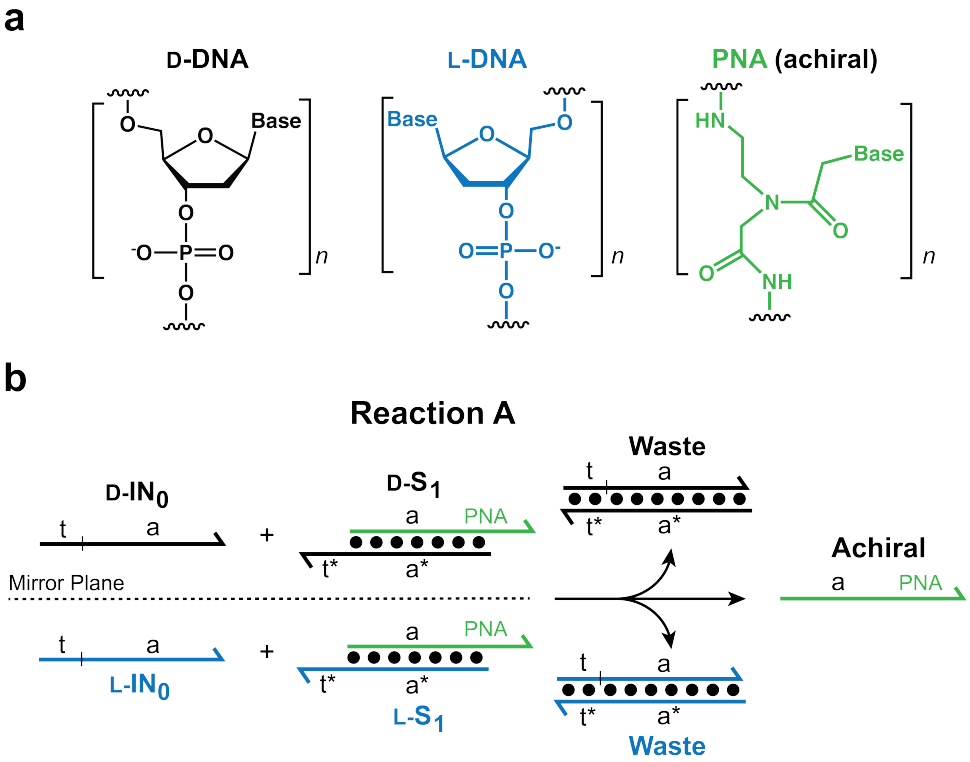


Figure 4.1: Heterochiral DNA strand-displacement reactions. (a) The three types of nucleic acids used in this work. D-DNA (black), L-DNA (blue), and PNA (green) are distinguished by color throughout the text. (b) Mechanism for heterochiral strand-displacement reaction A. DNA and PNA strands (in all figures) are depicted as lines with the half-arrow denoting the 3′ end (or C-terminus for PNA) and an asterisk indicating complementarity. Adapted from Ref. 125 with permission from ACS.

displacement reactions) that exploits a DNA/PNA heteroduplex in order to interface the two enantiomers of DNA . We will refer to this strand-displacement reaction as reaction A (Figure 4.1b). In reaction A, a DNA/PNA substrate complex ($S_1$) is activated via binding of a DNA input ($IN_0$) to its DNA toehold domain $t^*$) , resulting in displacement of the achiral PNA strand. In this reaction, the chirality of the input signal must match the chirality of the incumbent DNA strand on the DNA/PNA heteroduplex. Release of the PNA strand effectively decouples the stereochemical information from the sequence information present in the chiral input. At this point, the achiral PNA output can serve as a sequence-specific input for downstream reactions with either D-DNA or L-DNA components. Using reaction A as a starting point for developing a heterochiral DNA nanodevice, we designed a multilayer DNA strand-displacement circuit employing both enantiomers of each reaction component (Figure 4.2a). The input strand (e.g., D-$IN_1$) reacts with the chimeric DNA/PNA complex (e.g., D-$A_1$) via toehold domain (1), resulting in displacement of the achiral PNA intermediate ($PNA_1$). The activated domain ($2^*$) on the PNA serves as the input for a second reaction with complex $B_1$ (e.g., D-$B_1$), releasing the output strand (e.g., D-$OUT_1$). Depending on the chirality of the DNA components provided, the circuit can proceed through several possible reaction pathways (Figure 4.2c). For example, a circuit composed solely of components D-$A_1$ and D-$B_1$ can only generate D-$OUT_1$ in the presence of D-$IN_1$ (pathway P1). This is analogous to the traditional, homochiral approach (i.e., if the achiral PNA were to be replaced with a D-DNA strand having the same sequence). However, addition of L-$B_1$ to the same reaction mixture enables simultaneous production of both enantiomers of $OUT_1$ (pathway P3, Figure 4.2c), each of which can carry out unique downstream functions. To confirm our design, we first examined pathways P2 and P5 in isolation (Figure 4.2c), both of which produce a DNA output having the opposite chirality as the input. In order to stereospecifically monitor the outputs of the circuit, we utilized a pair of chiral reporter complexes (D-$R_1$ and L-$R_1$) having unique fluorophore-quencher pairs (Cy3/BHQ2 and Cy5/BHQ3, respectively) (Figure 4.2b). As shown in Figure 4.2d, when D-$IN_1$ was added to a reaction mixture containing only pathway P2 components (D-$A_1$ and L-$B_1$) along with both reporter complexes, only the fluorescence signal corresponding to activation of L-$R_1$ (Cy5) was

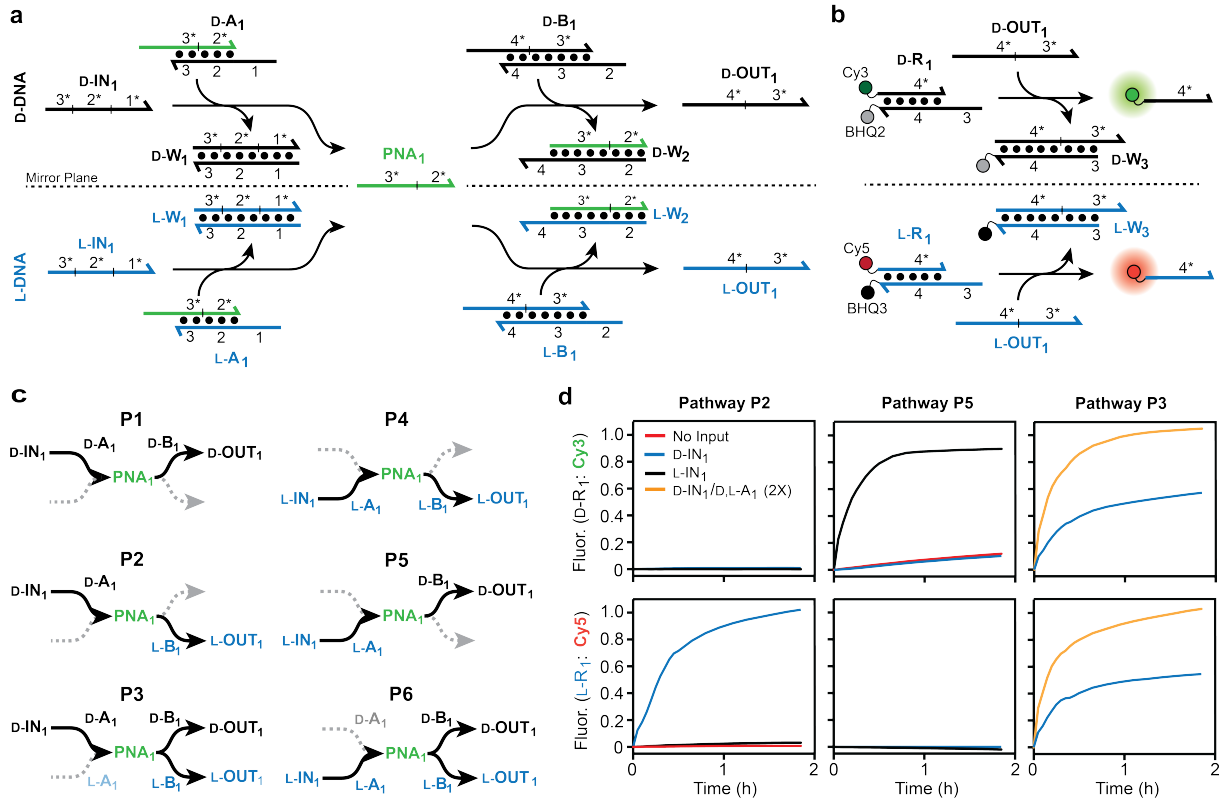


Figure 4.2: A heterochiral DNA strand-displacement circuit implemented with reaction A. (a) Schematic illustration of the heterochiral circuit. (b) Fluorescent reporter strategy. Domain 3* of the output strand from (a) (D-$OUT_1$ or L-$OUT_1$) reacts with toehold domain 3 of the corresponding reporter complex (D-$R_1$ or L-$R_1$, respectively), displacing the incumbent fluorescent strand. (c) Potential reaction pathways (P1-P6) for the circuit depicted in (a). (d) Demonstration of the heterochiral circuit (pathways P2, P3, and P5). Unless stated otherwise, all reaction cascades contained the indicated circuit components at 500 nM along with 300 mM NaCl, 1 mM EDTA, and 10 mM Tris (pH 7.6) and were carried out at 23 °C. All reaction mixtures also contained each reporter complex (D-$R_1$ and L-$R_1$) at 500 nM, and their corresponding fluorescent signals were monitored in parallel. Fluorescence (Fluor.) in all figures is reported in units such that 1.0 is the fluorescence of the triggered reporter (in this case 500 nM) and 0.0 is the background of the quenched reporter complex. Sequences of strands are listed in Figure C.1. Adapted from Ref. 125 with permission from ACS.

observed. Likewise, only reporter D-$R_1$ (Cy3) was activated when L-$IN_1$ was added to a reaction containing solely pathway P5 components (L-$A_1$ and D-$B_1$). In contrast, no significant fluorescence signal was observed for either reaction in the absence of an input or in the presence of an input with the opposite (orthogonal) chirality relative to complex $A_1$. These fluorescence data were further verified by gel electrophoresis (Figure 4.3) Together, these results confirm that pathways P2 and P5 of the heterochiral circuit function as intended and demonstrate for the first time an autonomous heterochiral DNA device.

Having demonstrated the proper function of pathways P2 and P5 in isolation, we combined their corresponding components into a single reaction mixture in order to construct the complete heterochiral circuit depicted in Figure 4.2a. All of the reaction components (D-$A_1$, L-$A_1$, D-$B_1$, and L-$B_1$) as well as both reporter complexes (D-$R_1$ and L-$R_1$) were present at equimolar concentrations (500 nM). Addition of 1 equivalent of D-$IN_1$ (500 nM) to the racemic circuit resulted in generation of approximately half the maximal fluorescence signal for each reporter complex (Figure 4.2d, pathway P3), suggesting that 0.5 equivalents of each output strand ( 250 nM) was produced relative to the input. This observation is consistent with the equal consumption of the achiral PNA strand ($PNA_1$) by each enantiomer of complex $B_1$ (pathway P3). Accordingly, doubling the concentration of the input (D-$IN_1$) as well as both complexes D-$A_1$ and L-$A_1$ resulted in near-stoichiometric activation of both chiral reporters (Figure 4.2d). As anticipated, similar results were obtained using L-$IN_1$ in place of D-$IN_1$ (pathway P6, figure 4.4). The fluorescence signal associated with L-$R_1$ (Cy5) remained unaffected when the reaction (pathway P3) was carried out in either the absence of reporter D-$R_1$ or in the presence of a 2-fold excess of D-$R_1$ relative to L-$R_1$ (Figure 4.5), further confirming the absolute orthogonality between D-$OUT_1$ and L-$OUT_1$ (and D-DNA and L-DNA in general). Because of its ability to convert an enantiomerically pure DNA input into a 1:1 mixture of orthogonal D-DNA and L-DNA outputs, we term this circuit a "racemization gate", the outputs of which offer a general route to parallelization of DNA circuitry or other dynamic DNA devices without a concomitant increase in crosstalk between reaction components.

L-DNA is resistant to both nuclease degradation and off target interactions with native

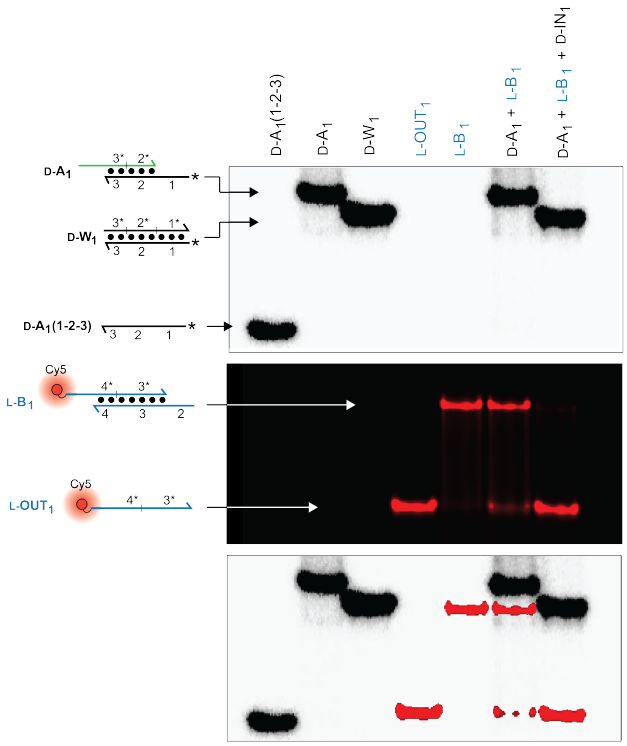


Figure 4.3: Native PAGE analysis of the heterochiral strand-displacement reaction depicted in Figure 2a. Here, heteroduplex D-$A_1$ is [5′-$^{32}$P-labeled (asterisk) via strandD-$A_1$ (1-2-3) (where 1-2-3 refers to the strand having domains 1, 2, and 3 arranged in the 5′ to 3′ direction) and duplex L-$B_1$ is labeled with Cy5 via strand L-$OUT_1$. Reaction mixtures contained the indicated components, 300 mM NaCl, 1 mM EDTA, and 10 mM Tris (pH 7.6) and the strand-displacement reaction was allowed to proceed for 2 hours at 23 °C. Samples were then run on a 20% native PAGE (19:1 acrilamide:bisacrylamide) at 140 volts for at least 6 hours and imaged by autoradiography (top) and fluorescence (middle). The overlay (bottom) is also depicted for clarity. Adapted from Ref. 125 with permission from ACS.

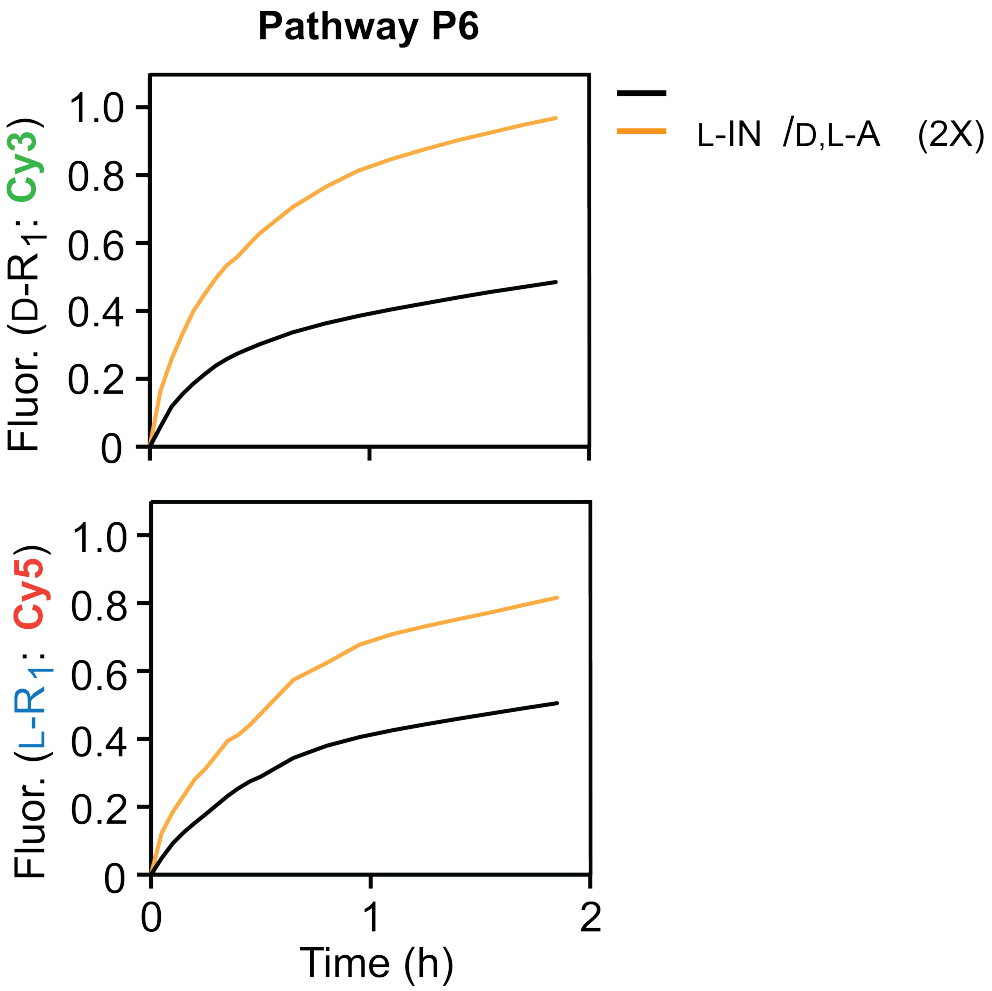


Figure 4.4: Demonstration of circuit pathway P6 (Fig. 2c). Refer to Fig. 2a in the main text for the complete reaction scheme. Reactions were carried out as described in Fig. 2d (pathway P3) except that they were initiated with L-$IN_1$ in place of D-$IN_1$. Adapted from Ref. 124 with permission from ACS.

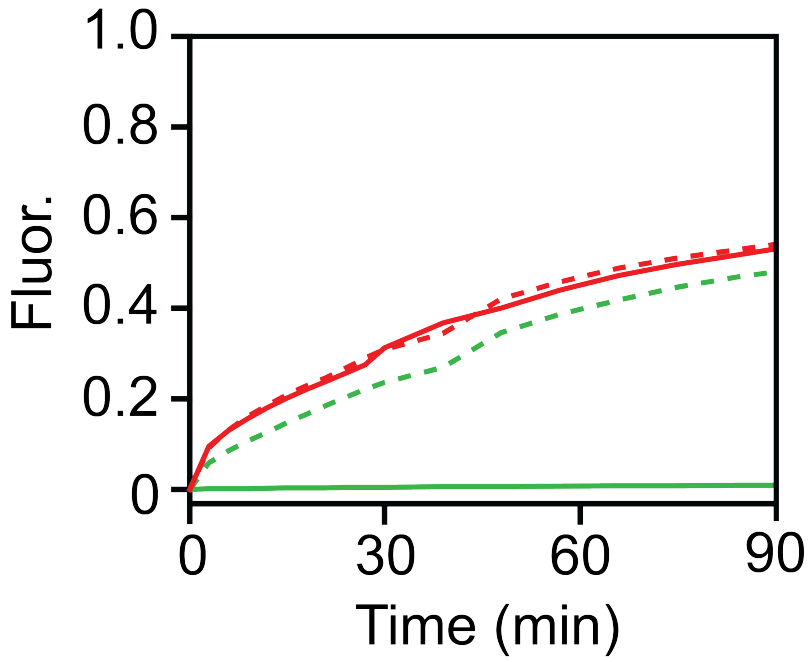


Figure 4.5: Confirmation of output ($OUT_1$) orthogonality for the heterochiral circuit depicted in Fig. 2a (pathway P3). Strand-displacement reactions were carried out as described in Fig. 2d (pathway P3), however, reporter complex D-$R_1$ was either omitted (solid lines) or present in 2-fold excess relative to L-$R_1$ (dashed lines). The fluorescent signals generated via activation of either reporter complex D-$R_1$ (Cy3) or L-$R_1$ (Cy5) are colored green or red, respectively. Adapted from Ref. 125 with permission from ACS.

nucleic acids and proteins. Thus, our demonstration of sequence-specific interfacing of a biologically relevant RNA species (microRNA) with L-DNA lays the foundation for integrating endogenous nucleic acid signals with L-DNA-based circuits capable of performing autonomous diagnostic and therapeutic tasks in living organisms free of obstruction from cellular components [12] [65]. Success in this area would remove a significant source of design constraints in the burgeoning field of in vivo DNA nanotechnology. Toward this goal, the heterochiral circuit depicted in Figure 4a could easily be employed as a bioorthogonal sensor for oncogenic microRNA-155. Moving forward, it will be important to explore the operation of heterochiral strand-displacement circuitry in live cells.

## 4.2 Materials and Methods

### 4.2.1 General

. Oligonucleotides were either purchased from Integrated DNA Technologies (Coralville,IA) or prepared by solid-phase synthesis on an Expedite 8909 DNA/RNA synthesizer. DNA synthesis reagents and D-nucleoside phosphoramidites were purchased from Glen Research (Sterling, Va), and L-nucleoside phosphoramidites were purchased from ChemGenes (Wilmington, Ma). Black Hole Quencher 2 (BHQ2) and Black Hole Quencher 3 (BHQ3) CPG resins were purchased from LGC Biosearch Technologies (Petaluma, CA). [Gamma-$^{32}$P]ATP was purchased from Perkin Elmer (Waltham, MA). Fluorescent dyes (NHS Cy3 and NHS Cy5) were purchased from Lumiprobe Life Science Solutions (Hallendale Beach, FL). Peptide nucleic acids (PNAs) were purchased from PNA Bio Inc. (Newbury Park, CA) at 99.9% purity and were not purified further.

### 4.2.2 Sequence Design

. DNA sequences (Table S1) for the strand-displacement circuit depicted in Fig. 2a were rationally designed and analyzed using NUPACK1 to ensure proper hybridization and eliminate spurious secondary structures. In particular, $PNA_1$ was designed to minimize the number of purine residues in order to ensure adequate solubility in aqueous media. The circuit depicted in Fig. 3a and Fig. 4a was designed around the sequence of microRNA-155 (D-$IN_{RNA}$; Table S1). The PNA sequence was chosen to be complementary to the 5′ end of the microRNA, while the L- and D-DNA strands, as well as reporter complexes, were rationally designed and verified via NUPACK. PNA melting temperatures were approximated using the PNA Tool from PNA Bio Inc. All DNA melting temperatures were approximated using the IDT Oligo Analyzer tool, utilizing the nearest neighbor approximation.

### 4.2.3 Oligonucleotide purification

. Unmodified D-oligonucleotides were purchased from IDT and all L-oligonucleotides were synthesized in house using standard solid-phase synthesis procedures. All oligonucleotides were purified by 20% denaturing polyacrylamide gel electrophoresis (PAGE; 19:1 acrylamide:bisacrylamide). Purified oligonucleotides were excised from the gel and eluted overnight at 23 °C in a buffer consisting of 200 mM NaCl, 10 mM EDTA, and 10 mM Tris (pH 7.6). The solution was then filtered to remove gel fragments, and eluted oligonucleotides were concentrated using an Amicon Ultra Centrifugal Filter (Millipore-Sigma) having a membrane pore size of 3 kDa. Following concentration, all samples were desalted by ethanol precipitation. All 3′ labeled oligonucleotides (Table S1) were prepared using commercial CPG resins functionalized with the corresponding modification (e.g. BHQ2) and purified as described above. Fluorescent dyes (N-hydroxysuccinimide esters) were conjugated to the 5′ end of oligonucleotides via a 5′ amino modification installed at the time of synthesis. Conjugation reactions were performed by combining the unpurified amino modified oligonucleotide ( 20 nmol) with the appropriate dye NHS ester (5 mM final concentration) in 0.1 mL of 0.1 M sodium borate buffer (pH 8.5). Reaction mixtures were vortexed intermittently over 2 hours before being rocked gently overnight at 23 °C. Samples were then passed through a NAP-5 Sephadex G-25 Column (GE Healthcare, Chicago, IL) to remove excess dye and the labeled oligonucleotide was purified by 20% denaturing PAGE as before.

### 4.2.4 Preparation of duplex reaction components.

Duplex reaction components for each stranddisplacement reaction were assembled via a hybridization titration approach in order to achieve an ideal 1:1 ratio of the corresponding strands. Here, one strand was held constant at 5 $\mu$M while the concentration of the second strand was varied across a narrow range around 5 $\mu$M. All hybridization mixtures contained the appropriate amount of each strand, 300 mM NaCl, 1 mM EDTA, 10 mM Tris (pH 7.6) and were heated to 90 °C for 3 minutes then cooled slowly to room temperature over 1 hour. The extent of hybridization was

quantified by 20% native PAGE (19:1 acrylamide:bisacrylamide) after staining with either ethidium bromide (EtBr) or, in the case of fluorescently labeled strands, fluorescence scanning with excitation/emission wavelengths at either 532 nm/560 nm (longpass filter; Cy3) or 635 nm/660 nm (longpass filter; Cy5) on a Typhoon FLA 9500 (GE Healthcare, Chicago, IL). Only those mixtures having an ideal 1:1 ratio of strands (i.e. no single-stranded oligonucleotide remained) were used further.

### 4.2.5 Monitoring of heterochiral strand-displacement reactions by spectrofluorimetry.

Eachstrand displacement reaction was monitored using a GloMax Discover multi-well plate reader from Promega Corp. (Madison, WI). Unless stated otherwise, all reactions contained 500 nM of the indicated reaction components, 300 mM NaCl, 1 mM EDTA, and 10 mM Tris (pH 7.6) and were carried out at 23 °C. Reactions involving D-$IN_{RNA}$ (Fig. 4) were carried out at 37 °C. Reaction mixtures were prepared to a final volume of 20 $\mu$L, transferred to a 384-well microplate, and initiated by the addition of the indicated amount of input strand. The fluorescence intensity of D-reporter complexes was monitored with excitation/emission wavelengths at 520 nm/580-640 nm (bandpass filter; Cy3), while the fluorescence intensity of Lreporter complexes was monitored with excitation/emission wavelengths at 627 nm/660-720 nm (bandpass filter; Cy5). All fluorescence data were normalized to a triggered reporter representing the maximum achievable signal using the following equation:

$$F_n = \frac{F - F_0}{F_c - F_0}$$

Where $F_n$ is the normalized fluorescence intensity, $F$ is the measured fluorescence, $F_0$ is the quenched fluorescence, and $F_c$ is the control fluorescence at each time a measurement was taken. This normalization equation allows for us to account for the loss in signal due to photobleaching, and enables the direct comparison of the different fluorophores representing each chiral system.

### 4.2.6 Monitoring of heterochiral strand-displacement reactions by native PAGE

In some instances, heterochiral strand-displacement reactions were analyzed by 20% native PAGE (19:1 acrylamide:bisacrylamide) (Fig. S1 and S4). Reactions were prepared as described above and incubated for 2 hours at 23 °C before an aliquot was taken (5 $\mu$L) and loaded onto a running gel. Native gels were run at 140 volts for at least 6 hours at 23 °C before being imaged as described above.

## 4.3 L-DNA-Based Catalytic Hairpin Assembly Circuit*

Due to the low abundance of most nucleic acid biomarkers in biological fluids and tissues, analytical application of DNA nanodevices often requires signal amplification. Thus, it is not surprising that significant effort has gone into engineering non-enzymatic DNA amplifier circuits that can detect and amplify nucleic acid signals based on strand-displacement mechanisms [165]. Examples of DNA amplifiers include entropy driven catalytic circuits [46], hybridization chain reactions [170] and various DNAzyme-based systems [171]. Perhaps one of the most versatile DNA amplifiers is the catalytic hairpin assembly (CHA), originally developed by Pierce and coworkers [44]. CHA circuits utilize a pair of complementary DNA hairpins to achieve isothermal, enzyme-free, signal amplification. Spontaneous hybridization between the two hairpins is kinetically hindered because the complementary sequence domains are embedded within the hairpin stems. However, in the presence of a target input strand, one of the hairpins can be opened via toehold-mediated strand-displacement reactions, which in turn enable the assembly (hybridization) of both hairpins. During this assembly process, the input strand is displaced from the annealed hairpin complex, allowing it to initiate further rounds of hairpin opening and assembly. CHA circuits provide rapid and efficient signal amplification with minimal background and fast turnover rates. Consequently, CHA circuits have been adapted to a variety of analytical applications, including the detection of quantification of therapeutically relevant nucleic acids in vitro and in living cells [172] [173] [53].

Despite the promise of DNA amplifiers in low-abundance biomarker discovery and clinical diagnosis, the straightforward implementation of such devices in harsh biological environments remains challenging for several reasons. In particular, natural DNA is susceptible to nuclease mediated degradation and non-specific interactions with other nucleic acids and proteins, both of which can lead to high background and/or poor signal amplification in living cells [12]. Although modifications of the 2′-OH group of the ribose sugar (e.g., 2′-O-methyl ribonucleotides [174] [175] and locked nucleic acids [53] [176]), as well as the phosphate backbone modifications

*Reprinted with permission from "L-dna based catalytic hairpin assembly circuit" by Adam M. Kabza and Jonathan T. Sczepanski, 2017 *Molecules*, 25, pp. 947

(e.g., phosphorothioates) [177], can confer nuclease stability, such modified oligonucleotides still have the potential for off-target hybridization, and in some cases, cellular toxicity [178]. Importantly, the majority of modified oligonucleotides have altered kinetic and thermodynamic properties relative to native DNA, making it very difficult to apply established design principles to the development of amplifier circuits composed of such polymers. Therefore, developing robust DNA amplifiers capable of catalytic amplification in biological environments remains an important challenge.

Recently, we challenged the idea of classical nucleic acid modifications by employing L-DNA, the enantiomer of natural D-DNA, in DNA circuit design. L-DNA is an ideal oligonucleotide analog because it is completely nuclease resistant, yet has identical kinetic and thermodynamic properties as its native counterpart, D-DNA [179]. Furthermore, L-oligonucleotides are incapable of forming contiguous WC base pairs with the native polymer [180] [123]. Thus, L-DNA avoids off-target interactions with myriad of cellular nucleic acids. Nevertheless, we previously reported a method to interface specific nucleic acid targets with L-DNA using strand-displacement reactions [125]. This approach, termed 'heterochiral' stand-displacement, employs an achiral peptide nucleic acid (PNA) in order to transfer sequence information between oligonucleotide enantiomers (Figure 4.6). The reaction involves of a complex between an achiral PNA strand and an L-DNA strand (L-OUT). We refer to this complex as an 'inversion gate'. Importantly, a single-stranded toehold domain t* resides on the achiral PNA strand, which facilitates binding of a D-input strand (D-IN) to the inversion gate via t/t* and subsequent displacement of the incumbent L-DNA strand (L-OUT) or vice versa. In this way, any D-oligonucleotide input, including disease biomarkers, can be sequence specifically interfaced with bio-stable L-DNA nanodevices or circuits, providing a promising approach for overcoming several key limitations of using such devices in cells or other harsh biological environments. For example, we recently used this approach to interface oncogenic microRNAs with an L-RNA-based fluorescent biosensor, enabling real-time imaging of microRNA expression levels in living mammalian cells [102]. Despite the potential advantages of L-DNA/RNA based devices, a heterochiral L-DNA amplifier circuit has not previously been re-

ported.

Here, we report the design and implementation of the first L-DNA amplifier circuit capable of detecting native D-oligonucleotides. The amplifier consists of a single PNA/L-DNA inversion gate, the output of which initiates an L-DNA-based CHA circuit allowing for the detection of the native D-input, microRNA-155 (miR-155), at sub-stoichiometric concentrations. We show that both D-DNA and L-DNA versions of the optimized amplifier circuit behave similarly, achieving signal amplification under physiological conditions. However, only the L-DNA amplifier retains faithful operation in the presence of 10% FBS. Overall, this work demonstrates that CHA circuits constructed from L-DNA, together with a heterochiral inversion gate, provide a robust and straightforward approach for detection low-abundance nucleic acids within harsh biological environments.

## 4.4 Results

Our goal was to design a CHA circuit comprised of L-DNA that could ultimately be interfaced with disease-relevant nucleic acid biomarkers. The target chosen for this study was miR-155, a prototypical oncogenic miR associated with various malignancies [181]. The overall heterochiral CHA amplifier circuit is illustrated in Figure 4.6. The reaction between D-miR-155 and the miR-155-specific inversion gate (L-$A_{155}$) results in the displacement of L-$OUT_{155}$, which subsequently initiates the opening of hairpin L-H1 via toehold domain 3*. The newly exposed single-stranded domains on L-H1 (5 and 6) then hybridize to hairpin L-H2 (via toehold-domain 5*), triggering the formation of product duplex L-H1/H2 and displacement of L-$OUT_{155}$ from L-H1. The recycled L-$OUT_{155}$ strand can then go on to initiate further rounds of hairpin L-H1 opening and catalysis. The reaction can be monitored by a reporter complex (L-R) that reacts with domain 4 on hairpin L-H1 (via 4*) only after opening of L-H1. The choice of target immediately restricts the overall circuit design because the sequence of the inversion gate ($A_1$) must have partially complementarity with sequence with D-miR-155 (domains 1-3). In turn, the toehold domain (3*) on hairpin L-H1 is also dependent on the sequence of miR-155. However, beyond domain 3, the remaining sequences for both hairpins H1 and H2, as well as the fluorescent reporter duplex L-R may be chosen as required for the particular application of the system.

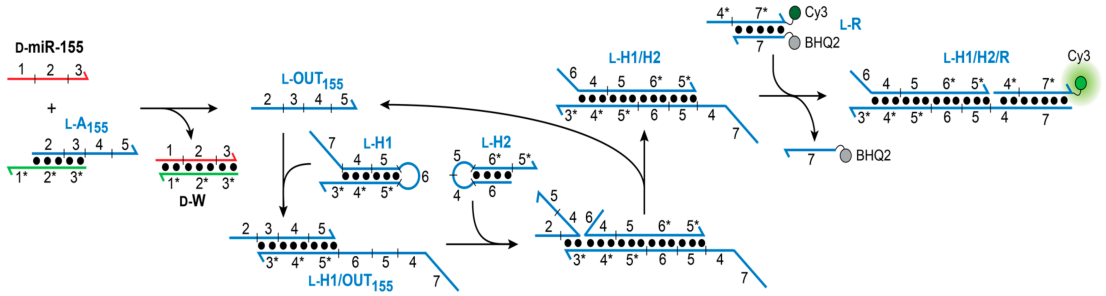


Figure 4.6: Schematic illustration of the heterochiral L-CHA circuit. Sequences of all strands are listed in Figure C.2. D-MiR-155 RNA is colored red. Adapted from Ref. 126 MDPI open access journal.

Following principles originally established by Ellington and coworkers [182], we designed and tested a series of hairpins by varying the length and nucleotide composition of complementary domains (domains 4-6). To increase the efficiency of this process, all experiments were carried out using D-DNA and hairpin assembly reactions were monitored by native gel electrophoresis (Figures 4.7 and 4.8). Ultimately, we identified a pair of hairpins, D-H1 and D-H2 (Table S1), which retained high stability under simulated physiological conditions (i.e., 50 mM KCl, 20 mM NaCl, 1 mM $MgCl_2$, pH 7.6, 37 °C), yet rapidly assembled into complex D-H1/H2 the presence of the initiator strand (D-$OUT_{155}$). Therefore, all further studies were based on these two hairpins. As shown in Figure 4.9a, the rate of the CHA reaction between D-H1 and D-H2 was highly dependent on the concentration of initiator D-$OUT_1$, as monitored by fluorescence (Cy3) using reporter D-R. When 2 nM D-$OUT_{155}$ was added, i.e., 100-fold lower concentration that the hairpins and reporter, 40% maximal fluorescent signal was observed after 3 h, representing 20-fold signal amplification. This data indicates that this CHA circuit can provide rapid and efficient signal amplification under physiological conditions. We note that despite the presence of stoichiometric initiator (200 nM D-$OUT_{155}$), the CHA circuit failed to achieve the maximum fluorescence signal for the reporter complex (D-R), indicating incomplete hairpin opening and/or reporter activation. Importantly, a negligible fluorescence signal was observed for up to 2 h prior to the addition of D-$IN_1$ to the reaction (Figure 4.9a), confirming that hairpins D-H1 and D-H2 do not spontaneously hybridize in the absence of the initiator strand. Furthermore, a scrambled version of D-$OUT_{155}$ (D-$OUT_S$) failed to initiate the reaction, demonstrating the specificity of this CHA circuit (Figure 4.9a).

Having confirmed the proper operation of the CHA circuit using D-DNA components, we prepare L-DNA versions of the same components (L-$OUT_{155}$, L-H1, L-H2, and L-R) using solid-phase phosphoramidites chemistry (Table S1). Overall, the L-DNA CHA circuit behaved similarly to its D-DNA counterpart (Figure 4.9b), but with a somewhat reduced rate of signal amplification. Initial rates for the D- and L-CHA reactions in the presence of stoichiometric initiator (200 nM) were calculated to be 54.02 $\pm$ 2.64 $min^{-1}$ and 24.78 $\pm$ 1.0 $min^{-1}$, respectively. We attribute this discrepancy to potential differences in oligonucleotide quality, as well as other experimental lim

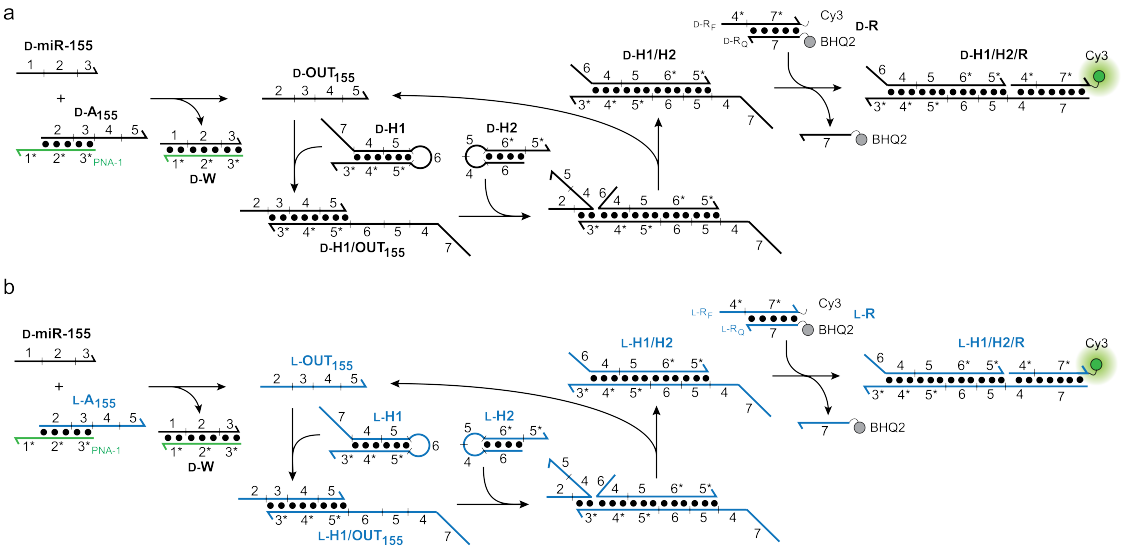


Figure 4.7: Schematic illustration of the D-DNA (a) and L-DNA (b) versions of the full CHA circuit. Sequences of all strands are listed in Figure C.2. Adapted from Ref. 126 MDPI open access journal.

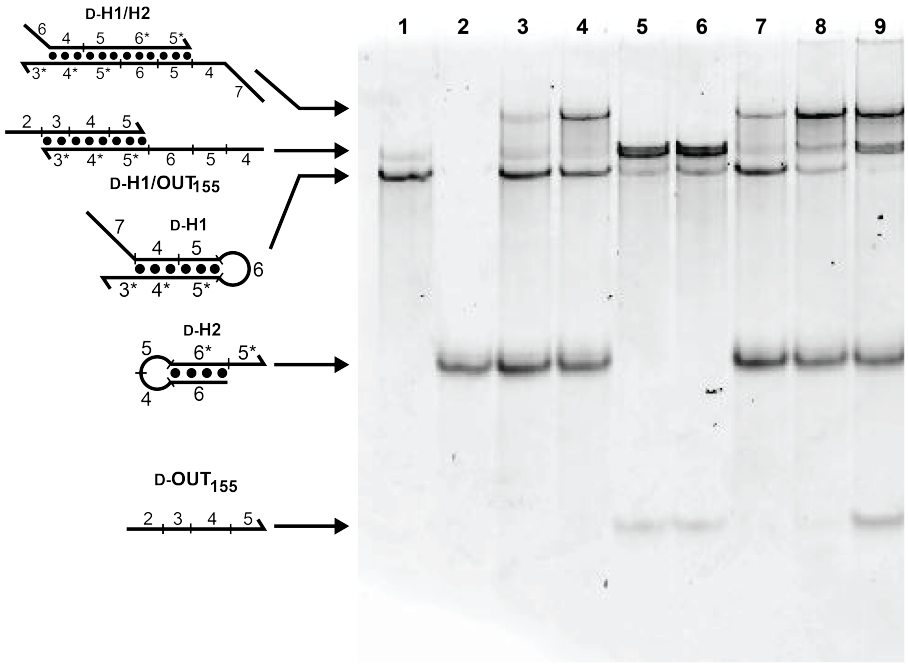


Figure 4.8: Native PAGE (20%; 19:1 acrylamide:bisacrylamide) analysis of the CHA reaction. Reaction conditions are identical to those described in Figure X above. Lane 1: D-H1; lane 2: D-H2; lane 3: D-H1 and D-H2; lane 4: D-H1 and D-H2 after annealing; lane 5: D-H1 and D-$OUT_{155}$; lane 6: D-H1 and D-$OUT_{155}$ after annealing; lane 7: D-H1, D-H2, and D-$OUT_{155}$ (4 nM); lane 8: D-H1, D-H2, and D-$OUT_{155}$ (40 nM); lane 9: D-H1, D-H2, and D-$OUT_{155}$ (200 nM). Unless stated otherwise, the concentration of all components was 200 nM. Adapted from Ref. 126 MDPI open access journal.

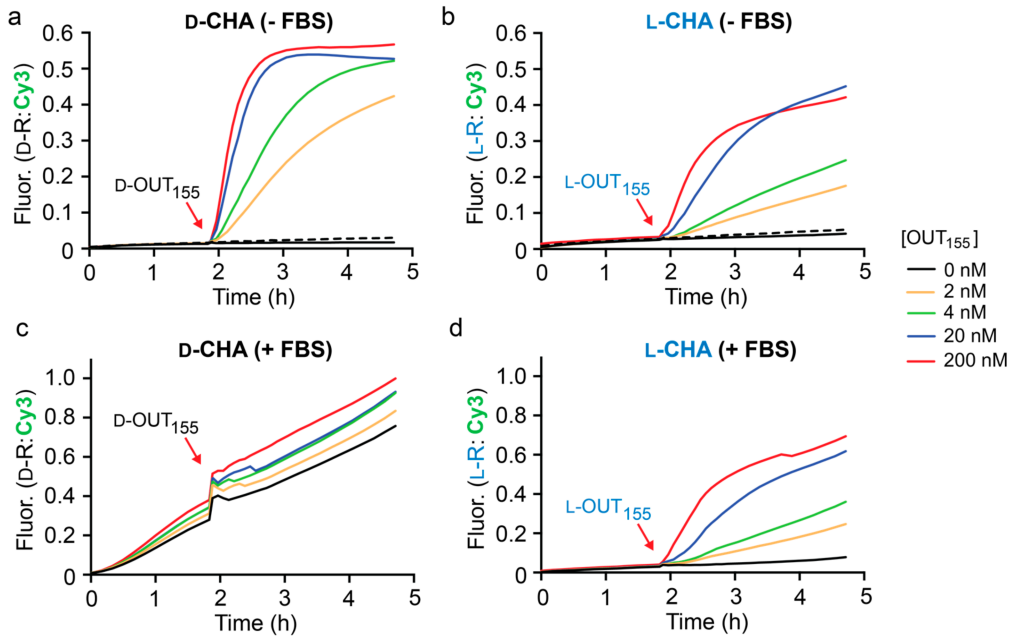


Figure 4.9: Fluorescence monitoring (Cy3) of CHA reactions in the absence (a,b) and presence (c,d) of 10% fetal bovine serum (FBS). All reaction mixtures contained 200 nM hairpins (H1 and H2) and 200 nM reporter complex (R) in the indicated stereochemistry, along with either 0% or 10% FBS, 50 mM KCl, 20 mM NaCl, 1 mM $MgCl_2$, and 25 mM TRIS (pH 7.6). Reactions were initiated with the indicated concentration of either D- or L-$OUT_{155}$ and were carried out at 37 °C. CHA reactions initiated with a scrambled input $OUT_S$ (200 nM) are indicated by dotted lines. Fluorescence (Fluor.) in all figures is reported in units such that 0.0 and 1.0 are the fluorescence of the quenched and activated reporter complex, respectively, at 200 nM. Average fluorescence data from triplicate experiments is plotted. Adapted from Ref. 126 MDPI open access journal.

-itations, such as pipetting and concentration errors. Nevertheless, the L-CHA circuit generated 20% maximal fluorescent signal in the presence of 2 nM L-$OUT_{155}$, representing ≈10-fold signal amplification. To the best of our knowledge, this represents the first example of a nucleic acid amplifier comprised entirely of mirror-image L-DNA.

With both D- and L-versions of the CHA circuit in hand, we compared their performance in the presence of 10% fetal bovine serum (FBS) as a model biological environment (Figure 4.9c,d). We have previously shown that both L-DNA and L-RNA are stable in 10% FBS for long periods of time [102] [183]. As before, the circuit components were allowed to incubate for 2 h prior to the addition of the in initiator strand $OUT_{155}$. As expected, the D-CHA circuit was rapidly degraded during the 2 h pre-incubation period, as evident by an initiator-independent gain in fluorescence signal (i.e., leak) (Figure 4.9c). Moreover, addition of the initiator strand (D-$OUT_{155}$) to the D-CHA circuit after 2 h failed to promote any meaningful signal amplification relative to background (i.e., no initiator). In contrast, the presence of 10% FBS had little effect on the operation of the L-DNA version of the CHA circuit (Figure 4.9d). Negligible fluorescence signal was observed during the 2 h pre-incubation period, indicating that the L-DNA circuit components, and in particular hairpins L-H1 and L-H2, remained intact in the presence of 10% FBS. This was confirmed by gel electrophoresis (Figure 4.10). Importantly, initiation of the L-CHA reaction using L-$OUT_{155}$ resulted in a concentration dependent fluorescence response, again reaching 20% maximal signal in the presence of 100-fold lower concentration of L-$OUT_{155}$ relative to reporter after 3 h. Overall, the fluorescent data obtained for the L-CHA circuit in the presence of 10% FBS (Figure 4.9d) closely mirrored data obtained in its absence (Figure 4.9b), demonstrating that complex biological matrixes do not significantly interfere with the operation of L-DNA-based CHA reactions.

The L-CHA reactions depicted in Figure 4.11 were initiated directly using either D- or L-$OUT_{155}$. However, our ultimate goal was to utilize an L-CHA circuit to detect D-miR-155, which required an inversion gate be placed upstream of the L-DNA hairpins (Figure 4.6). As discussed above, the sequence of the inversion gate (L-$A_{155}$) was dictated by the sequence of D-miR-155 (Table S1), and was designed such that binding of D-miR-155 to the achiral PNA toehold domain

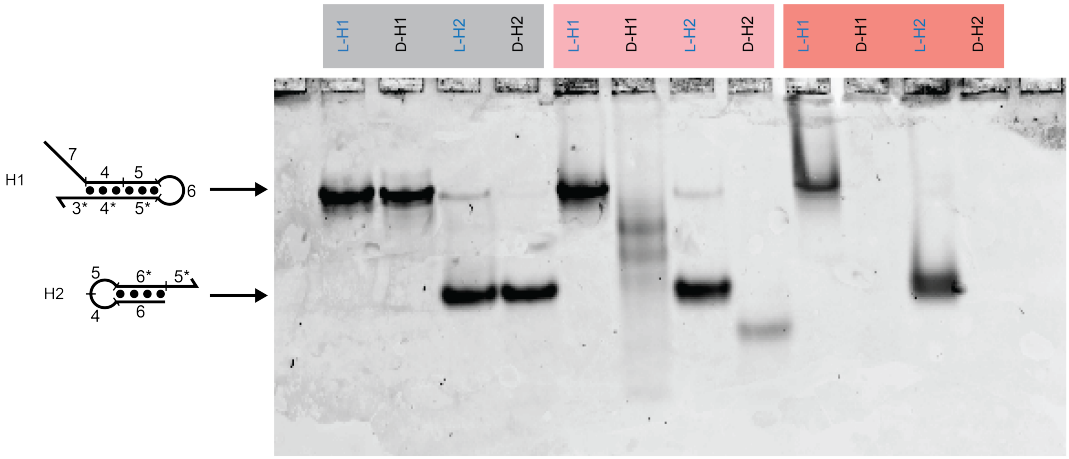


Figure 4.10: Denaturing PAGE (20%; 19:1 acrylamide:bisacrylamide) analysis of hairpins H1 and H2 in the presence of different amounts of FBS. The indicated hairpin (200 nM) was incubated with either 0%, 10%, or 100% FBS for 6 hours at 37 °C in a reaction mixture containing 50 mM KCl, 20 mM NaCl, 1 mM $MgCl_2$, and 25 mM TRIS (pH 7.6) Adapted from Ref. 126 MDPI open access journal.

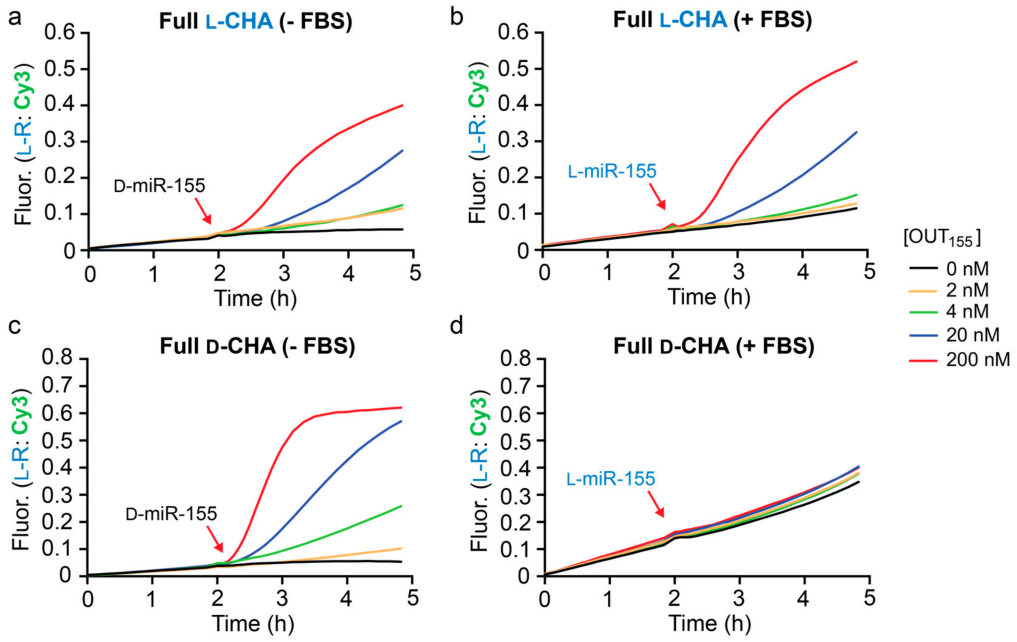


Figure 4.11: Fluorescence monitoring (Cy3) of the full heterochiral CHA circuit in the absence (a,c) and presence (b,d) of 10% FBS. Reaction conditions are identical to those described in Figure 3, except that 200 nM inversion gate $A_{155}$ was also included. Reactions were initiated with the indicated concentration of either D- or L-miR-155 as indicated and were carried out at 37 °C. Average fluorescence data from triplicate experiments is plotted. Adapted from Ref. 126 MDPI open access journal.

(1*) resulted in displacement of the incumbent strand L-OUT$_{155}$, which subsequently initiates the CHA reaction via domains 3/3*. We assembled and tested the full heterochiral CHA circuit depicted in Figure 4.7b, which consisted of L-A$_{155}$, L-H1, L-H2, and L-R1. All concentrations of D-miR-155 input tested resulted in the generation of a fluorescence signal that was greater than background (Figure 4.11a). However, it was clear that these reactions were significantly slower than the corresponding CHA reactions that were directly initiated with L-OUT$_{155}$ (Figure 4.9b). This likely reflects the relatively slow kinetics of the heterochiral strand-displacement reaction between D-miR-155 and L-A$_{155}$ [125]. Despite the reduced rate, however, the heterochiral amplifier was still capable of modest signal amplification (≈3-5-fold).

To test for selectivity, we attempted to initiate the heterochiral CHA reaction with D-miR-155-derived inputs containing either one or two mismatches (D-miR-155$_{M1}$ or D-miR-155$_{M2}$, respectively) in the toehold-binding domain 1 (Figure 4.6 and Table S1). These reactions were carried out for an extended period of time (6 h) to ensure that any small amount of non-specific initiation by the mismatched substrates could be detected through CHA amplification. At 20 nM input concentrations (10-fold less than reporter), both mismatched substrates resulted in significantly less signal generation then D-miR-155 (Figure 4.12), which achieved ≈4-fold amplification during the reaction. Increasing the concentration of both mismatched substrates by 10-fold did not greatly increase the signal generated by the system, allowing the CHA circuit to detect D-miR-155 (20 nM) in the presence of excess mismatched target RNA (200 nM). In all cases, the signal generated by the single and double mismatched substrates were similar. Overall, this data indicates that the heterochiral CHA circuit can discriminate against sequences containing a single mismatch, at least within the toehold domain.

Finally, we tested the full heterochiral CHA circuit in 10% FBS. The circuit maintained functionality in 10% FBS (Figure 4.11b), although with somewhat reduced sensitivity towards D-miR-155 due to a higher background fluorescence signal. This suggests possible circuit leakage due to an uninitiated reaction between the inversion gate (L-A$_1$) and hairpin L-H1 in serum. An L-RNA version of miR-155 (L-miR-155) was employed as the input during these experiments to avoid nu-

clease degradation prior to circuit activation. The full L-CHA circuit remained intact during the 2 h pre-incubation period in the presence of 10% FBS and treatment with 20 nM L-miR-155 resulted in the generation of a fluorescence signal equivalent to ≈3-fold amplification. Not surprisingly, incubation of the D-DNA version of the full CHA circuit (D-$A_{155}$, D-H1, D-H2, and D-$R_1$) in 10% FBS resulted in significant circuit leakage during the 2 h pre-incubation period and failed to activate upon the addition of L-miR-155 input (Figure 4.11c), further highlighting the advantage of L-DNA. While further optimization is needed, the above results demonstrate that the heterochiral L-CHA amplifier circuit described herein can be made compatible with the detection of low-abundance nucleic acids in complex biological samples.

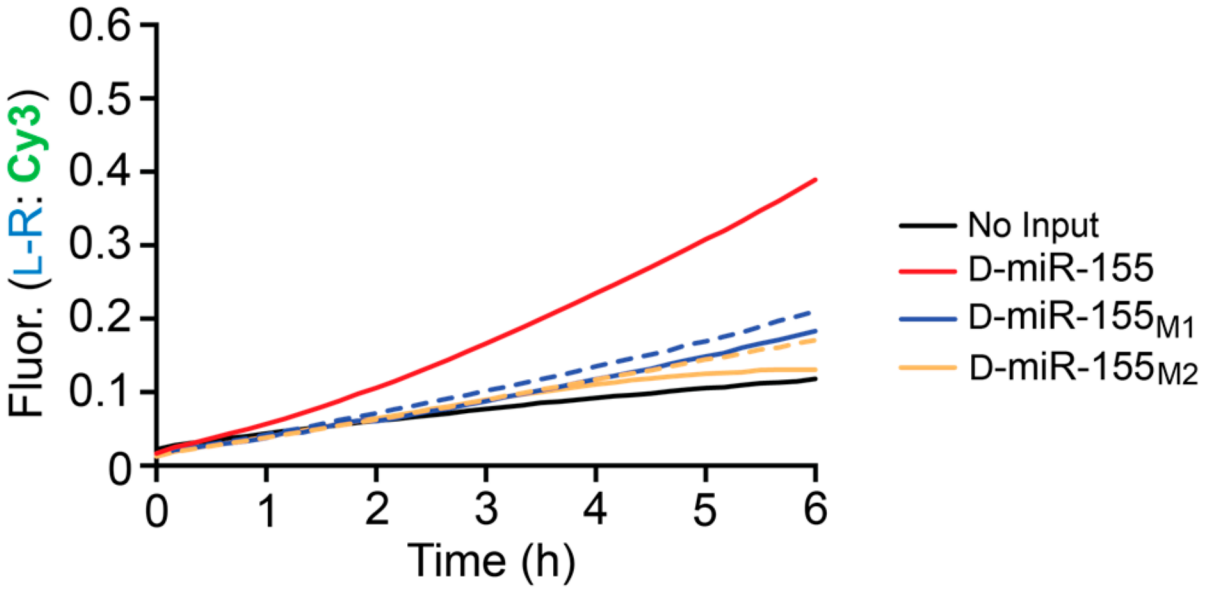


Figure 4.12: Mismatch discrimination by the full heterochiral CHA circuit. Reaction conditions are identical to those described in Figure 4. Reactions were initiated with either 20 nM input (solid lines) or 200 nM input (dotted lines) and were carried out at 37 °C. Adapted from Ref. 126 MDPI open access journal.

## 4.5 Materials and Methods

### 4.5.1 General

Oligonucleotides were either purchased from Integrated DNA Technologies (Coralville, IA, USA) or prepared by solid-phase synthesis on an Expedite 8909 DNA/RNA synthesizer (ThermoFisher Scientific, Waltham, MA, USA). Synthesizer reagents, D-nucleoside phosphoramidites, and Cy3 phosphoramidites were purchased from Glen Research (Sterling, VA, USA). L-nucleoside phosphoramidites were purchased from ChemGenes (Wilmington, MA, USA). Black Hole Quencher 2 resins were purchased from LGC Biosearch Technologies (Petaluma, CA, USA). Peptide nucleic acids (PNA) were purchased from PNA Bio Inc. (Newbury Park, CA, USA) at 99.9% purity and were not purified further. All other reagents were purchased from Sigma Aldrich (St. Louis, MO, USA).

### 4.5.2 Oligonucleotide Purification and Assembly

Unmodified D-oligonucleotides were purchased from IDT. All L-oligonucleotides were synthesized in house following the manufacturers recommended procedures, and completed L-oligonucleotides were deprotected using a 1:1 mixture of aqueous ammonium hydroxide and aqueous methylamine for 30 min at 65 °C. All oligonucleotides were purified by 20% denaturing polyacrylamide gel electrophoresis (PAGE, 19:1 acrylamide:bisacrylamide). Purified material was excised from the gel and eluted overnight at 23 °C in Buffer EB (200 mM NaCl, 10 mM EDTA, and 10 mM Tris pH 7.5). The solution was filtered to remove gel fragments, and the eluent was precipitated with ethanol. Duplex components ($A_{155}$ and R) for each CHA circuit were assembled via a hybridization titration approach in order to achieve an ideal 1:1 ratio of the corresponding strands. Here, one strand was held constant at 1 $\mu$M while the concentration of the second strand was varied across a narrow range around 1 $\mu$M (0.80-1.20 $\mu$M in 0.05 $\mu$M increments). All hybridization mixtures contained the appropriate amount of each strand, 300 mM NaCl, 1 mM EDTA, 10 mM Tris (pH 7.6) and were heated to 90 °C for 3 min then cooled slowly to room temperature over 2 h. The extent of

hybridization was quantified by 20% native PAGE (19:1 acrylamide:bisacrylamide) after staining with SYBR Gold (ThermoFisher Scientific, Waltham, MA, USA). Only those mixtures having an ideal 1:1 ratio of strands (i.e., no single-stranded oligonucleotide remained) were used further. The ideal 1:1 ratio of hairpins H1 and H2 strands were determined in a similar manner.

### 4.5.3 Fluorescence Monitoring of CHA Reactions

CHA reactions were monitored using a GloMax Discover multi-well plate reader from Promega Corp. (Madison, WI, USA). All reaction mixtures contained 200 nM each H1, H2, and reporter R in the indicated stereochemistry, along with either 0% or 10% FBS, 50 mM KCl, 20 mM NaCl, 1 mM $MgCl_2$, and 25 mM TRIS (pH 7.6). For reaction containing the full CHA circuit (Figure 4), 200 nM inversion gate $A_{155}$ was also included. Reactions were prepared to a final volume of 20 $\mu$L and transferred to a 384-well black-walled microplate. After the 2 h pre-incubation at 37 °C, the indicated concentration of initiator was added ($OUT_{155}$ for CHA only reactions or miR-155 for the full circuit) and the reaction allowed to proceed for 3 h. Fluorescence was monitored with excitation/emission wavelengths at 520/580-640 nm (bandpass filter: Cy3). Data was normalized to a control representing the maximum achievable signal using Equation (1):

$$F_n = \frac{F - F_0}{F_c - F_0}$$

where $F_n$ is the normalized fluorescence intensity, $F$ is the measured fluorescence, $F_0$ is the fluorescence of the quenched reporter, and $F_c$ is the fluorescence of the activated reporter at each time a measurement was taken.

### 4.5.4 Monitoring of Heterochiral Strand-Displacement Reactions by Native PAGE.

In some instances, CHA reactions were analyzed by 20% native PAGE (19:1 acrylamide:bisacrylamide) (Figure S2). Reactions were prepared as described above and incubated for 2 h at 37 °C before an aliquot was taken (5 $\mu$L) and loaded onto a running gel. Native gels were run at 140 volts for at

least 6 h at 23 °C before being imaged as described above

# 5. SUMMARY AND OUTLOOK

## 5.1 Summary

The work presented in this dissertation details the discovery and application of a novel strand-displacement reaction, the heterochiral strand-displacement reaction, which is the first example of sequence specific information transfer between unnatural L-DNA and natural D-DNA. Chapter 1 provides a general background of DNA and RNA describing their structure, biological function, and synthetic applications. Contemporary topics of DNA nanotechnology are discussed, including DNA strand displacement reactions, DNA computation, DNA cryptography, and aptamers. The generality of nucleic acids is discussed, stressing that all nucleic acid technologies may be integrated with one another through standard WC base pairing. L-oligonucleotides are introduced in the context of modified nucleic acids and their applications in aptamer technology are discussed. Importantly, chapter 1 establishes the current challenges facing DNA nanotechnologies, especially their application in living systems and states how we intend to address these challenges.

### 5.1.1 A chemically modified L-RNA aptamer

Chapter two focuses on the development of a chemically modified L-RNA aptamer that binds precursor microRNA-19a [124]. In this work, an L-RNA aptamer is selected with each uridine residue replaced with a chemically modified aminoallyl-uridine residue. L-aptamers bind D-RNA targets through tertiary interactions and we hypothesized that by reducing the overall negative charge of the L-aptamer via a positively charged chemically modified nucleotide, that we could increase the binding affinity of the aptamer for its target. We successfully isolated an L-RNA aptamer with the highest binding affinity of any L-aptamer for an RNA target. A detailed structural analysis was performed, in which we systematically replaced the modified uridine residues with cytosine residues, revealing which chemical modifications are absolutely necessary for function. In fact, nearly every chemically modified uridine residue was required for tight binding. We carried

out an in-line probing analysis which revealed that this aptamer binds the loop region of the pre-miR-19a hairpin. This is precisely the region of the target that Dicer binds to for processing. We performed a series of Dicer inhibition experiments, demonstrating the ability of MLRA to inhibit Dicer mediated cleavage of pre-miR-19a, stopping the generation of mature microRNA-19a. To test the specificity of MLRA for its target, pre-miR-19a, we transcribed 10 off-target RNA hairpins, including 3 from the same cluster as the target, and carried out an EMSA which clearly demonstrated that MLRA binds only its proper target. Similarly, we synthesized multiple off-target Dicer substrate hairpins and performed Dicer inhibition experiments. MLRA did not inhibit Dicer cleavage of any RNA molecule besides pre-miR-19a. Overall this work describes the first example of a chemically modified L-aptamer, expanding the chemical toolkit available to mirror image aptamers and providing impetus for the application of L-aptamers as oligonucleotide therapeutics against endogenous RNA species.

### 5.1.2 A Mirror Image FRET Assay for the Identification of Small Molecule RNA Inhibitors

Chapter 3 describes the design and execution of a mirror-image FRET assay for the identification of small molecule RNA inhibitors with specific activity. There are sparse examples of high throughput assays capable of screening for small molecules which bind a structured RNA specifically. A key challenge that this technology addresses is targeting RNA tertiary, rather than secondary structure. Essentially, an L-aptamer and its D-RNA target are labelled with a pair of FRET active fluorophores, such that upon binding, a positive FRET signal is generated. Consequently, if binding is prohibited, such as with a small molecule competitor, no FRET signal is observed. We demonstrate a FRET active fluorescent labeling scheme for the aptamer and target, including various alternative labeling schemes which serve to generalize the application of this approach. Conditions were chosen to mimic high throughput screening conditions. Furthermore, a second aptamer and target pair was utilized to demonstrate the generalizability of this procedure. An L-DNA aptamer and its target, pre-miR-155, were chosen because this aptamer is DNA, not RNA as in the original pair, and the target is a different sequence. Despite these differences, an identical FRET knockdown assay could be performed. We performed controls demonstrating that

our inhibitors knock down FRET through target binding and not nonspecific interactions with the aptamer. As a whole this project demonstrates the unique advantages of L-aptamers for applications in biotechnologies.

### 5.1.3 Heterochiral DNA strand-displacement circuits

Chapter 4 details the discovery, partial characterization, and application of heterochiral strand-displacement reactions. The two fundamental reactions utilize a PNA/DNA heteroduplex and are distinguished depending on which polymer strand, DNA or PNA, is the incumbent strand. We define a heterochiral strand displacement with an incumbent PNA, a racemization gate. If the incumbent strand is DNA we define it as an inversion gate. The racemization gate effectively decouples stereochemical information from the sequence information of the input strand, allowing downstream reactions to proceed through either D- or L-stereochemistry circuit components. The inversion gate inverts the chirality associated with a particular nucleic acid sequence from D- to L- or vice versa. Together these two reactions constitute the first examples of translating stereochemical information between enantiomers of oligonucleotides. These reactions make it possible for any existing DNA nanotechnology which utilize strand displacement to have L-oligonucleotides directly integrated into their components. We demonstrate this versatility by using an inversion gate in a catalytic signal amplification circuit, catalytic hairpin assembly (CHA), to detect an endogenously expressed RNA, microRNA-155. By utilizing a fully L-DNA based circuit, we were capable of detecting trace amounts of miR-155 in media containing 10% fetal bovine serum. We simultaneously demonstrate the ineffectiveness of the identical D-DNA circuit which degrades under such harsh conditions. This work, in conjunction with ongoing research in our lab, showcases the superiority of L-DNA to its natural counterpart for the design of complex nucleic acid circuitry capable of functioning under mimicked harsh biological conditions.

## 5.2 Outlook

This collective body of work represents an entirely new area of research in DNA nanotechnology by dissolving boundary between mirror image oligonucleotides. The enantiomer of natural

D-DNA, L-DNA, has three key characteristics which make it a superior modification for dynamic DNA nanotechnologies: 1) L-DNA is nuclease resistant, 2) L-DNA is incapable of forming contiguous WC base pairs with D-DNA, and 3) L-DNA has identical thermodynamic properties as D-DNA. Ongoing work in our lab continues to demonstrate ease of design and application of these styles of strand displacement reactions. Recently we have shown sequence specific detection of micro-RNA-155, which was artificially up-regulated in HeLa cells, through an inversion gate which releases an incumbent mango aptamer that subsequently folds into its active fluorescent conformation, thus coupling miR-155 detection to a fluorescent signal [102]. Other work in this area in our group is focused on sequence-detection based attenuation of DNA therapeutics, synthesis of L-DNA nanostructures (tetrahedrons), as well as studying delivery and trafficking of L-nucleic acids inside live cells. Despite the advantages L-DNA enjoys, there are numerous challenges which still require further study: 1) Increasing circuit complexity and depressing background leak signal, 2) delivery and trafficking of L-oligonucleotides within cells, and 3) developing synthetic strategies to generate much larger (>120nt) L-DNA fragments, potentially thousands of bases in length.

### 5.2.1 Increasing circuit complexity

Although we have designed and performed the fundamental heterochiral strand displacement reactions and applied them to create novel L-DNA circuits and detectors, much work remains to be done towards characterizing, developing, and testing L-nucleic acid circuits. Recent work by my colleagues has focused on the characterization of the kinetics of heterochiral strand displacement reactions. Modeling this work after Winfree and coworkers [25] previously published results, we are working to determine how parameters such as toehold length, base composition, branch-migration domain length, and salt concentration affect the rate of heterochiral strand displacement. This work is critical for future ease of circuit design and scalability. When all of the thermodynamic and kinetic parameters of this unique system are understood, it will be possible to design both in vitro and in vivo systems with complexity matching that of traditional homochiral systems.

Heterochiral strand-displacement reactions are still in the earliest stages of development. Consequently, it is difficult to predict where the application of such a technology would be most appro-

priate in the broad area of DNA nanotechnology. However, one area of research in particular that L-nucleic acids have immense potential for, is DNA cryptography and data storage. Specifically, the lack of sequencing technologies for L-oligonucleotides, as well as its immunity to enzymatic processing, make L-DNA an unrivaled candidate for the safe coding and storage of sensitive information. Already, laboratories are transcribing historical records, astronomical and meteorological data, as well as music and literature, onto DNA strands for long term storage of valuable cultural and scientific data. Applying L-nucleic acids in this context is now theoretically possible. On its own, DNA cryptography and data storage is a budding area of research, and it is expected that as advancements are made in this area, in parallel with heterochiral DNA technologies, there will be tremendous opportunities for collaboration and further growth of both fields. In particular, it is likely that upon broader application of L-nucleic acids for in biotechnology, technologies for sequencing [84] and enzymatically processing L-DNAs will likely concomitantly be developed, enriching our understanding of protein-nucleic acid interactions and the potential reasons for natures choice of D-DNA over L-DNA.

### 5.2.2 Delivery and trafficking of L-oligonucleotides within cells

The application of nucleic acid technologies in living cells still poses numerous challenges [184] [185] [186]. The polyanionic nature of the DNA phosphate backbone makes it impossible for oligonucleotides to directly pass through the phospholipid bilayer of cells. The most common methods for DNA transfection are polycationic transfection reagents [187] [188], which effectively cancel the negative charge of nucleic acid thus promoting endocytosis. Although these technologies have proven to be useful methods for nucleic acid delivery, almost any new set of oligonucleotides require optimization of transfection conditions. This lack of systematicity in transfection protocols has impeded progress in the application of nucleic acids as therapeutics. Furthermore, it is still poorly understood what parameters cause endosomal escape as well as what factors affect the trafficking of oligonucleotides that have made it into the cytoplasm [189] [190]. In our lab for example, we have observed that different fluorescent modifications cause identical DNA strands to be trafficked to different areas within cells. Looking to the future there are two critical

issues that stand out and must be addressed regarding the application of heterochiral DNA nanotechnologies (and by extension all DNA nanotechnologies) in vivo: 1) A more comprehensive understanding of the transfection conditions and cellular localization must be gained. Specifically, for heterochiral nucleic acid systems, delivery conditions and trafficking of all combinations of chimeric oligonucleotides must be better understood. 2) Determining all off-target interactions of L-DNA with endogenous cellular entities. Already in our lab we have observed a nonspecific binding interaction between an L-G-quadruplex and the Polycomb Repressive Complex 2 (PCR2) protein [191]. Further study through various pull-down and foot-printing methods is required to observe what endogenous proteins and nucleic acids interact with mirror image nucleic acids.

### 5.2.3 Developing improved L-DNA synthetic procedures

In this thesis and other work in our group, we have established that the utilization of unnatural stereoisomers of biologically relevant entities is a useful and powerful technique. Moving into the future it will be critical to scale up synthetic procedures for modified oligonucleotides, specifically L-oligonucleotides, in order to generate large nucleic acid polymers (<40kDa) synthetically. The ability to synthesize highly modified oligonucleotides, hundreds of bases in length, would greatly enrich our ability to study chemically modified large scale DNA architectures, simplify selections on large random libraries, and make it possible to replicate large natural nucleic acid architectures, such as nucleosomes with site specific modifications, for study. Currently the limit on L-DNA polymer length is $\approx$150 nucleotides. Conversely, D-DNA constructs several thousands of bases in length can be synthesized using G-block assembly [192]. However, G-block assembly requires first a solid phase synthesis of multiple overlapping duplexes followed by assembly of these duplexes into the final polymer by polymerase enzymes through multiple cycles of PCR. There is a critical need for the development of heterochiral enzymes, capable of interacting with stereoisomers of their natural targets. Not only would developing such enzymes further our understanding of the stereospecificity of nature, but also reshape how we design medical biotechnologies. The recent Nobel Laureate, Dr. Francis Arnold, received the Nobel prize for her work on synthetically evolving enzymes to perform unnatural chemistry [193] [194] [195]. In one example, a stereospe-

cific enzyme is evolved to invert the stereospecificity of the active site [196]. This work provides impetus for evolving a polymerase capable of accepting and polymerizing L-nucleotides into L-DNA/RNA. Recently, there has also been excitement concerning the enzyme TDT, and its potential ability to perform non-templated enzyme mediated nucleotide addition on oligonucleotides [197]. This is also a promising avenue toward improving oligonucleotide synthesis strategies. As our synthetic capabilities advance, so will the sophistication of all DNA nanotechnology.

### 5.2.4 RNA Nanotechnology and beyond

It is important to note that all of the ideas and technologies discussed herein also apply to RNA polymers. The distinction between RNA and DNA nanotechnology has only recently unfolded. Although RNA shares many commonalities with DNA in terms of base pair design parameters, its reduced stability, and greater structural flexibility provide unique opportunities for engineering complex nanodevices [198]. Already groups have exploited these differences to construct novel 3 dimensional architectures from RNA [199] [200] [201] [202].

Moving forward it will be exciting to see what new areas of research and ideas are unraveled. The simplicity of nucleic acid interactions makes it easy to develop general rules for operating sophisticated nanodevices of all variety. Additionally, nucleic acids are the natural genetic material for all living organisms, making the integration of nucleic acid technologies into biological systems straightforward. As this young area of science continues to mature, it will likely be instrumental in the development of future genetic medicines, synthetic biological systems, and countless unforseeable inventions.

# REFERENCES


[1] J. Watson and F. Crick, "A structure for deoxyribose nucleic acid," *Nature*, vol. 171, pp. 737–738, 1953.

[2] O. T. Avery, C. M. MacLeod, and M. McCarty, "Studies on the chemical nature of the substance inducing transformation of pneumococcal types," *The Journal of Experimental Medicine*, vol. 79, pp. 137–158, 1944.

[3] F. Crick, "Central dogma of molecular biology," *Nature*, vol. 227, pp. 561–563, 1970.

[4] E. Rutherford, "The structure of the atom," *Philosophical Magazine*, pp. 490–498, 1914.

[5] E. Schrodinger, "An undulatory theory of the mechanics of atoms and molecules," *The Physical Review*, vol. 28, pp. 1049–1070, 1926.

[6] P. Dirac, "On the theory of quantum mechanics," *Proceedings of the Royal Society of London*, pp. 661–677, 1926.

[7] L. Bragg, "X-ray crystallography," *Scientific American*, vol. 219, pp. 58–74, 1968.

[8] S. Dokka and Y. Rojanasakul, "Novel non-endocytic delivery of antisense oligonucleotides," *Advanced drug delivery reviews*, vol. 44, no. 1, pp. 35–49, 2000.

[9] S. T. Crooke, S. Wang, T. A. Vickers, W. Shen, and X. hai Liang, "Cellular uptake and trafficking of antisense oligonucleotides," *Nature Biotechnology*, vol. 35, pp. 230–237, 2017.

[10] P. D. Hsu, E. S. Lander, and F. Zhang, "Development and applications of crispr-cas9 for genome engineering," *Cell*, vol. 157, no. 6, pp. 1262–1278, 2014.

[11] D. Y. Zhang and G. Seelig, "Dynamic dna nanotechnology using strand-displacement reactions," *Nature chemistry*, vol. 3, no. 2, p. 103, 2011.

[12] Y.-J. Chen, B. Groves, R. A. Muscat, and G. Seelig, "Dna nanotechnology from the test tube to the cell," *Nature nanotechnology*, vol. 10, no. 9, p. 748, 2015.

[13] J. Chen and N. C. Seeman, "Synthesis from dna of a molecule with the connectivity of a cube," *Nature*, vol. 350, no. 6319, pp. 631–633, 1991.

[14] P. W. Rothemund, "Folding dna to create nanoscale shapes and patterns," *Nature*, vol. 440, no. 7082, pp. 297–302, 2006.

[15] T. H. Hamilton, "Control by estrogen of genetic transcription and translation.," *Science*, 1968.

[16] J. C. Venter, M. D. Adams, E. W. Myers, P. W. Li, R. J. Mural, G. G. Sutton, H. O. Smith, M. Yandell, C. A. Evans, R. A. Holt, *et al.*, "The sequence of the human genome," *science*, vol. 291, no. 5507, pp. 1304–1351, 2001.

[17] P. Andolfatto, "Adaptive evolution of non-coding dna in drosophila," *Nature*, vol. 437, no. 7062, pp. 1149–1152, 2005.

[18] Y. Zheng, S. Josefowicz, A. Chaudhry, X. P. Peng, K. Forbush, and A. Y. Rudensky, "Role of conserved non-coding dna elements in the foxp3 gene in regulatory t-cell fate," *Nature*, vol. 463, no. 7282, pp. 808–812, 2010.

[19] R. C. Lee, R. L. Feinbaum, and V. Ambros, "The c. elegans heterochronic gene lin-4 encodes small rnas with antisense complementarity to lin-14," *cell*, vol. 75, no. 5, pp. 843–854, 1993.

[20] G. A. Calin and C. M. Croce, "Microrna signatures in human cancers," *Nature reviews cancer*, vol. 6, no. 11, pp. 857–866, 2006.

[21] R. A. Gupta, N. Shah, K. C. Wang, J. Kim, H. M. Horlings, D. J. Wong, M.-C. Tsai, T. Hung, P. Argani, J. L. Rinn, *et al.*, "Long non-coding rna hotair reprograms chromatin state to promote cancer metastasis," *Nature*, vol. 464, no. 7291, pp. 1071–1076, 2010.

[22] M. Kozak, "Point mutations define a sequence flanking the aug initiator codon that modulates translation by eukaryotic ribosomes," *Cell*, vol. 44, no. 2, pp. 283–292, 1986.

[23] M. Brandon, P. Baldi, , and D. Wallace, "Mitochondrial mutations in cancer," *Oncogene*, vol. 25, no. 34, pp. 4647–4662, 2006.

[24] P. A. Muller and K. H. Vousden, "p53 mutations in cancer," *Nature cell biology*, vol. 15, no. 1, pp. 2–8, 2013.

[25] D. Y. Zhang and E. Winfree, "Control of dna strand displacement kinetics using toehold exchange," *Journal of the American Chemical Society*, vol. 131, no. 47, pp. 17303–17314, 2009.

[26] J. X. Zhang, J. Z. Fang, W. Duan, L. R. Wu, A. W. Zhang, N. Dalchau, B. Yordanov, R. Petersen, A. Phillips, and D. Y. Zhang, "Predicting dna hybridization kinetics from sequence," *Nature chemistry*, vol. 10, no. 1, pp. 91–98, 2018.

[27] J. SantaLucia, H. T. Allawi, and P. A. Seneviratne, "Improved nearest-neighbor parameters for predicting dna duplex stability," *Biochemistry*, vol. 35, no. 11, pp. 3555–3562, 1996.

[28] N. Zadeh, Joseph, D. Steenberg, Conrad, S. Bois, Justin, R. Wolfe, Brian, B. Pierce, Marshall, R. Khan, Asif, M. Dirks, Robert, and A. Pierce, Niles, "Nupack analysis and design of nucleic acid systems," *Journal of computational chemistry*, vol. 32, no. 1, pp. 170–173, 2011.

[29] F. P. Schwarz, S. Robinson, and J. M. Butler, "Thermodynamic comparison of pna/dna and dna/dna hybridization reactions at ambient temperature," *Nucleic acids research*, vol. 27, no. 24, pp. 4792–4800, 1999.

[30] G. E. Plum, A. P. Grollman, F. Johnson, and K. J. Breslauer, "Influence of the oxidatively damaged adduct 8-oxodeoxyguanosine on the conformation, energetics, and thermodynamic stability of a dna duplex," *Biochemistry*, vol. 34, no. 49, pp. 16148–16160, 1995.

[31] S. M. Freier and K.-H. Altmann, "The ups and downs of nucleic acid duplex stability: structure-stability studies on chemically-modified dna: Rna duplexes," *Nucleic acids research*, vol. 25, no. 22, pp. 4429–4443, 1997.

[32] M. Zuker, "Mfold web server for nucleic acid folding and hybridization prediction," *Nucleic acids research*, vol. 31, no. 13, pp. 3406–3415, 2003.

[33] J. C. García-Ramos, R. Galindo-Murillo, F. Cortés-Guzmán, and L. Ruiz-Azuara, "Metal-based drug-dna interactions," *Journal of the Mexican Chemical Society*, vol. 57, no. 3, pp. 245–259, 2013.

[34] N. C. Seeman, "Nucleic acid junctions and lattices," *Journal of theoretical biology*, vol. 99, no. 2, pp. 237–247, 1982.

[35] N. C. Seeman, "Interactive design and manipulation of macro-molecular architecture utilizing nucleic acid junctions," *Journal of Molecular Graphics*, vol. 3, no. 2, pp. 34–39, 1985.

[36] A. V. Pinheiro, D. Han, W. M. Shih, and H. Yan, "Challenges and opportunities for structural dna nanotechnology," *Nature nanotechnology*, vol. 6, no. 12, p. 763, 2011.

[37] F. Hong, F. Zhang, Y. Liu, and H. Yan, "Dna origami: scaffolds for creating higher order structures," *Chemical reviews*, vol. 117, no. 20, pp. 12584–12640, 2017.

[38] L. L. Ong, N. Hanikel, O. K. Yaghi, C. Grun, M. T. Strauss, P. Bron, J. Lai-Kee-Him, F. Schueder, B. Wang, P. Wang, *et al.*, "Programmable self-assembly of three-dimensional nanostructures from 10,000 unique components," *Nature*, vol. 552, no. 7683, pp. 72–77, 2017.

[39] S. Kotani and W. L. Hughes, "Multi-arm junctions for dynamic dna nanotechnology," *Journal of the American Chemical Society*, vol. 139, no. 18, pp. 6363–6368, 2017.

[40] N. Srinivas, J. Parkin, G. Seelig, E. Winfree, and D. Soloveichik, "Enzyme-free nucleic acid dynamical systems," *Science*, vol. 358, no. 6369, p. eaal2052, 2017.

[41] G. Seelig, D. Soloveichik, D. Y. Zhang, and E. Winfree, "Enzyme-free nucleic acid logic circuits," *science*, vol. 314, no. 5805, pp. 1585–1588, 2006.

[42] J.-S. Shin and N. A. Pierce, "A synthetic dna walker for molecular transport," *Journal of the American Chemical Society*, vol. 126, no. 35, pp. 10834–10835, 2004.

[43] B. Yurke, A. J. Turberfield, A. P. Mills, F. C. Simmel, and J. L. Neumann, "A dna-fuelled molecular machine made of dna," *Nature*, vol. 406, no. 6796, pp. 605–608, 2000.

[44] P. Yin, H. M. Choi, C. R. Calvert, and N. A. Pierce, "Programming biomolecular self-assembly pathways," *Nature*, vol. 451, no. 7176, pp. 318–322, 2008.

[45] Y. S. Jiang, S. Bhadra, B. Li, and A. D. Ellington, "Mismatches improve the performance of strand-displacement nucleic acid circuits," *Angewandte Chemie International Edition*, vol. 53, no. 7, pp. 1845–1848, 2014.

[46] D. Y. Zhang, A. J. Turberfield, B. Yurke, and E. Winfree, "Engineering entropy-driven reactions and networks catalyzed by dna," *Science*, vol. 318, no. 5853, pp. 1121–1125, 2007.

[47] A. J. Genot, D. Y. Zhang, J. Bath, and A. J. Turberfield, "Remote toehold: a mechanism for flexible control of dna hybridization kinetics," *Journal of the American Chemical Society*, vol. 133, no. 7, pp. 2177–2182, 2011.

[48] J. Fern and R. Schulman, "Design and characterization of dna strand-displacement circuits in serum-supplemented cell medium," *ACS synthetic biology*, vol. 6, no. 9, pp. 1774–1783, 2017.

[49] C. Thachuk, E. Winfree, and D. Soloveichik, "Leakless dna strand displacement systems," in *International Workshop on DNA-Based Computers*, pp. 133–153, Springer, 2015.

[50] L. Qian and E. Winfree, "Scaling up digital circuit computation with dna strand displacement cascades," *Science*, vol. 332, no. 6034, pp. 1196–1201, 2011.

[51] L. Qian and E. Winfree, "A simple dna gate motif for synthesizing large-scale circuits," *Journal of the Royal Society Interface*, vol. 8, no. 62, pp. 1281–1297, 2011.

[52] G. Chatterjee, N. Dalchau, R. A. Muscat, A. Phillips, and G. Seelig, "A spatially localized architecture for fast and modular dna computing," *Nature nanotechnology*, vol. 12, no. 9, p. 920, 2017.

[53] C. Wu, S. Cansiz, L. Zhang, I.-T. Teng, L. Qiu, J. Li, Y. Liu, C. Zhou, R. Hu, T. Zhang, *et al.*, "A nonenzymatic hairpin dna cascade reaction provides high signal gain of mrna imaging inside live cells," *Journal of the American Chemical Society*, vol. 137, no. 15, pp. 4900–4903, 2015.

[54] S. D. Patil, D. G. Rhodes, and D. J. Burgess, "Dna-based therapeutics and dna delivery systems: a comprehensive review," *The AAPS journal*, vol. 7, no. 1, pp. E61–E77, 2005.

[55] R. Jungmann, C. Steinhauer, M. Scheible, A. Kuzyk, P. Tinnefeld, and F. C. Simmel, "Single-molecule kinetics and super-resolution microscopy by fluorescence imaging of transient binding on dna origami," *Nano letters*, vol. 10, no. 11, pp. 4756–4761, 2010.

[56] R. Jungmann, M. S. Avendaño, J. B. Woehrstein, M. Dai, W. M. Shih, and P. Yin, "Multiplexed 3d cellular super-resolution imaging with dna-paint and exchange-paint," *Nature methods*, vol. 11, no. 3, p. 313, 2014.

[57] S. Ko, H. Liu, Y. Chen, and C. Mao, "Dna nanotubes as combinatorial vehicles for cellular delivery," *Biomacromolecules*, vol. 9, no. 11, pp. 3039–3043, 2008.

[58] S. Tyagi and F. R. Kramer, "Molecular beacons: probes that fluoresce upon hybridization," *Nature biotechnology*, vol. 14, no. 3, pp. 303–308, 1996.

[59] D. P. Bratu, B.-J. Cha, M. M. Mhlanga, F. R. Kramer, and S. Tyagi, "Visualizing the distribution and transport of mrnas in living cells," *Proceedings of the National Academy of Sciences*, vol. 100, no. 23, pp. 13308–13313, 2003.

[60] T. Lee, J. Weng, and S. Tseng, "Teaching boolean logic through game rule tuning," *IEEE Transactions on Learning Technologies*, vol. 3, pp. 319–328, oct 2010.

[61] L. M. Adleman, "Molecular computation of solutions to combinatorial problems," *Science*, pp. 1021–1024, 1994.

[62] R. M. Dirks, M. Lin, E. Winfree, and N. A. Pierce, "Paradigms for computational nucleic acid design," *Nucleic acids research*, vol. 32, no. 4, pp. 1392–1403, 2004.

[63] Y. Erlich and D. Zielinski, "Dna fountain enables a robust and efficient storage architecture," *Science*, vol. 355, no. 6328, pp. 950–954, 2017.

[64] L. Qian, E. Winfree, and J. Bruck, "Neural network computation with dna strand displacement cascades," *Nature*, vol. 475, no. 7356, pp. 368–372, 2011.

[65] J. Hemphill and A. Deiters, "Dna computation in mammalian cells: microrna logic operations," *Journal of the American Chemical Society*, vol. 135, no. 28, pp. 10512–10518, 2013.

[66] D. Wilhelm, J. Bruck, and L. Qian, "Probabilistic switching circuits in dna," *Proceedings of the National Academy of Sciences*, vol. 115, no. 5, pp. 903–908, 2018.

[67] D. Soloveichik, G. Seelig, and E. Winfree, "Dna as a universal substrate for chemical kinetics," *Proceedings of the National Academy of Sciences*, vol. 107, no. 12, pp. 5393–5398, 2010.

[68] A. Joesaar, S. Yang, B. Bögels, A. van der Linden, P. Pieters, B. P. Kumar, N. Dalchau, A. Phillips, S. Mann, and T. F. de Greef, "Dna-based communication in populations of synthetic protocells," *Nature nanotechnology*, vol. 14, no. 4, pp. 369–378, 2019.

[69] W. A. Lim, "Designing customized cell signalling circuits," *Nature reviews Molecular cell biology*, vol. 11, no. 6, pp. 393–403, 2010.

[70] J. P. Cox, "Long-term data storage in dna," *TRENDS in Biotechnology*, vol. 19, no. 7, pp. 247–250, 2001.

[71] G. Jacob, "Dna based cryptography: An overview and analysis," *International Journal of Emerging Sciences*, vol. 3, no. 1, p. 36, 2013.

[72] K. Kruger, P. J. Grabowski, A. J. Zaug, J. Sands, D. E. Gottschling, and T. R. Cech, "Self-splicing rna: autoexcision and autocyclization of the ribosomal rna intervening sequence of tetrahymena," *cell*, vol. 31, no. 1, pp. 147–157, 1982.

[73] A. D. Ellington and J. W. Szostak, "In vitro selection of rna molecules that bind specific ligands," *nature*, vol. 346, no. 6287, pp. 818–822, 1990.

[74] C. Tuerk and L. Gold, "Systematic evolution of ligands by exponential enrichment: Rna ligands to bacteriophage t4 dna polymerase," *science*, vol. 249, no. 4968, pp. 505–510, 1990.

[75] D. L. Robertson and G. F. Joyce, "Selection in vitro of an rna enzyme that specifically cleaves single-stranded dna," *Nature*, vol. 344, no. 6265, pp. 467–468, 1990.

[76] W. Xu and Y. Lu, "Label-free fluorescent aptamer sensor based on regulation of malachite green fluorescence," *Analytical chemistry*, vol. 82, no. 2, pp. 574–578, 2010.

[77] J. Liu and Y. Lu, "A colorimetric lead biosensor using dnazyme-directed assembly of gold nanoparticles," *Journal of the American Chemical Society*, vol. 125, no. 22, pp. 6642–6643, 2003.

[78] S. Song, L. Wang, J. Li, C. Fan, and J. Zhao, "Aptamer-based biosensors," *TrAC Trends in Analytical Chemistry*, vol. 27, no. 2, pp. 108–117, 2008.

[79] P. Burgstaller, A. Girod, and M. Blind, "Aptamers as tools for target prioritization and lead identification," *Drug discovery today*, vol. 7, no. 24, pp. 1221–1228, 2002.

[80] L. Cerchia, F. Ducongé, C. Pestourie, J. Boulay, Y. Aissouni, K. Gombert, B. Tavitian, V. de Franciscis, and D. Libri, "Neutralizing aptamers from whole-cell selex inhibit the ret receptor tyrosine kinase," *PLoS Biol*, vol. 3, no. 4, p. e123, 2005.

[81] D. Eulberg and S. Klussmann, "Spiegelmers: biostable aptamers," *Chembiochem*, vol. 4, no. 10, pp. 979–983, 2003.

[82] M. Cho, Y. Xiao, J. Nie, R. Stewart, A. T. Csordas, S. S. Oh, J. A. Thomson, and H. T. Soh, "Quantitative selection of dna aptamers through microfluidic selection and high-throughput sequencing," *Proceedings of the National Academy of Sciences*, vol. 107, no. 35, pp. 15373–15378, 2010.

[83] J. T. Sczepanski and G. F. Joyce, "Binding of a structured d-rna molecule by an l-rna aptamer," *Journal of the American Chemical Society*, vol. 135, no. 36, pp. 13290–13293, 2013.

[84] E. R. Mardis, "Dna sequencing technologies: 2006–2016," *Nature protocols*, vol. 12, no. 2, p. 213, 2017.

[85] S. Klußmann, A. Nolte, R. Bald, V. A. Erdmann, and J. P. Fürste, "Mirror-image rna that binds d-adenosine," *Nature biotechnology*, vol. 14, no. 9, pp. 1112–1115, 1996.

[86] A. Nolte, S. Klußmann, R. Bald, V. A. Erdmann, and J. P. Fürste, "Mirror-design of l-oligonucleotide ligands binding to l-arginine," *Nature biotechnology*, vol. 14, no. 9, pp. 1116–1119, 1996.

[87] A. Vater and S. Klussmann, "Turning mirror-image oligonucleotides into drugs: the evolution of spiegelmer® therapeutics," *Drug discovery today*, vol. 20, no. 1, pp. 147–155, 2015.

[88] K. P. Williams, X.-H. Liu, T. N. Schumacher, H. Y. Lin, D. A. Ausiello, P. S. Kim, and D. P. Bartel, "Bioactive and nuclease-resistant l-dna ligand of vasopressin," *Proceedings of the National Academy of Sciences*, vol. 94, no. 21, pp. 11285–11290, 1997.

[89] R. d. Milton, S. Milton, and S. Kent, "Total chemical synthesis of a d-enzyme: the enantiomers of hiv-1 protease show reciprocal chiral substrate specificity [corrected]," *Science*, vol. 256, no. 5062, pp. 1445–1448, 1992.

[90] R. T. Batey, R. P. Rambo, and J. A. Doudna, "Tertiary motifs in rna structure and folding," *Angewandte Chemie International Edition*, vol. 38, no. 16, pp. 2326–2343, 1999.

[91] C. Baugh, D. Grate, and C. Wilson, "2.8 å crystal structure of the malachite green aptamer," *Journal of molecular biology*, vol. 301, no. 1, pp. 117–128, 2000.

[92] C. Laing and T. Schlick, "Computational approaches to rna structure prediction, analysis, and design," *Current opinion in structural biology*, vol. 21, no. 3, pp. 306–318, 2011.

[93] M. A. Convery, S. Rowsell, N. J. Storehouse, A. D. Ellington, I. Hirao, J. B. Murray, D. S. Peabody, S. E. Phillips, and P. G. Stockley, "Crystal structure of an rna aptamer–protein complex at 2.8 å resolution," *Nature structural biology*, vol. 5, no. 2, pp. 133–139, 1998.

[94] P. L. Adams, M. R. Stahley, A. B. Kosek, J. Wang, and S. A. Strobel, "Crystal structure of a self-splicing group i intron with both exons," *Nature*, vol. 430, no. 6995, pp. 45–50, 2004.

[95] N. Ban, P. Nissen, J. Hansen, M. Capel, P. B. Moore, and T. A. Steitz, "Placement of protein and rna structures into a 5 å-resolution map of the 50s ribosomal subunit," *Nature*, vol. 400, no. 6747, pp. 841–847, 1999.

[96] R. Nutiu and Y. Li, "Structure-switching signaling aptamers," *Journal of the American Chemical Society*, vol. 125, no. 16, pp. 4771–4778, 2003.

[97] R. Nutiu and Y. Li, "In vitro selection of structure-switching signaling aptamers," *Angewandte Chemie International Edition*, vol. 44, no. 7, pp. 1061–1065, 2005.

[98] P. S. Lau, B. K. Coombes, and Y. Li, "A general approach to the construction of structure-switching reporters from rna aptamers," *Angewandte Chemie International Edition*, vol. 49, no. 43, pp. 7938–7942, 2010.

[99] J. Zhu, L. Zhang, Z. Zhou, S. Dong, and E. Wang, "Molecular aptamer beacon tuned dna strand displacement to transform small molecules into dna logic outputs," *Chemical Communications*, vol. 50, no. 25, pp. 3321–3323, 2014.

[100] Y.-M. Wang, Z. Wu, S.-J. Liu, and X. Chu, "Structure-switching aptamer triggering hybridization chain reaction on the cell surface for activatable theranostics," *Analytical chemistry*, vol. 87, no. 13, pp. 6470–6474, 2015.

[101] A. Autour, S. C. Jeng, A. D. Cawte, A. Abdolahzadeh, A. Galli, S. S. Panchapakesan, D. Rueda, M. Ryckelynck, and P. J. Unrau, "Fluorogenic rna mango aptamers for imaging small non-coding rnas in mammalian cells," *Nature communications*, vol. 9, no. 1, pp. 1–12, 2018.

[102] W. Zhong and J. T. Sczepanski, "A mirror image fluorogenic aptamer sensor for live-cell imaging of micrornas," *ACS sensors*, vol. 4, no. 3, pp. 566–570, 2019.

[103] S.-F. Torabi, P. Wu, C. E. McGhee, L. Chen, K. Hwang, N. Zheng, J. Cheng, and Y. Lu, "In vitro selection of a sodium-specific dnazyme and its application in intracellular sensing," *Proceedings of the National Academy of Sciences*, vol. 112, no. 19, pp. 5903–5908, 2015.

[104] Z. Tang, P. Mallikaratchy, R. Yang, Y. Kim, Z. Zhu, H. Wang, and W. Tan, "Aptamer switch probe based on intramolecular displacement," *Journal of the American Chemical Society*, vol. 130, no. 34, pp. 11268–11269, 2008.

[105] H. G. Khorana, "Nucleic acid synthesis," *Pure and Applied Chemistry*, vol. 17, no. 3-4, pp. 349–382, 1968.

[106] S. P. Adams, K. S. Kavka, E. J. Wykes, S. B. Holder, and G. R. Galluppi, "Hindered dialkylamino nucleoside phosphite reagents in the synthesis of two dna 51-mers," *Journal of the American Chemical Society*, vol. 105, no. 3, pp. 661–663, 1983.

[107] L. McBride and M. Caruthers, "An investigation of several deoxynucleoside phosphoramidites useful for synthesizing deoxyoligonucleotides," *Tetrahedron Letters*, vol. 24, no. 3, pp. 245–248, 1983.

[108] A. H. Alhasan, P. C. Patel, C. H. J. Choi, and C. A. Mirkin, "Exosome encased spherical nucleic acid gold nanoparticle conjugates as potent microrna regulation agents," *Small*, vol. 10, no. 1, pp. 186–192, 2014.

[109] G. W. Ashley, "Modeling, synthesis, and hybridization properties of (l)-ribonucleic acid," *Journal of the American Chemical Society*, vol. 114, no. 25, pp. 9731–9736, 1992.

[110] G. F. Joyce, "Rna evolution and the origins of life," *Nature*, vol. 338, no. 6212, pp. 217–224, 1989.

[111] D. G. Blackmond, "The origin of biological homochirality," *Cold Spring Harbor perspectives in biology*, vol. 2, no. 5, p. a002147, 2010.

[112] R. Breslow and Z.-L. Cheng, "On the origin of terrestrial homochirality for nucleosides and amino acids," *Proceedings of the National Academy of Sciences*, vol. 106, no. 23, pp. 9144–9146, 2009.

[113] F. Pellestor and P. Paulasova, "The peptide nucleic acids (pnas), powerful tools for molecular genetics and cytogenetics," *European journal of human genetics*, vol. 12, no. 9, pp. 694–700, 2004.

[114] M. Egholm, O. Buchardt, P. E. Nielsen, and R. H. Berg, "Peptide nucleic acids (pna). oligonucleotide analogs with an achiral peptide backbone," *Journal of the American Chemical Society*, vol. 114, no. 5, pp. 1895–1897, 1992.

[115] P. Wittung, P. E. Nielsen, O. Buchardt, M. Egholm, B. Norde, *et al.*, "Dna-like double helix formed by peptide nucleic acid," *Nature*, vol. 368, no. 6471, pp. 561–563, 1994.

[116] M. Egholm, O. Buchardt, L. Christensen, C. Behrens, S. M. Freier, D. A. Driver, R. H. Berg, S. K. Kim, B. Norden, and P. E. Nielsen, "Pna hybridizes to complementary oligonucleotides obeying the watson–crick hydrogen-bonding rules," *Nature*, vol. 365, no. 6446, pp. 566–568, 1993.

[117] U. Giesen, W. Kleider, C. Berding, A. Geiger, H. Ørum, and P. E. Nielsen, "A formula for thermal stability (t m) prediction of pna/dna duplexes," *Nucleic acids research*, vol. 26, no. 21, pp. 5004–5006, 1998.

[118] I. Autiero, M. Saviano, and E. Langella, "Molecular dynamics simulations of pna–pna and pna–dna duplexes by the use of new parameters implemented in the gromacs package: a conformational and dynamics study," *Physical Chemistry Chemical Physics*, vol. 16, no. 5, pp. 1868–1874, 2014.

[119] G. B. Fields and R. L. NOBLE, "Solid phase peptide synthesis utilizing 9-fluorenylmethoxycarbonyl amino acids," *International journal of peptide and protein research*, vol. 35, no. 3, pp. 161–214, 1990.

[120] N. J. Peffer, J. C. Hanvey, J. E. Bisi, S. A. Thomson, C. F. Hassman, S. A. Noble, and L. E. Babiss, "Strand-invasion of duplex dna by peptide nucleic acid oligomers," *Proceedings of the National Academy of Sciences*, vol. 90, no. 22, pp. 10648–10652, 1993.

[121] R. Shrestha, Y. Shen, K. A. Pollack, J.-S. A. Taylor, and K. L. Wooley, "Dual peptide nucleic acid-and peptide-functionalized shell cross-linked nanoparticles designed to target mrna toward the diagnosis and treatment of acute lung injury," *Bioconjugate chemistry*, vol. 23, no. 3, pp. 574–585, 2012.

[122] U. Koppelhus and P. E. Nielsen, "Cellular delivery of peptide nucleic acid (pna)," *Advanced drug delivery reviews*, vol. 55, no. 2, pp. 267–280, 2003.

[123] K. Hoehlig, L. Bethge, and S. Klussmann, "Stereospecificity of oligonucleotide interactions revisited: no evidence for heterochiral hybridization and ribozyme/dnazyme activity," *PloS one*, vol. 10, no. 2, 2015.

[124] A. M. Kabza and J. T. Sczepanski, "An l-rna aptamer with expanded chemical functionality that inhibits microrna biogenesis," *ChemBioChem*, vol. 18, no. 18, pp. 1824–1827, 2017.

[125] A. M. Kabza, B. E. Young, and J. T. Sczepanski, "Heterochiral dna strand-displacement circuits," *Journal of the American Chemical Society*, vol. 139, no. 49, pp. 17715–17718, 2017.

[126] A. M. Kabza and J. T. Sczepanski, "l-dna-based catalytic hairpin assembly circuit," *Molecules*, vol. 25, no. 4, p. 947, 2020.

[127] C. M. Croce, "Causes and consequences of microrna dysregulation in cancer," *Nature reviews genetics*, vol. 10, no. 10, pp. 704–714, 2009.

[128] V. Bernat and M. D. Disney, "Rna structures as mediators of neurological diseases and as drug targets," *Neuron*, vol. 87, no. 1, pp. 28–46, 2015.

[129] A. Engelman and P. Cherepanov, "The structural biology of hiv-1: mechanistic and therapeutic insights," *Nature Reviews Microbiology*, vol. 10, no. 4, pp. 279–290, 2012.

[130] L. Guan and M. D. Disney, "Recent advances in developing small molecules targeting rna," *ACS chemical biology*, vol. 7, no. 1, pp. 73–86, 2012.

[131] J. R. Thomas and P. J. Hergenrother, "Targeting rna with small molecules," *Chemical reviews*, vol. 108, no. 4, pp. 1171–1224, 2008.

[132] H. Tafer, S. L. Ameres, G. Obernosterer, C. A. Gebeshuber, R. Schroeder, J. Martinez, and I. L. Hofacker, "The impact of target site accessibility on the design of effective sirnas," *Nature biotechnology*, vol. 26, no. 5, pp. 578–583, 2008.

[133] A. L. Jackson, S. R. Bartz, J. Schelter, S. V. Kobayashi, J. Burchard, M. Mao, B. Li, G. Cavet, and P. S. Linsley, "Expression profiling reveals off-target gene regulation by rnai," *Nature biotechnology*, vol. 21, no. 6, pp. 635–637, 2003.

[134] J. T. Sczepanski and G. F. Joyce, "Specific inhibition of microrna processing using l-rna aptamers," *Journal of the American Chemical Society*, vol. 137, no. 51, pp. 16032–16037, 2015.

[135] Y. Feng, J. Liu, Y. Kang, Y. He, B. Liang, P. Yang, and Z. Yu, "mir-19a acts as an oncogenic microrna and is up-regulated in bladder cancer," *Journal of experimental & clinical cancer research*, vol. 33, no. 1, p. 67, 2014.

[136] K. Lu, C. Liu, T. Tao, X. Zhang, L. Zhang, C. Sun, Y. Wang, S. Chen, B. Xu, and M. Chen, "Microrna-19a regulates proliferation and apoptosis of castration-resistant prostate cancer cells by targeting btg1," *FEBS letters*, vol. 589, no. 13, pp. 1485–1490, 2015.

[137] T. Schoetzau, J. Langner, E. Moyroud, I. Roehl, S. Vonhoff, and S. Klussmann, "Aminomodified nucleobases: functionalized nucleoside triphosphates applicable for selex," *Bioconjugate chemistry*, vol. 14, no. 5, pp. 919–926, 2003.

[138] N. K. Vaish, R. Larralde, A. W. Fraley, J. W. Szostak, and L. W. McLaughlin, "A novel, modification-dependent atp-binding aptamer selected from an rna library incorporating a cationic functionality," *Biochemistry*, vol. 42, no. 29, pp. 8842–8851, 2003.

[139] C. E. Lünse, G. Michlewski, C. S. Hopp, A. Rentmeister, J. F. Cáceres, M. Famulok, and G. Mayer, "An aptamer targeting the apical-loop domain modulates pri-mirna processing," *Angewandte Chemie International Edition*, vol. 49, no. 27, pp. 4674–4677, 2010.

[140] G. A. Soukup and R. R. Breaker, "Relationship between internucleotide linkage geometry and the stability of rna," *Rna*, vol. 5, no. 10, pp. 1308–1325, 1999.

[141] J. L. Childs-Disney and M. D. Disney, "Approaches to validate and manipulate rna targets with small molecules in cells," *Annual review of pharmacology and toxicology*, vol. 56, pp. 123–140, 2016.

[142] U. J. Desai and P. K. Pfaffle, "Single-step purification of a thermostable dna polymerase expressed in escherichia coli.," *Biotechniques*, vol. 19, no. 5, pp. 780–2, 1995.

[143] J. Van Meerloo, G. J. Kaspers, and J. Cloos, "Cell sensitivity assays: the mtt assay," in *Cancer cell culture*, pp. 237–245, Springer, 2011.

[144] J. G. Bruno, M. P. Carrillo, T. Phillips, and C. J. Andrews, "A novel screening method for competitive fret-aptamers applied to e. coli assay development," *Journal of fluorescence*, vol. 20, no. 6, pp. 1211–1223, 2010.

[145] L. S. Green, C. Bell, and N. Janjic, "Aptamers as reagents for high-throughput screening," *Biotechniques*, vol. 30, no. 5, pp. 1094–1110, 2001.

[146] A. S. Piatek, S. Tyagi, A. C. Pol, A. Telenti, L. P. Miller, F. R. Kramer, and D. Alland, "Molecular beacon sequence analysis for detecting drug resistance in mycobacterium tuberculosis," *Nature biotechnology*, vol. 16, no. 4, pp. 359–363, 1998.

[147] J. C. Owicki, "Fluorescence polarization and anisotropy in high throughput screening: perspectives and primer," *Journal of biomolecular screening*, vol. 5, no. 5, pp. 297–306, 2000.

[148] M. Wade, J. Méndez, N. P. Coussens, M. R. Arkin, and M. A. Glicksman, "Inhibition of protein-protein interactions: cell-based assays," in *Assay Guidance Manual [Internet]*, Eli Lilly & Company and the National Center for Advancing Translational Sciences, 2017.

[149] T. Hermann, "Small molecules targeting viral rna," *Wiley Interdisciplinary Reviews: RNA*, vol. 7, no. 6, pp. 726–743, 2016.

[150] R. Penchovsky and C. C. Stoilova, "Riboswitch-based antibacterial drug discovery using high-throughput screening methods," *Expert opinion on drug discovery*, vol. 8, no. 1, pp. 65–82, 2013.

[151] S. E. Butcher and A. M. Pyle, "The molecular interactions that stabilize rna tertiary structure: Rna motifs, patterns, and networks," *Accounts of chemical research*, vol. 44, no. 12, pp. 1302–1311, 2011.

[152] H. Sahoo, "Förster resonance energy transfer–a spectroscopic nanoruler: Principle and applications," *Journal of Photochemistry and Photobiology C: Photochemistry Reviews*, vol. 12, no. 1, pp. 20–30, 2011.

[153] R. del Villar-Guerra, R. D. Gray, J. O. Trent, and J. B. Chaires, "A rapid fluorescent indicator displacement assay and principal component/cluster data analysis for determination of ligand–nucleic acid structural selectivity," *Nucleic Acids Research*, vol. 46, no. 7, pp. e41–e41, 2018.

[154] C. Dingwall, I. Ernberg, M. J. Gait, S. M. Green, S. Heaphy, J. Karn, A. D. Lowe, M. Singh, M. A. Skinner, and R. Valerio, "Human immunodeficiency virus 1 tat protein binds trans-activation-responsive region (tar) rna in vitro," *Proceedings of the National Academy of Sciences*, vol. 86, no. 18, pp. 6925–6929, 1989.

[155] S. Wang, P. W. Huber, M. Cui, A. W. Czarnik, and H.-Y. Mei, "Binding of neomycin to the tar element of hiv-1 rna induces dissociation of tat protein by an allosteric mechanism," *Biochemistry*, vol. 37, no. 16, pp. 5549–5557, 1998.

[156] F. Mattiroli, Y. Gu, and K. Luger, "Fret-based stoichiometry measurements of protein complexes in vitro," *Bio-protocol*, vol. 7, no. 3, 2018.

[157] N. N. Patwardhan, L. R. Ganser, G. J. Kapral, C. S. Eubanks, J. Lee, B. Sathyamoorthy, H. M. Al-Hashimi, and A. E. Hargrove, "Amiloride as a new rna-binding scaffold with activity against hiv-1 tar," *MedChemComm*, vol. 8, no. 5, pp. 1022–1036, 2017.

[158] N. N. Patwardhan, Z. Cai, C. N. Newson, and A. E. Hargrove, "Fluorescent peptide displacement as a general assay for screening small molecule libraries against rna," *Organic & biomolecular chemistry*, vol. 17, no. 7, pp. 1778–1786, 2019.

[159] N. N. Patwardhan, Z. Cai, A. U. Juru, and A. E. Hargrove, "Driving factors in amiloride recognition of hiv rna targets," *Organic & biomolecular chemistry*, vol. 17, no. 42, pp. 9313–9320, 2019.

[160] S. Dey and J. T. Sczepanski, "In vitro selection of l-dna aptamers that bind a structured d-rna molecule," *Nucleic Acids Research*, 2020.

[161] H. Ulrich, C. A. Trujillo, A. A. Nery, J. M. Alves, P. Majumder, R. R. Resende, and A. H. Martins, "Dna and rna aptamers: from tools for basic research towards therapeutic applications," *Combinatorial chemistry & high throughput screening*, vol. 9, no. 8, pp. 619–632, 2006.

[162] K. Lund, A. J. Manzo, N. Dabby, N. Michelotti, A. Johnson-Buck, J. Nangreave, S. Taylor, R. Pei, M. N. Stojanovic, N. G. Walter, *et al.*, "Molecular robots guided by prescriptive landscapes," *Nature*, vol. 465, no. 7295, pp. 206–210, 2010.

[163] T. Omabegho, R. Sha, and N. C. Seeman, "A bipedal dna brownian motor with coordinated legs," *Science*, vol. 324, no. 5923, pp. 67–71, 2009.

[164] M. N. Stojanovic, D. Stefanovic, and S. Rudchenko, "Exercises in molecular computing," *Accounts of chemical research*, vol. 47, no. 6, pp. 1845–1852, 2014.

[165] C. Jung and A. D. Ellington, "Diagnostic applications of nucleic acid circuits," *Accounts of chemical research*, vol. 47, no. 6, pp. 1825–1835, 2014.

[166] J. Elbaz, O. Lioubashevski, F. Wang, F. Remacle, R. D. Levine, and I. Willner, "Dna computing circuits using libraries of dnazyme subunits," *Nature nanotechnology*, vol. 5, no. 6, p. 417, 2010.

[167] M. R. Jones, N. C. Seeman, and C. A. Mirkin, "Programmable materials and the nature of the dna bond," *Science*, vol. 347, no. 6224, p. 1260901, 2015.

[168] K. K. Jensen, H. Ørum, P. E. Nielsen, and B. Nordén, "Kinetics for hybridization of peptide nucleic acids (pna) with dna and rna studied with the biacore technique," *Biochemistry*, vol. 36, no. 16, pp. 5072–5077, 1997.

[169] M. Froeyen, F. Morvan, J.-J. Vasseur, P. Nielsen, A. Van Aerschot, H. Rosemeyer, and P. Herdewijn, "Conformational and chiral selection of oligonucleotides," *Chemistry & biodiversity*, vol. 4, no. 4, pp. 803–817, 2007.

[170] R. M. Dirks and N. A. Pierce, "Triggered amplification by hybridization chain reaction," *Proceedings of the National Academy of Sciences*, vol. 101, no. 43, pp. 15275–15278, 2004.

[171] H. Peng, A. M. Newbigging, Z. Wang, J. Tao, W. Deng, X. C. Le, and H. Zhang, "Dnazyme-mediated assays for amplified detection of nucleic acids and proteins," *Analytical chemistry*, vol. 90, no. 1, pp. 190–207, 2018.

[172] F. C. Simmel, B. Yurke, and H. R. Singh, "Principles and applications of nucleic acid strand displacement reactions," *Chemical reviews*, vol. 119, no. 10, pp. 6326–6369, 2019.

[173] F.-X. Su, C.-X. Yang, and X.-P. Yan, "Intracellular messenger rna triggered catalytic hairpin assembly for fluorescence imaging guided photothermal therapy," *Analytical chemistry*, vol. 89, no. 14, pp. 7277–7281, 2017.

[174] B. Groves, Y.-J. Chen, C. Zurla, S. Pochekailov, J. L. Kirschman, P. J. Santangelo, and G. Seelig, "Computing in mammalian cells with nucleic acid strand exchange," *Nature nanotechnology*, vol. 11, no. 3, p. 287, 2016.

[175] C. Molenaar, S. Marras, J. Slats, J.-C. Truffert, M. Lemaitre, A. Raap, R. Dirks, and H. Tanke, "Linear 2? o-methyl rna probes for the visualization of rna in living cells," *Nucleic acids research*, vol. 29, no. 17, pp. e89–e89, 2001.

[176] X. Olson, S. Kotani, B. Yurke, E. Graugnard, and W. L. Hughes, "Kinetics of dna strand displacement systems with locked nucleic acids," *The Journal of Physical Chemistry B*, vol. 121, no. 12, pp. 2594–2602, 2017.

[177] A. Khvorova and J. K. Watts, "The chemical evolution of oligonucleotide therapies of clinical utility," *Nature biotechnology*, vol. 35, no. 3, p. 238, 2017.

[178] J. B. Bramsen, M. B. Laursen, A. F. Nielsen, T. B. Hansen, C. Bus, N. Langkjær, B. R. Babu, T. Højland, M. Abramov, A. Van Aerschot, *et al.*, "A large-scale chemical modification screen identifies design rules to generate sirnas with high activity, high stability and low toxicity," *Nucleic acids research*, vol. 37, no. 9, pp. 2867–2881, 2009.

[179] N. C. Hauser, R. Martinez, A. Jacob, S. Rupp, J. D. Hoheisel, and S. Matysiak, "Utilising the left-helical conformation of l-dna for analysing different marker types on a single universal microarray platform," *Nucleic acids research*, vol. 34, no. 18, pp. 5101–5111, 2006.

[180] A. Garbesi, M. L. Capobinanco, F. P. Colonna, L. Tondelli, F. Arcamone, G. Manzini, C. W. Hilbers, J. M. Aelen, and M. J. Blommers, "L-dnas as potenital antimessenger oligonucleotides: a reassessment," *Nucleic acids research*, vol. 21, no. 18, pp. 4159–4165, 1993.

[181] G. Higgs and F. Slack, "The multiple roles of microrna-155 in oncogenesis," *Journal of clinical bioinformatics*, vol. 3, no. 1, p. 17, 2013.

[182] Y. Jiang, B. Li, J. N. Milligan, S. Bhadra, and A. D. Ellington, "Real-time detection of isothermal amplification reactions with thermostable catalytic hairpin assembly," *Journal of the American Chemical Society*, vol. 135, no. 20, pp. 7430–7433, 2013.

[183] B. E. Young and J. T. Sczepanski, "Heterochiral dna strand-displacement based on chimeric d/l-oligonucleotides," *ACS synthetic biology*, 2019.

[184] P. Guo, F. Haque, B. Hallahan, R. Reif, and H. Li, "Uniqueness, advantages, challenges, solutions, and perspectives in therapeutics applying rna nanotechnology," *Nucleic acid therapeutics*, vol. 22, no. 4, pp. 226–245, 2012.

[185] K. S. Schmidt, S. Borkowski, J. Kurreck, A. W. Stephens, R. Bald, M. Hecht, M. Friebe, L. Dinkelborg, and V. A. Erdmann, "Application of locked nucleic acids to improve aptamer in vivo stability and targeting function," *Nucleic acids research*, vol. 32, no. 19, pp. 5757–5765, 2004.

[186] D. Bousmail, L. Amrein, J. J. Fakhoury, H. H. Fakih, J. C. Hsu, L. Panasci, and H. F. Sleiman, "Precision spherical nucleic acids for delivery of anticancer drugs," *Chemical science*, vol. 8, no. 9, pp. 6218–6229, 2017.

[187] S. Kawai and M. Nishizawa, "New procedure for dna transfection with polycation and dimethyl sulfoxide.," *Molecular and Cellular Biology*, vol. 4, no. 6, pp. 1172–1174, 1984.

[188] B. Dalby, S. Cates, A. Harris, E. C. Ohki, M. L. Tilkins, P. J. Price, and V. C. Ciccarone, "Advanced transfection with lipofectamine 2000 reagent: primary neurons, sirna, and high-throughput applications," *Methods*, vol. 33, no. 2, pp. 95–103, 2004.

[189] R. Zhou, R. C. Geiger, and D. A. Dean, "Intracellular trafficking of nucleic acids," *Expert opinion on drug delivery*, vol. 1, no. 1, pp. 127–140, 2004.

[190] A. Lacroix, E. Vengut-Climent, D. De Rochambeau, and H. F. Sleiman, "Uptake and fate of fluorescently labeled dna nanostructures in cellular environments: A cautionary tale," *ACS central science*, vol. 5, no. 5, pp. 882–891, 2019.

[191] C. E. Deckard and J. T. Sczepanski, "Polycomb repressive complex 2 binds rna irrespective of stereochemistry," *Chemical communications*, vol. 54, no. 85, pp. 12061–12064, 2018.

[192] E. H. Akama-Garren, N. S. Joshi, T. Tammela, G. P. Chang, B. L. Wagner, D.-Y. Lee, W. M. Rideout III, T. Papagiannakopoulos, W. Xue, and T. Jacks, "A modular assembly platform for rapid generation of dna constructs," *Scientific reports*, vol. 6, p. 16836, 2016.

[193] F. H. Arnold, "Design by directed evolution," *Accounts of chemical research*, vol. 31, no. 3, pp. 125–131, 1998.

[194] L. Giver, A. Gershenson, P.-O. Freskgard, and F. H. Arnold, "Directed evolution of a thermostable esterase," *Proceedings of the National Academy of Sciences*, vol. 95, no. 22, pp. 12809–12813, 1998.

[195] H. Zhao, L. Giver, Z. Shao, J. A. Affholter, and F. H. Arnold, "Molecular evolution by staggered extension process (step) in vitro recombination," *Nature biotechnology*, vol. 16, no. 3, pp. 258–261, 1998.

[196] O. May, P. T. Nguyen, and F. H. Arnold, "Inverting enantioselectivity by directed evolution of hydantoinase for improved production of l-methionine," *Nature biotechnology*, vol. 18, no. 3, pp. 317–320, 2000.

[197] S. Barthel, S. Palluk, N. J. Hillson, J. D. Keasling, and D. H. Arlow, "Enhancing terminal deoxynucleotidyl transferase activity on substrates with 3? terminal structures for enzymatic de novo dna synthesis," *Genes*, vol. 11, no. 1, p. 102, 2020.

[198] D. Jasinski, F. Haque, D. W. Binzel, and P. Guo, "Advancement of the emerging field of rna nanotechnology," *Acs Nano*, vol. 11, no. 2, pp. 1142–1164, 2017.

[199] D. Liu, C. W. Geary, G. Chen, Y. Shao, M. Li, C. Mao, E. S. Andersen, J. A. Piccirilli, P. W. Rothemund, and Y. Weizmann, "Branched kissing loops for the construction of diverse rna homooligomeric nanostructures," *Nature Chemistry*, vol. 12, no. 3, pp. 249–259, 2020.

[200] L. Jaeger and A. Chworos, "The architectonics of programmable rna and dna nanostructures," *Current opinion in structural biology*, vol. 16, no. 4, pp. 531–543, 2006.

[201] W. W. Grabow and L. Jaeger, "Rna self-assembly and rna nanotechnology," *Accounts of chemical research*, vol. 47, no. 6, pp. 1871–1880, 2014.

[202] C. Geary, A. Chworos, E. Verzemnieks, N. R. Voss, and L. Jaeger, "Composing rna nanostructures from a syntax of rna structural modules," *Nano letters*, vol. 17, no. 11, pp. 7095–7101, 2017.

APPENDIX A

CHAPTER 2 SUPPLEMENTARY DATA

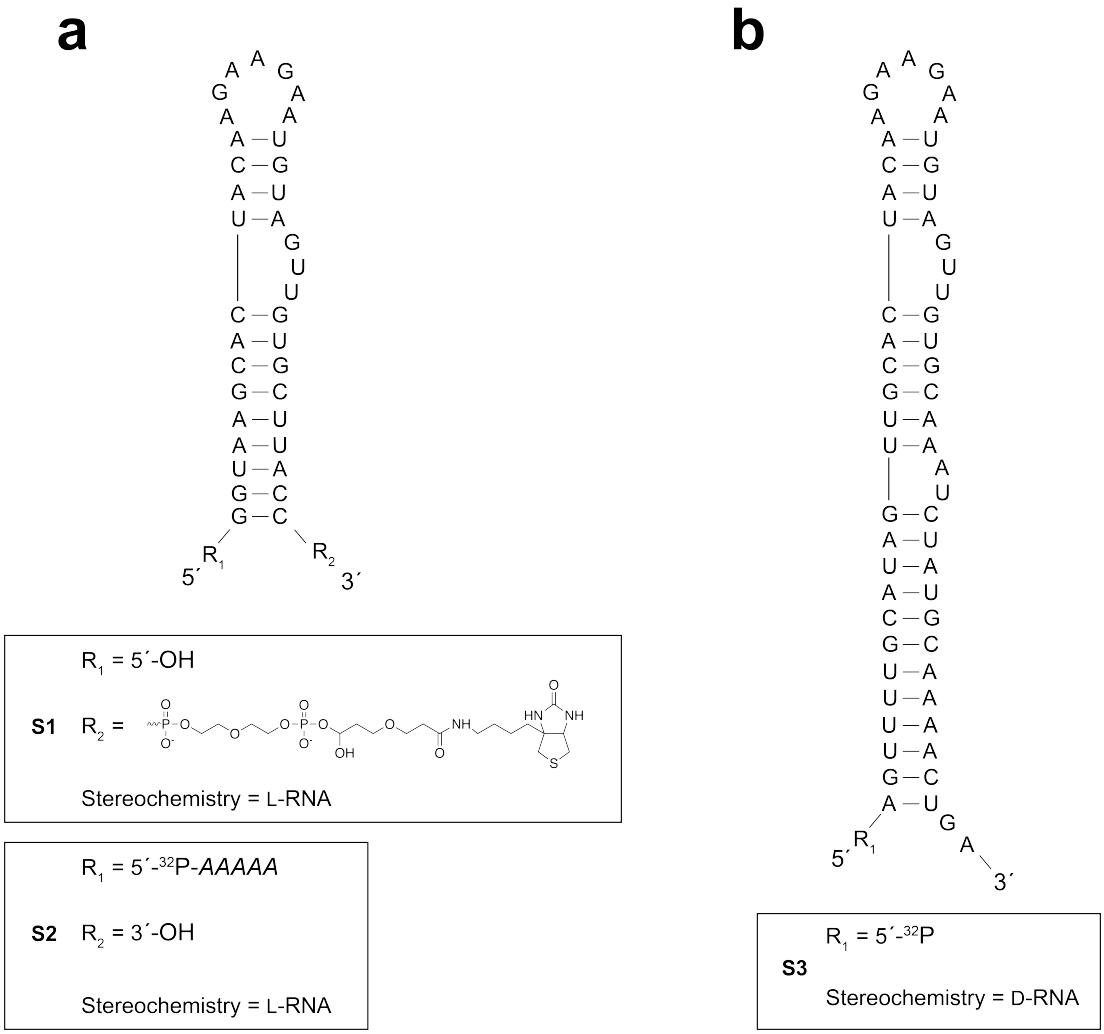


Figure A.1: Pre-miR-19a RNA constructs. (a) Pre-miR RNA **S1** was used during the in vitro selection experiment and pre-miR RNA **S2** was used to determine the dissociation constant of D-19a-6t (see Figure 2.3a in the main text) and to analyze D-19a-6t mutants (see figure 2.4 in the main text). Italicized nucleotides in **S2** are comprised D-DNA, which enabled [5′-$^{32}$P] labeling of the L-RNA. (b) Full length pre-miR-19a. Adapted from Ref. 123 with permission from Wiley.

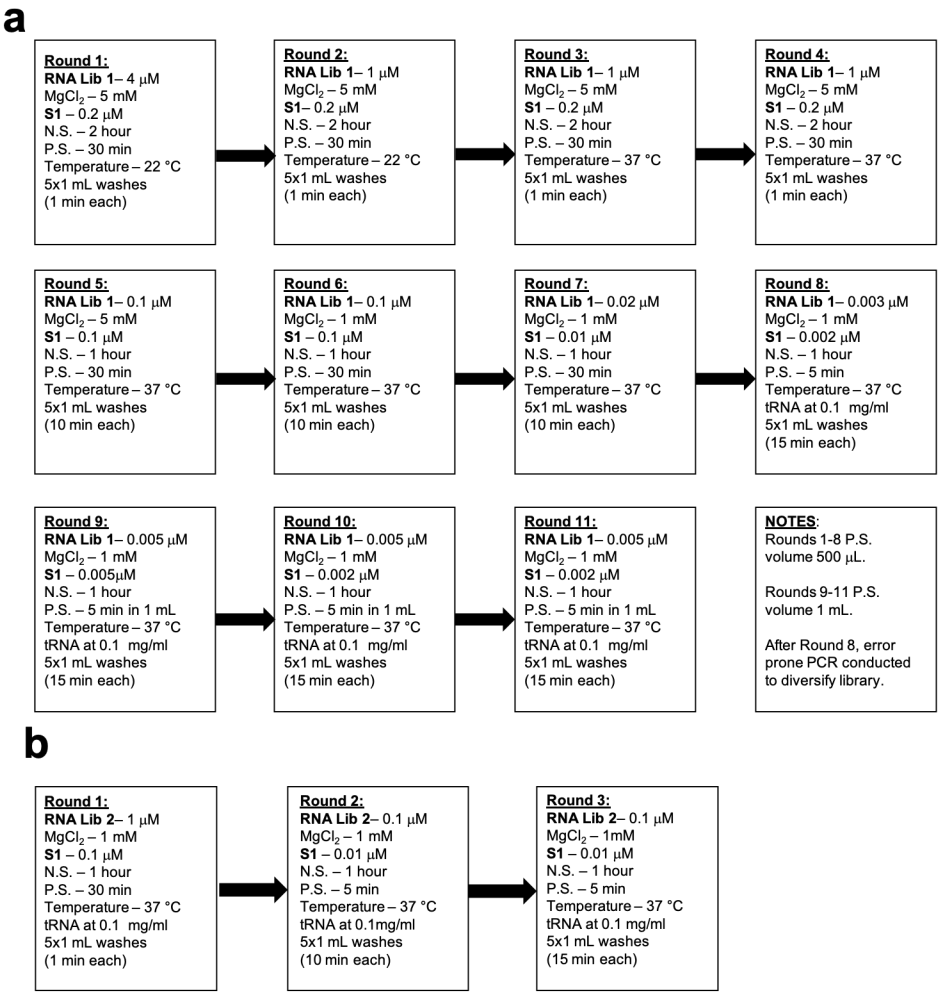


Figure A.2: Flow charts depicting selection conditions used in (a) each of the initial 11 rounds of in vitro selection and (b) each of the 3 rounds of reselection. See **Materials and Methods** for details. N.S. (negative selection) and P.S. (positive selection) indicate the time that the RNA library was incubated with either streptavidin-coated beads or pre-miR-19a (**S1**), respectively. Washes were carried out for the indicated time using a buffer having the same composition as the selection buffer (50 mM KCl, 20 mM NaCl, and 25 mM Tris pH 7.6) and with the indicated $MgCl_2$ concentration. Adapted from Ref. 123 with permission from Wiley.

**a**

Lib1
5'-TTCTAATACGACTCACTATAGGTTACCAGCCTTCACTGC(N50)GCACCACGGTCGGTCACAC-3'

R1
3'-CGTGGTGCCAGCCAGTGTG-5'

RNA Pool 1
5'-GGUUACCAGCCUUCACUGC(N50)GCACCACGGUCGGUCACAC-3'

**b**

19a-6 (11) UUAGCUGGAGGGGAGUGGGGUUGCAUUAACUUUUGGGUUAAGCCAGCUGC

19a-1 (1) AUAGCUGUAGGGGAGUGGGGUUGCAUUAACUUUUGGGUUAAGCCAGCUGC

19a-4 (1) UUAGCUGGAGGGGAGUGGGGUUGCAUUAACUUUUGGGUUAAGCCAGUUGC

19a-5 (1) UUAGCUGGAGGGGAGUGGGGUUGCAUUAACUUUUGGGUAAGCCAGCUGC

19a-10 (1) UUAGCGGGAGGGGAGUGGGGUUGCAUUAACUUUUGGGUUAAGCCUGCUGC

**c**

Lib2
5'-TTCTAATACGACTCACTATAGGTTACCAGCCTTCACTGCttagctggaggggagtgg
ggttgcattaacttttgggttaagccagctgcGCACCACGGTCGGTCACAC-3'

RNA pool 2
5'-GGUUACCAGCCUUCACUGCuuagcuggaggggaguggggguugcauuaac
uuuuggguuaagccagcugcGCACCACGGUCGGUCACAC-3'

Figure A.3: Sequences of starting pool, PCR primers, and selected clones. (a) Pool of synthetic DNA molecules (Lib1), each containing a 50 random nucleotide sequence flanked by binding sites for F1 and R1. T7 RNA polymerase promoter sequence is underlined. The corresponding pool of RNA molecules (RNA Pool 1) containing 50 random nucleotides flanked by fixed primer sites is shown below. (b) Sequences of individual clones isolated after eleven rounds of in vitro selection. Clone number is written on the left with the number in parentheses indicating redundancy of the sequences among the 15 clones analyzed. (c) Sequence of reselection library (Lib2). The italicized portion corresponds to clone 19a-6 sequence which was synthesized using doped reagent bottles to achieve a degeneracy of 0.12, or 7 mutations per molecule, within the italicized portion. Fixed primer binding sights are shown flanking the mutagenized region and were synthesized using pure reagents to avoid mutation in the primer binding domain. RNA pool 2 italicized sequence corresponds to mutated aptamer region (Figure A.4 shows reselection results). Adapted from Ref. 123 with permission from Wiley.

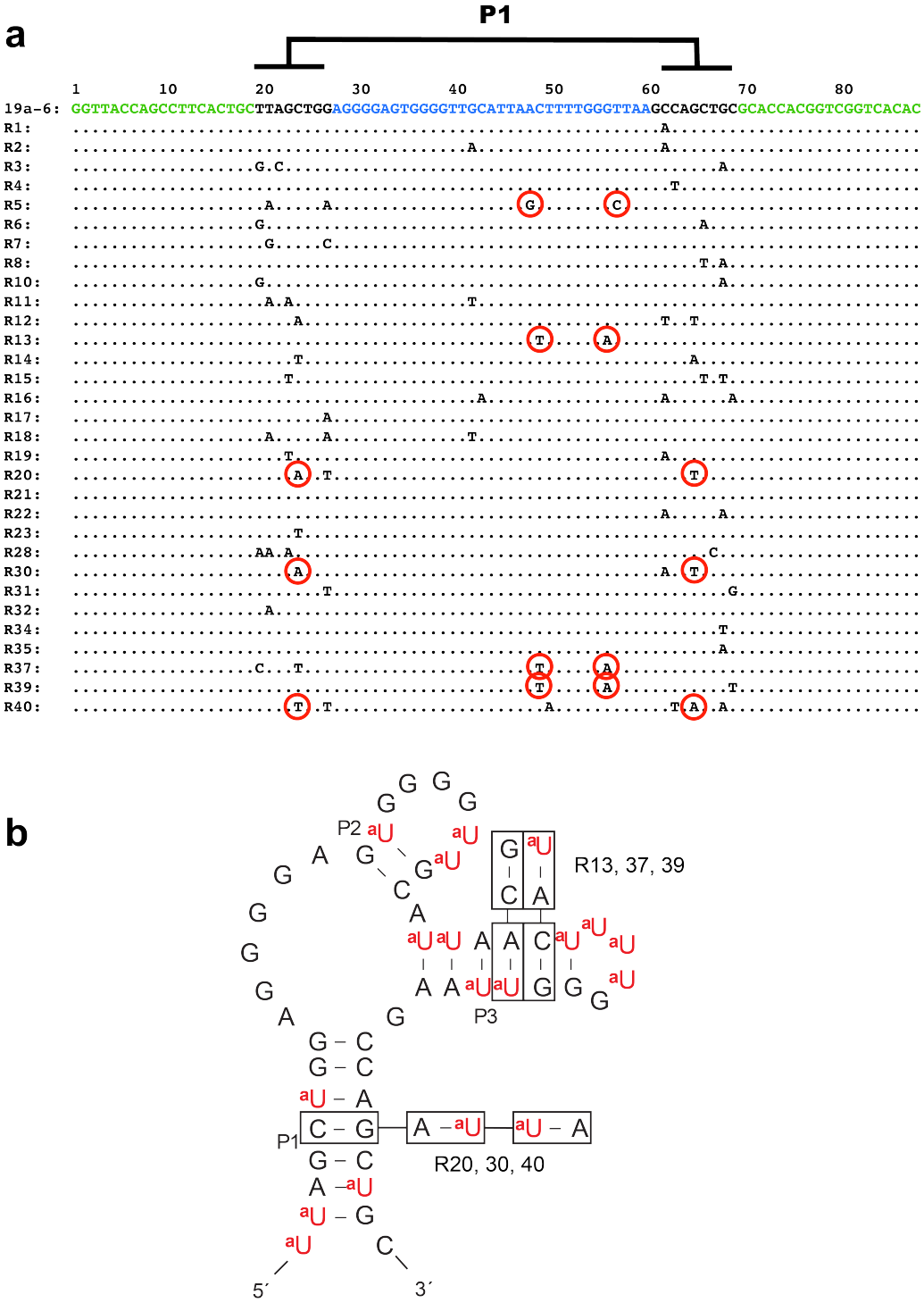


Figure A.4: Sequences of individual clones isolated following the reselection of mutagenized 19a-6 (RNA Pool 2). (a) Sequences of individual clones isolated following three rounds of reselection using Lib2. Green highlighted regions correspond to fixed primer binding sights. Blue highlighted region designates the highly conserved region. Compensatory mutations are circled in red and indicated in (b). (b) Predicted secondary structure of 19a-6 (Primer binding sites are not shown). Boxed nucleotides correspond to compensatory mutations within the P1 and P3 stems. Adapted from Ref. 123 with permission from Wiley.

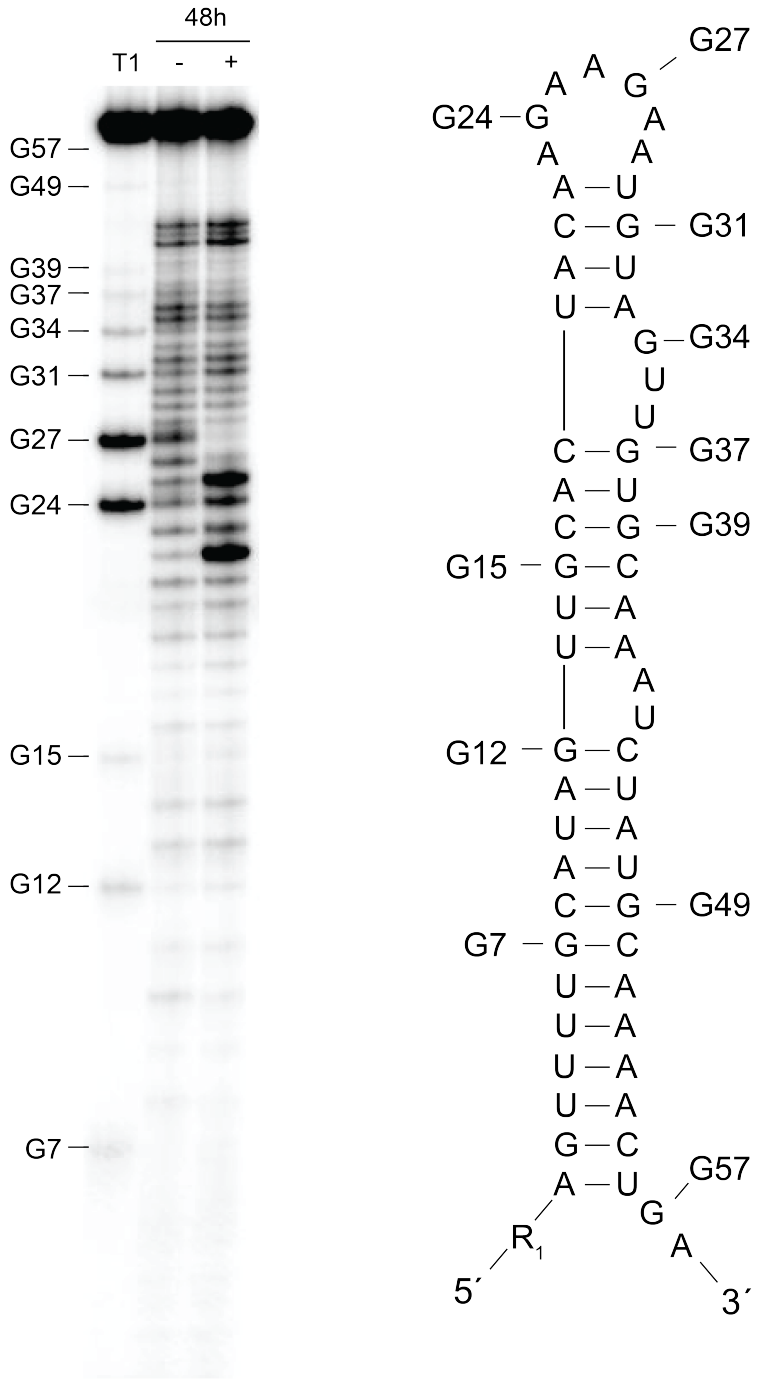


Figure A.5: In-line probing analysis of pre-miR-19a S3 in the presence and absence of MLRA-19a. Reaction mixtures contained 3 $\mu$M of [5′-$^{32}$P]-labeled **S3**, either none or 18 $\mu$M MLRA-19a, 5 mM $MgCl_2$, 150 mM KCl, 20 mM NaCl, and 25 mM Tris (pH 7.6), and were incubated at 37 °C for 48 hours. Material partially digested by ribonuclease T1 (cleaves after G residues) is shown at the left. Refer to Figure 2.5 in the main text. Adapted from Ref. 123 with permission from Wiley.

| | |
|---|---|
| M1 | M1a 5′-TTCGACTCACTATAGGCCGGAGGGGAGTGGGGTTGC3′<br>M1b 5′-GGCCGGCTTAACCCAAAAGTTAATGCAACCCCACTCCCCTCCGG-3′ |
| M2 | M2a 5′-TTCTAATACGACTCACTATAGACTGGAGGGGAGCGGGGTTGC-3′<br>M2b 5′-GACTGGCTTAACCCAAAAGTTAATGCAACCCCGCTCCCCT-3′ |
| M3 | M3a 5′-TTCTAATACGACTCACTATAGACTGGAGGGGAGTGGGGCCGC-3′<br>M3b 5′-GACTGGCTTACCCAAAAGGTTAATGCGGCCCCACTCCCCT-3′ |
| M4 | M4a 5′-TTCTAATACGACTCACTATAGACTGGAGGGGAGTGGGGTTGC-3′<br>M4b 5′-GACTGGCTTACCCAAGGTTAATGCAACCCCACTCCCCT-3′ |
| M5 | M5a 5′-TTCTAATACGACTCACTATAGACTGGAGGGGAGTGGGGTTGC-3′<br>M5b 5′-GACTGGCTTACCCAAGAGTTAATGCAACCCCACTCCCCT-3′ |
| M6 | M6a 5′-TTCTAATACGACTCACTATAGACTGGAGGGGAGTGGGGTTGC-3′<br>M6b 5′-GACTGGCTTACCCAGAAGTTAATGCAACCCCACTCCCCT-3′ |
| M7 | M7a 5′-TTCTAATACGACTCACTATAGACTGGAGGGGAGTGGGGTTGC-3′<br>M7b 5′-GACTGGCTTACCCGAAAGTTAATGCAACCCCACTCCCCT-3′ |
| M8 | M8a 5′-TTCTAATACGACTCACTATAGACTGGAGGGGAGTGGGGTTGC-3′<br>M8b 5′-GACTGGCTTGGCCAAAGCCAATGCAACCCCACTCCCCT-3′ |
| M9 | M9a 5′-TTCTAATACGACTCACTATAGACTGGAGGGGAGTGGGGTTGC-3′<br>M9b 5′-GACTGGCCCAACCAAAGTTGGTGCAACCCCACTCCCCT-3′ |

Figure A.6: Oligonucleotides used to prepare D-19a-6t and related mutants. Refer to Figure 2.4 in the main text. Red letters indicate mutations relative to D-19a-6t. Adapted from Ref. 123 with permission from Wiley.

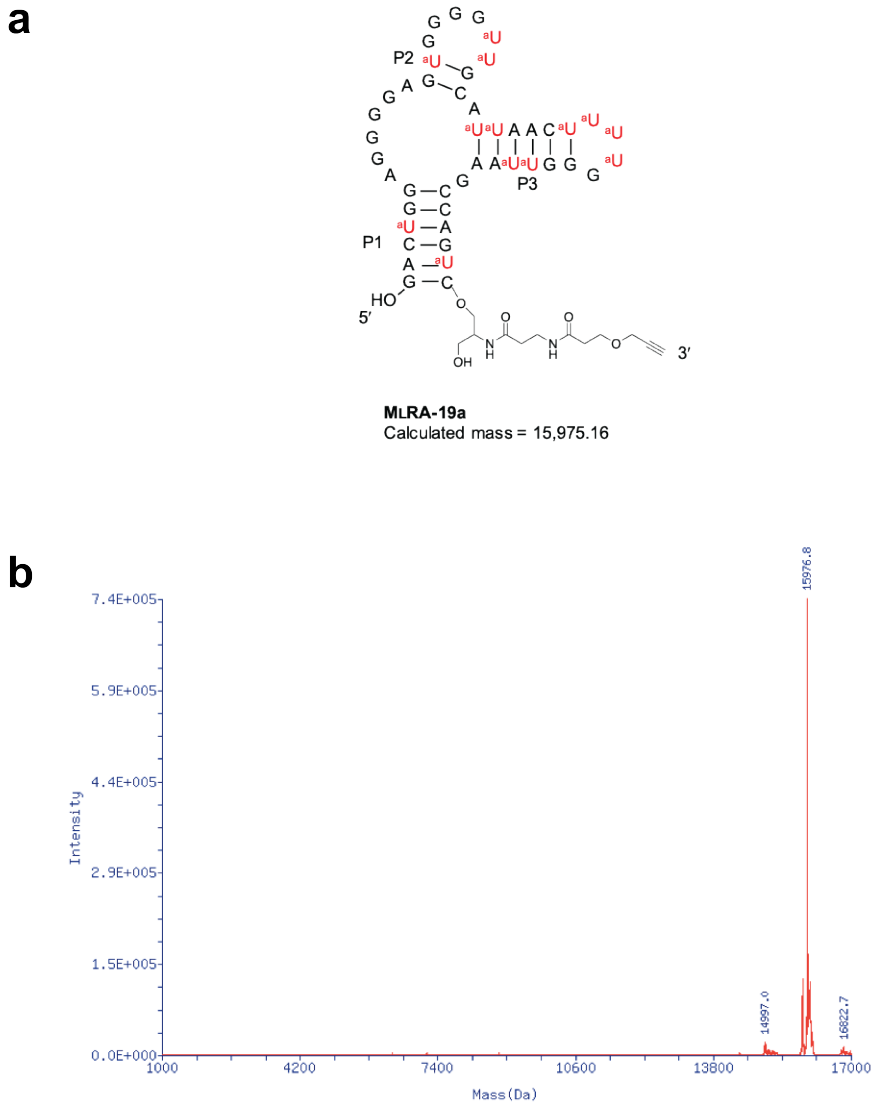


Figure A.7: Sequence and ESI-MS spectrum of MLRA-19a. (top) Sequence and proposed secondary structure of MLRA-19a prepared synthetically using L-nucleoside phosphoramidites. The 3′-alkyne modification was introduced during solid-phase RNA synthesis of MLRA-19a using the 3′-alkyne modified CPG support available from Glen Research (Sterling, VA). (bottom) ESI-MS spectrum of MLRA-19a. Mass calculated: 15,975.16; mass found: 15,976.8. Adapted from Ref. 123 with permission from Wiley.

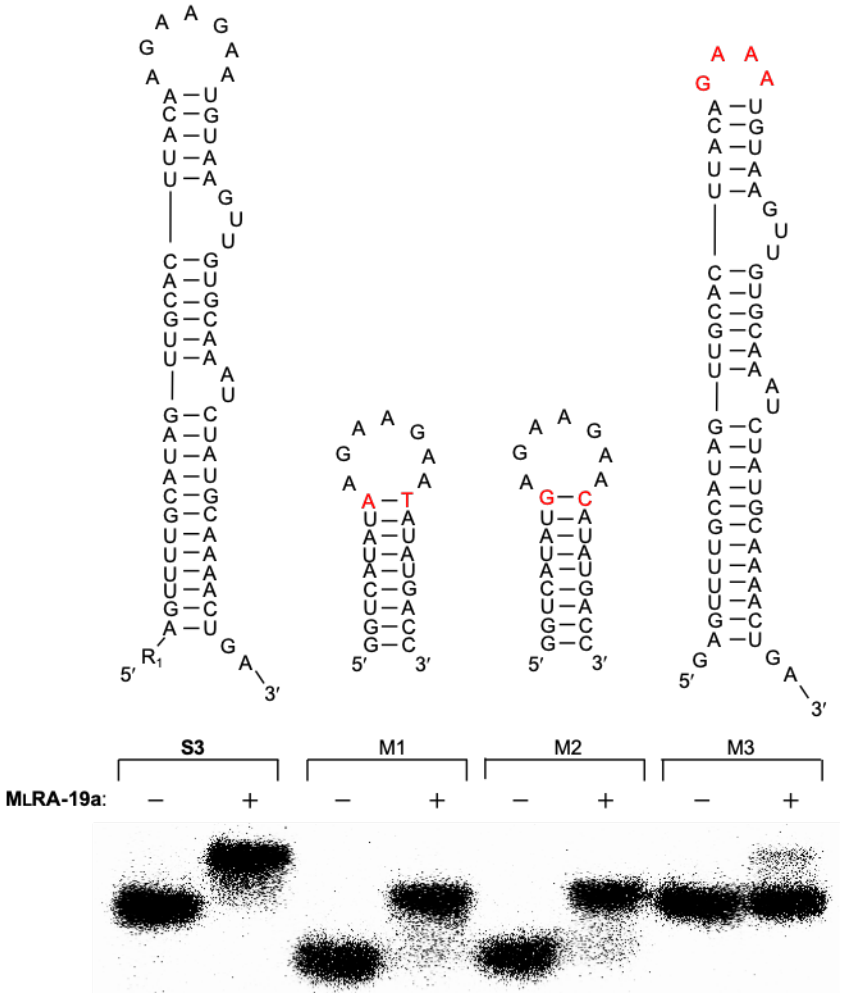


Figure A.8: Loop-dependent binding of MLRA-19a to S3. Mutations relative to pre-miR-19a are highlighted in red. MLRA-19a binds hairpins with random stem and correct pre-miR-19a distal loop (M1 and M2). Each reaction mixture contained 10 nM MLRA-19a and 1 nM of substrate. Buffer conditions were identical to EMSA conditions. Adapted from Ref. 123 with permission from Wiley.

# APPENDIX B

# CHAPTER 3 SUPPLEMENTARY DATA

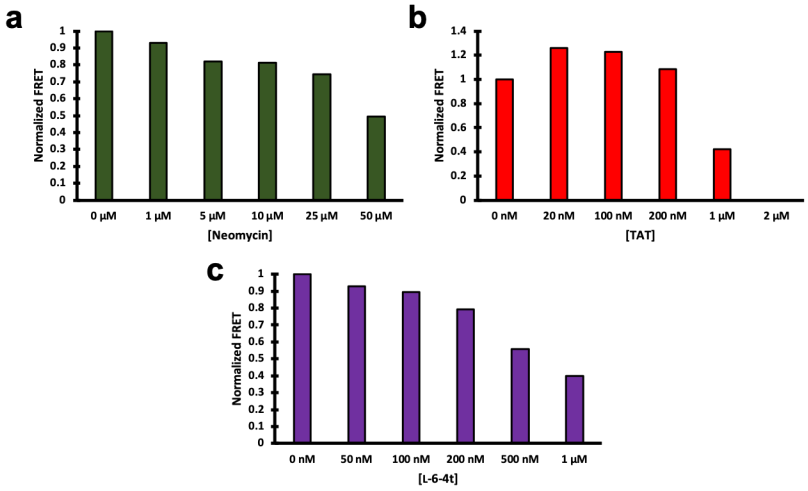


Figure B.1: Control aptamer displacement FRET inhibition assays. a) Neomycin titration from 1 to 50 $\mu$M with approximately 40% FRET signal reduction at 50 $\mu$M. b) TAT peptide titration from 20 nM to 2 $\mu$M with complete loss of FRET signal beyond 1 $\mu$M concentration. c) Unlabeled L-6-4t aptamer titration up to 1 $\mu$M.

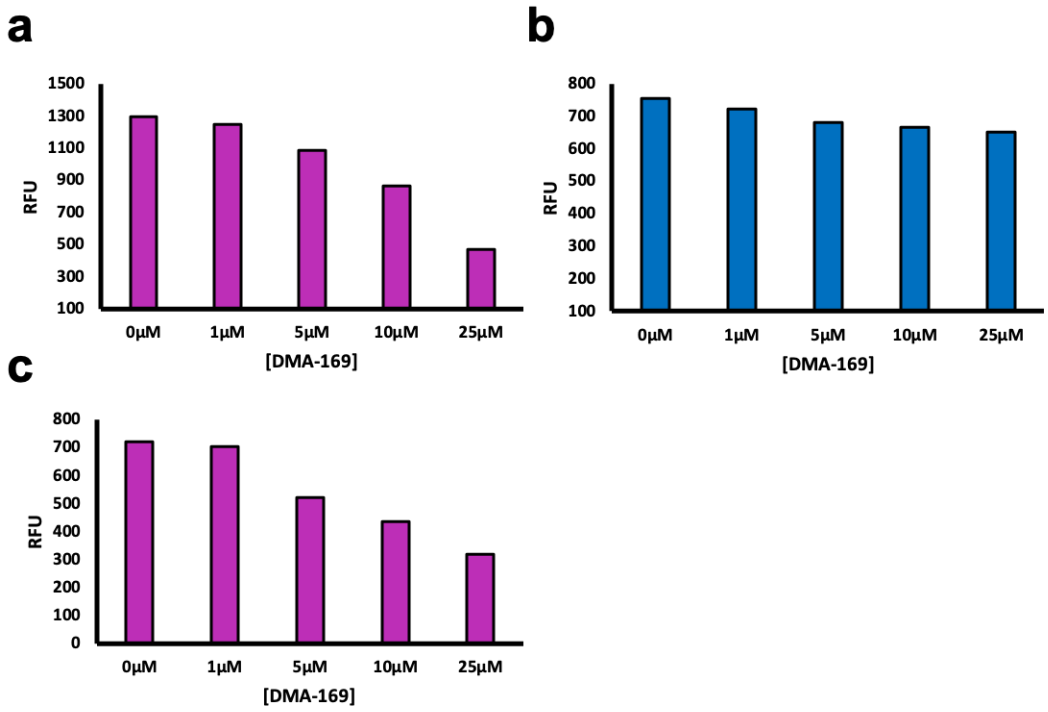


Figure B.2: Concentration dependence of fluorescence attenuation of various fluorescent species by DMA-169. a) A single stranded DNA oligonucleotide (18 nt) labeled at the 3′ end with Cy3 by phosphoramidite coupling. b) Cy5-maleimide labeling dye preemptively reacted with DTT. c) A g-quadruplex forming L-DNA aptamer (53 nt) labeled at the 5′ end with Cy3 by phosphoramidite coupling. These data, in addition to observations made in the main text (Figure 3.8) demonstrate that DMA-169 inherently affects the fluorescence of cyanine dyes to varying degrees in a non-specific manner. These data also necessitate our control reaction schemes discussed in Chapter 3 regarding a control at each concentration of competitor molecule.

**a**

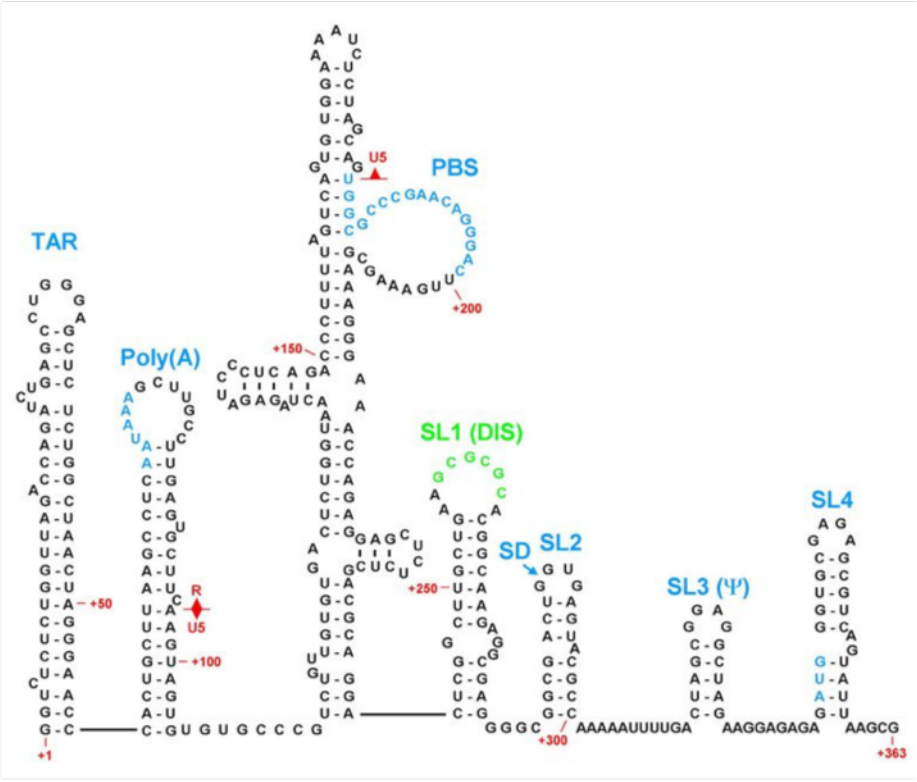


**b**

5′
GGCACUGCUUAAGCCUCAAUAAAGCUUGCCUUGAGUGCUU
CAAGUAGUGUGUGCCCGUCUGUUGUGUGACUCUGGUAACU
AGAGAUCCCUCAGACCCUUUUAGUCAGUGUGGAAAAUCUC
UAGCAGUGGCGCCCGAACAGGGACUUGAAAGCGAAAGGGA
AACCAGAGGAGCUCUCUCGACGCAGGACUCGGCUUGCUGA
AGCGCGCACGGCAAGAGGCGAGGGGCGGCGACUGGUGAG
UACGCCAAAAAUUUUGACUAGCGGAGGCUAGAAGGAGAGA
GAUGGGUGCGAGAGCGUCAGUAUUAAGCG 3′

Figure B.3: 363 bp HIV-RNA transcript construct. In the experiments depicted in Chapter 3 Figure 3.10, this template excluding the TAR hairpin at the 5′ end is used as a nonspecific blocker RNA. a) Predicted secondary structure of the full length TAR HIV transcript (363 bp). b) The 308 bp sequence lacking the TAR hairpin domain which was ordered from a commercial source as a G-block assembly for PCR assembly followed by transcription.

# APPENDIX C

## CHAPTER 4 SUPPLEMENTARY DATA

| Sequence Name | Sequence Identity 5′→3′ | Oligomer Stereochemistry |
|---|---|---|
| Reaction A | | |
| D-IN1 | CCCTCATTCATTCATCTCCATAGTGCACGG | D |
| PNA1 | ACATCATATTCCCTCATTCATTCA | achiral |
| D-A1(1-2-3) | CCGTGCACTATGGAGATGAATGAATGAGGG | D |
| D-OUT1 | GTATCTTAGTGTCCATTGCACATCATATTCCCTCA | D |
| D-B1(2-3-4) | TGAATGAATGAGGGAATATGATGTGCAAT | D |
| D-R1(4*) | **Cy3**-GTATCTTAGTGTCCATTGCA | D |
| D-R1(3-4) | ATGATGTGCAATGGACACTAAGATAC-**BHQ2** | D |
| L-IN1 | CCCTCATTCATTCATCTCCATAGTGCACGG | L |
| L-A1(1-2-3) | CCGTGCACTATGGAGATGAATGAATGAGGG | L |
| L-OUT1 | GTATCTTAGTGTCCATTGCACATCATATTCCCTCA | L |
| L-B1(2-3-4) | TGAATGAATGAGGGAATATGATGTGCAAT | L |
| L-R1(4*) | **Cy5**-GTATCTTAGTGTCCATTGCA | L |
| L-R1(3-4) | ATGATGTGCAATGGACACTAAGATAC-**BHQ3** | L |

Figure C.1: Names, sequences, and chirality of strand used in this work. For strands not named in the main text figures, they are named here based upon the complex they are associated with before initiation of the reaction, followed by their sequence domains listed in the 5′←3′ direction (in parenthesis). For example, strand D-$B_1$(2-3-4) is the bottom strand of complex D-$B_1$ illustrated in Fig. 4.2a. D-DNA (black), L-DNA (blue), and PNA (green) are indicated by color. Adapted from Ref. 124 with permission from ACS.

| Sequence Name | Sequence Identity 5' → 3' | Oligonucleotide Stereochemistry |
|---|---|---|
| D-H1 | ACGTTACCTGCCCTATAGGATCGAACTGGTAAGATGTGTACTACCAGTTC GATCCTATCACGAT | D |
| L-H1 | ACGTTACCTGCCCTATAGGATCGAACTGGTAAGATGTGTACTACCAGTTC GATCCTATCACGAT | L |
| D-H2 | AGATGTGTACATAGGATCGAACTGGTAGTACACATCTTACCAG | D |
| L-H2 | AGATGTGTACATAGGATCGAACTGGTAGTACACATCTTACCAG | L |
| D-$R_F$ | ATCCTATAGGGCAGGTAACGTC/3Cy3/ | D |
| L-$R_F$ | ATCCTATAGGGCAGGTAACGTC/3Cy3/ | L |
| D-$R_Q$ | /5BHQ2/GACGTTACCTGCCCTAT | D |
| L-$R_Q$ | /5BHQ2/GACGTTACCTGCCCTAT | L |
| D-$OUT_{155}$ | GCTAATCGTGATAGGATCGAACTGGTA | D |
| L-$OUT_{155}$ | GCTAATCGTGATAGGATCGAACTGGTA | L |
| D-$OUT_S$ | GCTATAGCACATAGGATCGAACTGG | D |
| L-$OUT_S$ | GCTATAGCACATAGGATCGAACTGG | L |
| PNA-1 | CCTATCACGATTAGCATTAA | Achiral |
| D-miR-155 | UUAAUGCUAAUCGUGAUAGGGUU | D |
| D-$miR\text{-}155_{M1}$ | UUAAU**C**CUAAUCGUGAUAGGGUU | D |
| D-$miR\text{-}155_{M2}$ | UU**T**AU**C**CUAAUCGUGAUAGGGUU | D |
| L-miR-155 | UUAAUGCUAAUCGUGAUAGGGUU | L |

Figure C.2: Names, sequences, and chirality of all oligonucleotides used in this work. D-DNA (Black, D-RNA (red), L-DNA (blue), and PNA (green) are indicated by color. 3Cy3 = cyanine 3 dye; 5BHQ2 = Black Hole Quencher 2. Refer to figure 4.7. Adapted from Ref. 125 MDPI open access journal.